ÇUKUROVA UNIVERSITY
INSTITUTE OF NATURAL AND APPLIED SCIENCES

PhD THESIS

Rahmi İlker KAYAALP

MODELLING AND ANALYSIS OF HYBRID REGENERATIVE POWER SYSTEM COMBINING WITH GRID AND SOLAR ENERGY

DEPARTMENT OF ELECTRICAL AND ELECTRONICS ENGINEERING

ADANA-2022

ÇUKUROVA UNIVERSITY
INSTITUTE OF NATURAL AND APPLIED SCIENCES

MODELLING AND ANALYSIS OF HYBRID REGENERATIVE POWER SYSTEM WITH GRID AND SOLAR ENERGY

Rahmi İlker KAYAALP

PhD THESIS

DEPARTMENT OF ELECTRICAL AND ELECTRONICS ENGINEERING

We certify that the thesis titled above was reviewed and approved for the award of the degree of the Philosophy of Doctorate by the board of jury on 03/08/2022.

…………………………….	…………………………...	…………….……………………
Prof. Dr. Mehmet TÜMAY	Doç. Dr. M. Uğraş CUMA	Prof. Dr. K. Çağatay BAYINDIR
SUPERVISOR	II.SUPERVISOR	MEMBER

………………………………..	…………………………...........
Doç. Dr. M. Mustafa SAVRUN	Dr. Öğr. Üyesi Adnan TAN
MEMBER	MEMBER

PhD Thesis is written at the Department of Biotechnology of Institute of Naturaland Applied Sciences of Çukurova University
Registration Number:

Prof. Dr. Sadık DİNÇER
Director
Institute of Natural and Applied Sciences

This study supported by Çukurova University Scientific Research Projects Unit.
(Project No: FDK-2017-9349).

ABSTRACT

PhD THESIS

MODELLING AND ANALYSIS OF HYBRID REGENERATIVE POWER SYSTEM WITH GRID AND SOLAR ENERGY

Rahmi İlker KAYAALP

ÇUKUROVA UNIVERSITY
INSTITUTE OF NATURAL AND APPLIED SCIENCES
DEPARTMENT OF ELECTRICAL AND ELECTRONICS ENGINEERING

Supervisor : Prof. Dr. Mehmet TÜMAY
Year: 2022, Pages: 173
Jury : Prof. Dr. Mehmet TÜMAY
: Prof. Dr. Kamil Çağatay BAYINDIR
: Assoc. Prof. Dr. Mehmet Uğraş CUMA
: Assoc. Prof. Dr. Murat Mustafa SAVRUN
: Asst. Prof. Dr. Adnan TAN

In this thesis, the Hybrid Regenerative Power System (HRPS) was studied and operated at low powers with a designing a new Central Energy Management System (CEMS). It is suitable for the critical AC & DC loads and efficient thanks to the regenerative effect. Firstly, equipments in the power system were created and operated seperately and the results of these equipments were obtained in different cases. HRPS consists of a bidirectional inverter connected with LCL filter and grid, a bidirectional isolated DC-DC converter connected with batteries and an isolated unidirectional DC-DC converter connected to photovoltaic panels and combining AC & DC loads. After the HRGS topology emerged, an innovative, efficient, unique rule-based CEMS is created. It can automatically manage power flow scenarios in order to operate power system efficiently and accurately by evaluating load demands and power balances in the system. Power flow scenarios were first run alone according to different situations and then they were operated together with CEMS using real irradiance and temperature spectrums. Then, how efficient the power system is in itself was calculated according to the results obtained and when compared to the literature, it was emphasized in which cases it has advantageous than the other energy management systems.

Key Words: Hybrid, Regenerative, Photovoltaic, Batteries, LCL Filter, Grid-connected Inverter, Energy Management System.

ÖZ

DOKTORA TEZİ

ŞEBEKE VE GÜNEŞ ENERJİSİ BAĞLANTILI HİBRİT REJENERATİF GÜÇ SİSTEMİNİN MODELLENMESİ VE ANALİZİ

Rahmi İlker KAYAALP

ÇUKUROVA ÜNİVERSİTESİ
FEN BİLİMLERİ ENSTİTÜSÜ
ELEKTRİK – ELEKTRONİK MÜHENDİSLİĞİ ANABİLİM DALI

Danışman : Prof. Dr. Mehmet TÜMAY
Yıl: 2022, Sayfa: 173
Jüri : Prof. Dr. Mehmet TÜMAY
: Prof. Dr. Kamil Çağatay BAYINDIR
: Doç. Dr. Mehmet Uğraş CUMA
: Doç. Dr. Murat Mustafa SAVRUN
: Dr. Öğr. Üyesi Adnan TAN

Bu tezde doğru akımlı ve alternatif akımlı kritik yük taleplerine uygun, rejeneratif etki sayesinde verimli, yeni bir Merkezi Enerji Yönetim Sistemi (MEYS) tasarımı yapılarak düşük güçlerde çalışabilecek Hibrit Rejeneratif Güç Sistemi (HRGS) üzerinde çalışılmıştır. Bu güç sisteminin içinde bulunan ekipmanlar öncelikle ayrı ayrı oluşturularak çalıştırılmış ve farklı durumlarda bu ekipmanlara ait sonuçlar alınmıştır. HRGS; şebekeye LCL filtre ile bağlı çift yönlü çalışabilen DA-AA dönüştürücüsü, bataryalara bağlı çift yönlü çalışabilen izoleli DA-DA dönüştürücüsü, fotovoltaik panellere bağlı izoleli H-köprü DA-DA dönüştürücüsü ile DA ve AA yüklerinin birleştirilmesinden oluşmaktadır. HRGS topolojisi ortaya çıktıktan sonra ise güç sisteminin en verimli ve doğru şekilde çalışabilmesi için güç akış senaryolarını otomatik olarak yönetebilen, yenilikçi, verimli, yük taleplerine ve sistemdeki güç dengelerine uygun, özgün, kural tabanlı bir MEYS tasarımı yapılmıştır. Güç akış senaryoları ise öncelikle farklı durumlara göre tek başlarına çalıştırılmış olup daha sonrasında gerçek ışıma ve sıcaklık spektrumları kullanılarak MEYS ile birlikte çalıştırılmıştır. Daha sonra ise alınan sonuçlara göre güç sisteminin kendi içinde ne kadar verimli olduğu hesaplanmış ve literatürle karşılaştırıldığında diğer enerji yönetim sistemlerine göre hangi durumlarda avantajlı olduğu vurgulanmıştır.

Anahtar Kelimeler: Hibrit, Rejeneratif, Fotovoltaik, Bataryalar, LCL Filtre, Şebeke-bağlantılı Evirici, Enerji Yönetim Sistemi.

EXTENDED SUMMARY

Studies with renewable energy sources are increasing and diversifying day by day. For this reason, new and more efficient controllers are improved on different renewable energy sources. Thus, renewable energy power systems can vary with the development of both topological, power system element controllers and energy management system controllers in line with the desired demands. These various power system topologies belong to renewable energy sources both reduce the cost and become more useful. Their aim to work more efficiently for a long time and they prevent fossil fuel energy conversion systems. In recent years, especially with the development of renewable energy technologies, lots of studies studies have been carried out to create an interconnected smart grid systems that can operate effectively at high or low power. At this point, the aim is producing more efficient topologies by working in harmony with each other of the equipments in the power system and keeping the errors minimum level. Central energy management system applications are developed in order to realize this purpose and control the power flow between the equipments in the power system. There are lots of various central energy management systems in literature. In general, we can say that each energy management system can work very efficiently in this environment where it can be created according to the total powers of components at own topology.

The general purpose of the thesis; using solar panels and batteries with isolated converters that is seen hybrid with DC connections for uninterrupting energy transfer a long time to low power critical loads. In addition, the other aim is designing a unique, high-level central energy management system that can control the power flows between the equipments on top of this hybrid structure, it operates the entire system efficiently in real radiation and temperature spectrums and different load demands. MATLAB / Simulink program is used in all of these studies.

It can be partially understand the path taken in the thesis work and which studies were carried out from the table of contents. When we make a general

summary of the studies and the results obtained in this section, firstly, grid connected 2-level AC-DC converter is designed and bidirectional operation is achieved. The designed converter is bidirectional because it should both feed the DC loads from the grid, charge the batteries and inject the power produced from the batteries and solar panels into the grid to provide savings thanks to the regenerative effect. Phase-locked-loop method is used for transferring power to grid and LCL filter design is made between the grid and the inverter, just after the AC loads, in order to reduce the harmonics. Transfer function and resonance frequency of LCL filter were calculated and plotted in MATLAB environment. Both DC-Link voltage controller and reactive power controller are made by using Clarke and Park transformations in the phase locked loop method.

Then, batteries connected bidirectional isolated DC-DC converter is created. The reason for the bidirectional operation of the converter is performing both charging and discharging of the batteries. IGBTs, which are more durable, are used for the switching signals of the DC-DC converter and signal triggers are made by using DPS method, which is the most efficient phase shift technique in order to obtain high efficient operation. The fact that the converter is preferred an isolated, H-bridge topology that ensures its long-lasting operability. The batteries used are 14 pieces and they are 24 V and 10 Ah lithium-ion type. All the parameters of the batteries are written by using the data sheets of the battery manufacturer companies. Constant Current – Constant Voltage method is used while charging the batteries. In this charging method, it is possible to charge the batteries with the current value that we want. When discharging operation, 2 different controllers are made. When the DC-Link voltage controller is started, the discharge current of the batteries is determined automatically and when we operate it with the discharge current controller, the DC load at the converter output can be fed by the desired discharge current value.

Afterwards, these chapters of the hybrid regenerative power system was completed, photovoltaic panels connected an isolated, unidirectional H-bridge DC-

DC converter is designed. At this point, total of 48 solar panels with 4 parallel and 12 serial connections of 1Soltech 1STH-215-P branded in MATLAB's own library are used. After drawing I-V and P-V graphics for solar panels at different irradiance and temperature values, the P&O method, which is one of the maximum power point tracking techniques, is used on the panels. The P&O method is preferred, because it is easier to design than other maximum power point tracking techniques and it is very useful.

Afterwards, all hybrid regenerative power system equipments, which are modeling and analysis were completed, are combined each other and the power flow scenarios that were required to be operated manually in a smooth and efficient manner. These scenarios are operated one by one at different load conditions. After obtaining the results of 7 different power flow scenarios in the power system, a high-level, centralized and unique rule-based energy management system is designed. It can automatically operate and control the all power system in accordance with changing load demands and weather conditions. The created central energy management system provides the transition between power flow scenarios with the mechanism of controlling the switches connected to DC-Link voltage of the converters in the power system. These transitions are completely dependent on load demands, produced powers, irradiation and temperature.

Efficiency analyzes are made by evaluating the results obtained in all of the cases examined and finally a profit analysis are made by looking at the daily consumed and produced power according to the hours in the hybrid regenerative power system topology operated together with the central energy management system for residential and commercial areas.

At the end of the thesis, comments about the obtained results by operating the proposed and hybrid regenerative power system and the central energy management system together are given at conclusion part. When the proposed hybrid regenerative power system and energy management system are compared with other applications in literature, we can emphasize that it has an efficient and long-lasting operating performance. It can be customized for different regenerative renewable power system topologies that feed critical loads, especially made at low power and it can provide quickly transition between power flow scenarios.

Finally, the proposed system with its regenerative effect, it supports uninterrupted power transfer to the critical loads and it has important contributions to minor smart grid literature.

GENİŞLETİLMİŞ ÖZET

Yenilenebilir enerji kaynakları ile yapılan çalışmalar gün geçtikçe daha da artmakta ve çeşitlenmektedir. Bu sebeple çeşitlendirilmiş yenilenebilir enerji kaynakları üzerinde yeni ve daha verimli çalışabilecek kontrolcü tasarımları da geliştirilmektedir. Böylelikle yenilenebilir enerji güç sistemleri istenen talepler doğrultusunda hem topolojik, hem güç sistemi elemanları kontrolcüleri, hem de enerji yönetim sistemi kontrolcülerinin geliştirilebilmesiyle değişkenlik gösterebilir. Yenilenebilir enerji kaynaklarına ait bu çeşitli güç sistemi topolojileri hem maliyeti düşürüp giderek daha kullanışlı hale gelmekle hem de daha verimli ve uzun ömürlü çalışabilmeyi amaçlayarak fosil yakıtlı enerji dönüşüm sistemlerinin önüne geçmektedirler. Son yıllarda özellikle yenilenebilir enerji teknolojilerinin gelişmesiyle birlikte yüksek ya da düşük güçte etkin çalışabilen birbiriyle bağlantılı akıllı şebeke oluşturma çalışmaları yapılmaktadır. Bu noktada amaç; güç sistemi içinde bulunan ekipmanların birbirleriyle uyum içinde çalışarak ve oluşabilecek hataları minimum düzeyde tutarak, daha verimli topolojiler üretmektir. Bu amacı gerçekleştirebilmek ve güç sistemi içinde ekipmanlar arasındaki güç akışını kontrol edebilmek için merkezi enerji yönetim sistemi uygulamaları geliştirilmektedir. Merkezi enerji yönetim sistemleri ise literatürde çeşitlilik göstermektedir. Genel olarak her enerji yönetim sistemi, kendisine ait topolojinin toplam gücüne göre şekillendirilebildiği bu ortamda oldukça verimli çalışabildiklerini söyleyebiliriz.

Buradaki tez çalışmasında da genel amaç; düşük güçlü kritik yük bağlantılarına sahip bir güç sistemi topolojisinde kesintisiz bir şekilde enerji iletiminin yapılabilmesi için DA bağlantıları ile hibrit görünümde, uzun ömürlü çalışabilecek izoleli dönüştürücüler yardımıyla solar paneller ve bataryalar kullanmaktır. Ayrıca bu yapının üstüne de ekipmanlar arasındaki güç akışlarını kontrol edebilecek özgün, yüksek seviyeli bir merkezi enerji yönetim sistemi tasarlayarak tüm sistemi gerçek ışıma ve sıcaklık spektrumlarında ve farklı yük

taleplerinde verimli bir şekilde çalıştırmaktır. Yapılan çalışmalarının tamamında MATLAB / Simulink programı kullanılmıştır.

Tez çalışmasında gidilen yol ve sırayla hangi çalışmaların yapıldığı içindekiler bölümünden de kısmi şekilde anlaşılabilir. Fakat bu bölümde yapılan çalışmaların ve alınan sonuçların genel bir özetini yaparsak ilk olarak şebeke bağlantılı, çift yönlü çalışabilen 2 seviyeli AA-DA dönüştürücüsü tasarımı yapılmıştır. Buradaki dönüştürücünün çift yönlü istenmesinin sebebi ise hem şebekeden DA yüklerini besleyip bataryaları şarj edebilmek hem de bataryalardan ve solar panellerden üretilen gücü şebekeye enjekte ederek rejeneratif etki sayesinde tasarruf sağlamaktır. Şebekeye aktarılacak gücün iletilmesi için faz kilitleme yöntemi kullanılmış olup oluşan harmonikleri de azaltabilmek için şebeke ve dönüştürücü arasına, AA yüklerinden hemen sonrasında LCL filtre tasarımı yapılmıştır. LCL filtrenin transfer fonksiyonu ve resonans frekansı hesaplanıp grafik halinde MATLAB ortamında çizdirilmiştir. Faz kilitleme yöntemi içerisinde ise Clarke ve Park dönüşümleri kullanılarak hem DA-Link gerilim kontrolcüsü hem de reaktif güç kontrolcüsü yapılmıştır.

Sonrasında bataryalarla bağlantılı çift yönlü çalışabilen izoleli DA-DA dönüştürücüsünün tasarımı yapılmıştır. Dönüştürücünün çift yönlü çalışmasının sebebi ise bataryaların hem şarjını hem de deşarjını gerçekleştirebilmektir. DA-DA dönüştürücüsünün tetikleme sinyalleri için daha dayanıklı olan IGBTler kullanılmış olup yüksek verimde çalışabilmesi için de faz kaydırma tekniklerinden en verimli olan DPS metoduyla sinyal tetiklemeleri yapılmıştır. Dönüştürücünün izoleli, H-köprü topolojisinde tercih edilmesi de uzun ömürlü çalışabilirliğini sağlamaktır. Kullanılan bataryalar ise 14 adet olup 24 V ve 10 Ah lik lityum-iyon tiptedir. Bataryaların tüm parametreleri ise batarya üreticisi şirketlerin veri sayfalarından yararlanılarak yazılmıştır. Bataryaları şarj ederken Sabit Akım – Sabit Gerilim metodu kullanılmıştır. Bu şarj yönteminde istediğimiz akım değeriyle bataryaları şarj etmemiz mümkündür. Deşarjı yapılırken ise 2 farklı kontrolcü yapılmıştır. DA-Link gerilimi kontrolcüsü çalıştırıldığında bataryaların deşarj akımı otomatik olarak belirlenirken, deşarj akımı kontrolcüsü ile çalıştırdığımızda istenilen deşarj akımı değeriyle dönüştürücü çıkışındaki DA yük beslenebilmektedir.

Hibrit rejeneratif güç sisteminin bu aşamaları bitirildikten sonra fotovoltaik panellere bağlı, izoleli, tek yönlü çalışabilen yine H-köprü DA-DA dönüştürücüsü tasarımı yapılmıştır. Bu noktada MATLAB'ın kendi kütüphanesinde bulunan 1Soltech 1STH-215-P markalı 4 paralel ve 12 seri bağlantılı olacak şekilde toplam 48 adet solar panel kullanılmıştır. Solar paneller için farklı ışıma ve sıcaklık değerlerinde I-V ve P-V grafikleri çizdirildikten sonra paneller üzerinde maksimum güç noktası izleme tekniklerinden biri olan P&O metodu kullanılmıştır. P&O metodu hem tasarımının diğer güç noktası izleme tekniklerinden daha kolay olması hem de oldukça kullanışlı olması bakımından tercih edilmiştir.

Bu aşamadan sonra ise tasarımları biten solar panellere bağlı DA-DA dönüştürücüsü ile şebeke bağlantılı AA-DA dönüştürücüsü DC-Link gerilimleri üzerinden birbirine bağlanarak 3 farklı yük durumunda çalıştırılıp sonuçları alınmıştır.

Devamında modellenmesi ve analizleri biten tüm hibrit rejeneratif güç sistemi ekipmanları birleştirilerek manuel olarak düzgün ve verimli bir şekilde çalıştırılması istenen güç akış senaryoları teker teker farklı yük koşulları dikkate alınarak çalıştırılmıştır. Güç sistemi içerisinde 7 farklı güç akış senaryosuna ait sonuçlar da alındıktan sonra tüm sistemi değişebilen yük taleplerine ve hava koşullarına uygun şekilde otomatik olarak çalıştırıp kontrol edebilen yüksek seviyeli, merkezi ve kural tabanlı, özgün bir enerji yönetim sistemi tasarımı yapılmıştır. Oluşturulan merkezi enerji yönetim sistemi güç sistemi içerisinde bulunan dönüştürücülerin DC-Link gerilimine bağlı anahtarlarını kontrol edebilme mekanizmasıyla güç akış senaryoları arasında geçişi sağlamaktadır. Bu geçişler ise tamamen yük taleplerine, üretilen güçlere, ışımaya ve sıcaklığa bağlı olarak değişmektedir.

İncelenen durumların tamamında alınan sonuçlar değerlendirilerek verimlilik analizleri yapılmış olup son olarak merkezi enerji yönetim sistemi ile birlikte çalıştırılan hibrit rejeneratif güç sistemi topolojisinde saatlere göre günlük harcanan ve üretilen güçlere bakılarak hem evler hem de iş yerleri için kâr analizi yapılmıştır.

Tez çalışmasının sonunda ise yapılan ve önerilen hibrit rejeneratif güç sistemi ile merkezi enerji yönetim sisteminin birlikte çalıştırılmasıyla elde edilen sonuçlar yorumlanarak sonuç bölümünde verilmiştir. Önerilen hibrit rejeneratif güç sistemi ve enerji yönetim sistemi literatürdeki diğer uygulamalarla karşılaştırıldığında; özellikle düşük güçte yapılmış kritik yükleri besleyen topolojilere yönelik özelleştirilebilen, güç akış senaryoları arasında hızlı geçiş yapabilen, verimli ve uzun ömürlü bir çalışma performansına sahip olduğunu vurgulayabiliriz.

Son olarak, önerilen sistemin rejeneratif etkisi sayesinde kritik yüklere kesintisiz güç aktarımını desteklemekte olup minör yapıdaki akıllı şebeke literatürüne de önemli katkıları vardır.

ACKNOWLEDGEMENTS

First of all, I would like to present my endless deepest gratitude to my esteemed supervisor Prof. Dr. Mehmet TÜMAY for his chiefery, deep knowledge and scientific approaches. It has been a great honor to have Prof. Dr. Mehmet TÜMAY as supervisor.

I am also grateful to my second supervisor Assoc. Prof. Dr. Mehmet Uğraş CUMA who supports me with his wide knowledge and excellent comments so that I can complete my thesis research and reach a solid scientific structure.

I would also like to thank my respectable lecturer, Prof. Dr. Kamil Çağatay BAYINDIR, especially for his extensive knowledge of the scientific literature, for opening my horizon and supporting me by specifying the details that I need to do and add my thesis.

In this process, I owe special thanks to Assoc. Prof. Dr. Murat Mustafa SAVRUN and Asst. Prof. Dr. Adnan TAN because of they always generously provided the necessary help for my scientific development, encouraged me to overcome difficulties and offered helpful suggestions.

Additionally, I would like extra to thank library and Scientific Research Projects Unit of Çukurova University, which provides necessary resource research and financial support for my PhD thesis (Project Number: FDK-2017-9349).

I would also like to extend my special thanks to my fellow Research Assistants, who have worked in our department in the past or are still continuing their studies, for their academic and moral support at every stage of my thesis work.

Finally, I wish to express my deepest gratitude to my mother Nimet KAYAALP, my father Prof. Dr. Gökhan Tamer KAYAALP and my lovely wife Elif KAYAALP who are always with me, helped me keep my motivation high, their patience and I am grateful for their all kinds of support.

CONTENTS **PAGE**

LIST OF TABLES **PAGE**

LIST OF FIGURES **PAGE**

LIST OF ABBREVIATIONS

AC	: Alternating Current
ACO	: Ant Colony Optimization
APC	: Adaptive Power Converter
APU	: Auxiliary Power Unit
BESS	: Battery Energy Storage System
BMS	: Battery Management System
BPVS	: Batteries and PV panels to System
BQZSI	: Bidirectional Quasi-Z-Source Inverter
BS	: Batteries to System
BTB	: Back To Back
CC-CV	: Constant Current – Constant Voltage
CEMS	: Central Energy Management System
CHB	: Cascaded H-Bridge
CSI	: Current Source Inverter
DAB	: Dual Active Bridge
DC	: Direct Current
DPS	: Dual Phase Shift
DSCC	: Double Star Chopper Cells
EMI	: Electromagnetic Interference
EMS	: Energy Management System
EPS	: Extended Phase Shift
EV	: Electric Vehicle
FL	: Fuzzy Logic
GA	: Genetic Algorithm
GL	: Grid to Loads
GS	: Grid to System
GT	: Game Theory

HESS	: Hybrid Energy Storage System
HEV	: Hybrid Electric Vehicle
HPF	: High Pass Filter
HRPS	: Hybrid Regenerative Power System
IBDC	: Isolated Bidirectional DC-DC Converter
IEEE	: Institude of Electrical and Electronic Engineers
IGBT	: Isolated Gate Bipolar Transistor
INC	: Incremental Conductance
IUDC	: Isolated Unidirectional DC-DC Converter
LF	: Loop Filter
LPF	: Low Pass Filter
MA	: Multi Agent
MILP	: Mixed Integer Linear Programming
MINLP	: Mixed Integer Non-Linear Programming
MMCI	: Modular Multilevel Cascade Inverter
MOSFET	: Metal Oxide Semiconductor Field Effect Transistor
MPC	: Model Predictive Control
MPPT	: Maximum Power Point Tracking
P&O	: Perturb & Observe
PD	: Phase Detector
PF	: Power Flow
PLL	: Phase Locked Loop
PS	: Phase Shift
PSO	: Partical Swarm Obtimization
PV	: Photovoltaic
PVBDC	: PV panels and Batteries to DC Load
PVBWG	: PV panels to Batteries Without Grid
PVS	: PV panels to System
PVSWB	: PV panels to System Without Batteries

PWM	: Pulse Width Modulation
RB	: Rule Based
RPS	: Regenerative Power System
SoC	: State of Charge
SoH	: State of Health
SPS	: Single Phase Shift
SRF	: Synchronous Reference Frame
THD	: Total Harmonic Distortion
TPC	: Three Port Converter
UC	: Ultra Capacitor
UPS	: Uninterruptable Power Supply
VCO	: Voltage Controlled Oscillator
VSC	: Voltage Source Converter
VSI	: Voltage Source Inverter
ZCS	: Zero Current Switching
ZVS	: Zero Voltage Switching

1. INTRODUCTION

There are lots of academic studies about power quality today. Scopes of these studies are making suitable form of current and voltage waveforms on grid lines. In recent years, lots of studies which increase efficiency, are done about power quality literature by improving smart grid methods. Using the renewable energy sources is the perfect way for increasing efficiency according to transmission and distribution lines. Thus, these renewable energy sources should be proper creation for working total of system and feeding loads compatibly.

There are lots of various renewable energy sources and solar energy is the most common used energy type. In this work, regenerative power system combined with grid will be designed by benefiting from the power that is produced in solar energy. There are different working condition types of renerative power system and these conditions can be various according to different scenarios in grid. Briefly, mitigating negative effects in grid cause to increase total efficiency of the system. The power system that can be worked at different scenerios have various equipments and suitable working each other with improved control methods are important. Therefore, these are the regenerative power system components that will be modelled and analysed: Alternative Current (AC) Grid, Photovoltaic (PV) Panels, Batteries, Bidirectional and Unidirectional Direct Current – Direct Current (DC-DC) Converters, AC-DC and DC-AC Converter and lastly AC/DC Load cells.

The general scope of this regenerative power system and the most important advantage is providing and emphasising regenerative effect on the grid by using PV panels and batteries systems. Moreover, the system will not be affected from various fault conditions and increased efficiency of transferred power owing to different working conditions. The designed power system is used in many areas in the literature. The regenerative power effect is very important for critical loads connected to the batteries of electric cars, trains and aircrafts. These critical loads that require uninterrupted or as little interruption as possible, must be operated by creating a proper Energy Management System (EMS) with a Hybrid Regenerative Power System (HRPS) topology. In addition, this system is very important for patients who depend on electricity in hospitals. For example, when a patient is connected to a dialysis device, this device needs an alternative HRPS topology that can be operated as a UPS to avoid any power outages. At this point, power can be transferred to the critical load groups at necessary areas in the hospital by designing a suitable EMS that can be operated with renewable energy sources. Apart from this, these systems are necessary in order to keep radar systems at the airports in a continuous state of operation. Especially in military applications, these systems are useful. Because protection of data and providing uninterrupted communication in the command – operation center are very important. Also developed EMS combined HRPSs are made for smart home systems in recent years.

Especially in recent years, regenerative power system comes to the forefront in renewable energy applications such as wind, solar and electric vehicles and they use battery but different topologies confront us (Chiang et al. 2010; Veerappan et al. 2014; Zulauf et al. 2015; Del Moral et al. 2015; Itani et al. 2016; Cao et al. 2012; Choi et al. 2012a; Choi et al. 2012b; Zhao et al. 2012; Agamy et al. 2012). Figure 1.1. shows topologic block diagram of regenerative power system and connections of using equipments. General system topology which will be designed, is similar with (Chiang et al. 2010)

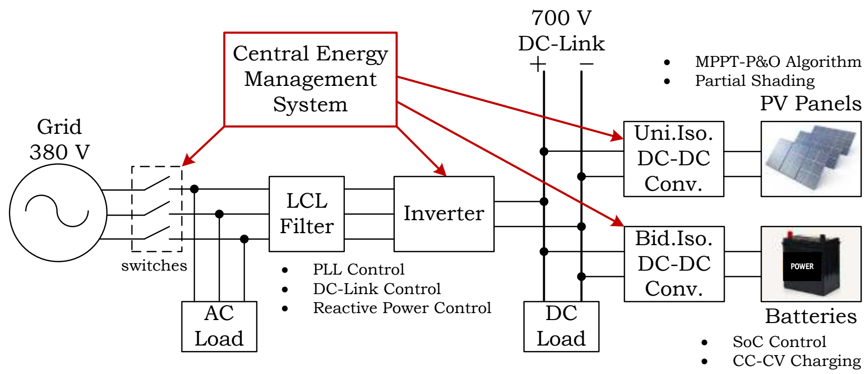

Figure 1.1. Proposed Block Diagram of Hybrid Regenerative Power System

Hybrid Regenerative Power System (HRPS) consists of grid, 2-level inverter with LCL filter, dc link line, photovoltaic (PV) panels, batteries, DC/AC loads, isolated unidirectional DC-DC converter (IUDC) and isolated bidirectional DC-DC converter (IBDC). There are lots of topologies about PV and Battery Energy Storage Systems (BESS) connected renewable energy systems and they can be classified as three types. These PV + BESS topologies are defined as;

(a) Modular cell connected cascade inverters (Chiang et al. 2010; Choi et al. 2012b; Zhao et al. 2012; Agamy et al. 2012; Lu et al. 2018; Essakiappan et al. 2015; Sochor et. al. 2018; Essakiappan et al. 2012; Bragard et al. 2010; Borrega et al. 2013; Elsayad et al. 2017; Choi et al. 2015; Islam et al. 2019)
(b) Modular cell connected on high frequency link (Veerappan et al. 2014; Choi et al. 2012a)
(c) Common dc link connected cascade dc-dc converters (Zulauf et al. 2015; Del Moral 2015; Itani et al. 2016; Zhang et al. 2018; Sayed et al. 2018)

In the light of these classification, it is realised that (c) type topologies are more useful than (a) and (b) types because of obtaining more smooth dc link voltage-current waveforms and compatible for HRPS. Moreover, if there is a fault in common dc link connected cascade dc-dc converters, system can be operated easily by mitigating these errors. It will be better to illustrate this with an example, when one PV or battery connected module is breakdown, modular multilevel dc-dc converters compensate this fault and give the same sufficient voltage value for dc-link. Thus, (c) type topologies demonstrate advantages than the other topologies. (a) and (b) type topologies are generally used for directly connecting AC grid and especially they are connected to more transformers so it causes more cost. Additionally, common frequency equalization and more flactuations on AC-Link can be harmful for other system equipments cause to decrease their lifetime. These topologies are classified above and shown in Figure 1.2.

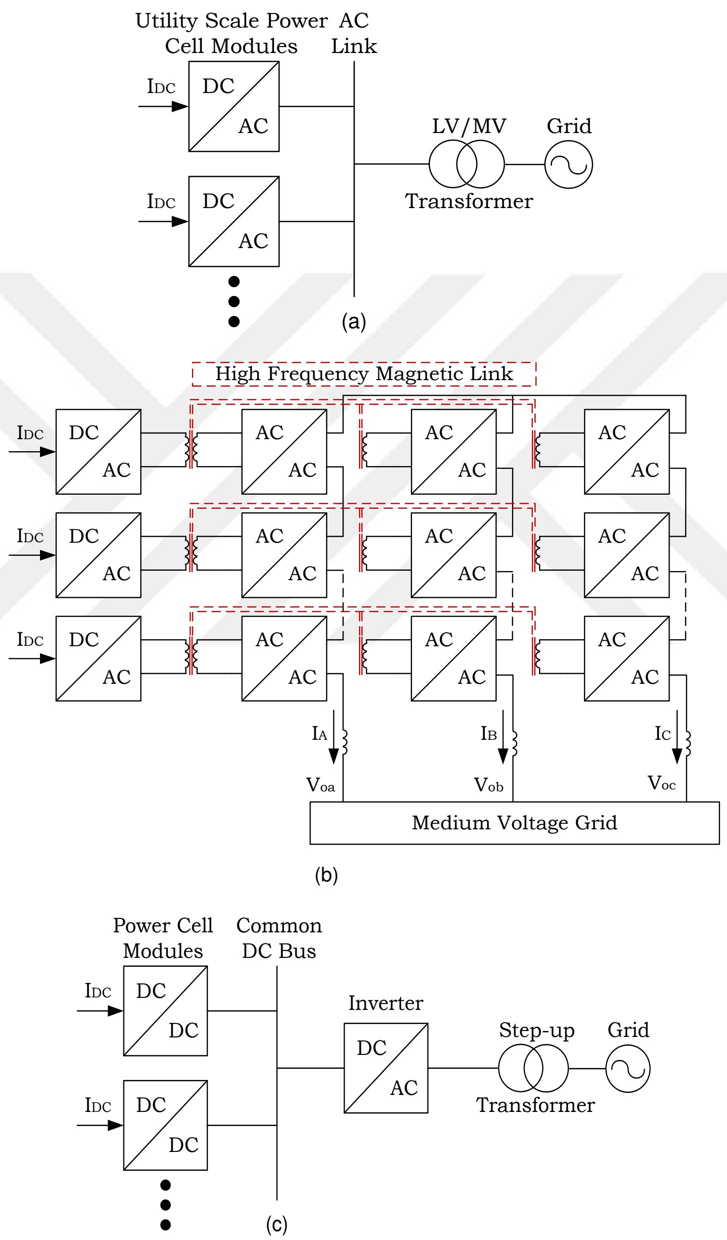

Figure 1.2. Classification of Grid connected Medium Voltage Power Systems

In recent years, efficient power transmission is very important for new proposed DC-DC and DC-AC converters in literature. Thus, especially comparison studies are very popular in order to show power loss effects. Reference (Zhang et al. 2018) compares power losses on switching elements and proposes new PV and BESS connected cell combination modular dc-dc converter for decreasing power losses and total cost. Some system topologies such as PDSR, PPSR, PDDS and PPDS combinations in category (b) demonstrates different efficiency results (Barrios et al. 2018). Additionally, reference (Choi et al. 2015) defines that SSIB converter topology increase the efficiency gradually than the other conventional type DC-DC converters for large scale PV applications in (c) category.

Therefore, in this thesis proposed HRPS is created by benefiting (c) type topologies. The proposed HRPS will be shown later and its components are introduced one by one. Each components are operated firstly. Then combination of these equipments are simulated according to 380 V AC grid connected 700 V DC link low voltage system. Additionally, different power flow scenarios are investigated and executed for all system after the individual operations. Then, proposed central energy management system is introduced with operation principle and it is operated with the proposed HRPS. Finally, efficiency results of the all system is calculated in order to show regenerative effect.

Moreover, different types of HRPSs are expressed by giving examples at different application areas such as photovoltaic power, wind power and hybrid electric vehicle systems.

Innovative ways of the proposed study can be arranged below;

1) In literature, there is not any regenerative power system study with central energy management system in low voltage applications for critical loads and it works like UPS with different power flow operations.

2) Grid voltage is 10 kW, 380 V and it is combined to 700 V DC-link with 2-level inverter with LCL filter for mitigating current harmonics.
3) Totally, 3.6 kW, 14 batteries connected IBDC topology operates with DPS + Soft Switching + ZVS and ZCS.
4) Totally, 10.2 kW, 48 PV panels are connected to Unidirectional Isolated DC-DC Converter topology and it is operated with Perturb and Observe (P&O) Maximum Power Point Tracking (MPPT) technique.
5) All of the DC-DC converters are controlled by phase-shift algorithm.
6) 2 Level inverter operates bidirectionally with Phase Locked Loop (PLL) algorithm and it feeds AC load even though without grid.
7) A new battery package will be designed for suitable low voltage power system by using CC-CV charging controller and discharge current controller methods.
8) A new high level central Energy Management System (EMS) controller which measures the power flows between all of the equipments, will be created by using novel rule-based algorithm for operating the all system automatically.
9) Results of the proposed HRPS topology with EMS are covered in its entirety and these results are used for emphasising the efficiency of regenerative effect by calculations of electricity prices at commercial and residential areas.

2. LITERATURE REVIEW

In this chapter, literature review of Regenerative Power Systems (RPSs) or PV-Storage Systems are explained firstly. Then, literature review of Energy Management Systems (EMSs) are defined. The most important and present studies are given in these topics.

2.1. Literature Review of Regenerative Power Systems

Conventional type of Regenerative Power System (RPS) is represented with solar and wind energy in (Chiang et al. 2010) and its topology is shown in Figure-2.1. In this study, different scenerios are investigated and power flows demonstrated between the equipments. But this study is not very effective in terms of feasibility because of using simple control methods. It will be better to illustrate this with an example, adaptive MPPT (Maximum Power Point Tracking) controller is used in proposed PV system and simple PWM controllers are used in converters for low voltage (1200V) experimental system. This operation do not show the better results in high voltage systems. Thus, modified Partical Swarm Optimization (PSO) based MPPT controller will be used in PV system for obtaining high efficiency results in high voltage RPS. In this way, effects of partial shading will be investigated for 500kW high voltage system for approaching reality. Moreover, previous studies show that phase-shift (PS) controllers are more suitable than conventional PWM method for converters. Bidirectional DC-DC (BDC), unidirectional DC-DC (UDC) or AC-DC and DC-AC converters can operate effectively when they are used with PS controllers.

In this system, 150W, 4 PV panels and 12V, 4A, 10 batteries are used in 60 Hz. These equipments are located to different arms of secondary side of the 3 arm rectifier-inverter. Furthermore, 3 different scenarios are investigated and transitional stages are shown with current, voltage and power graphics. But these transitional stages are not operated automatically because of lacking high level controller. Apart from all these cases, if the proposed system uses modular multilevel inverter at the load side, it will work better than the old system according to demand of the load and partial shading effects. To sum up, this study brings an effective solution for only low voltage renewable energy applications.

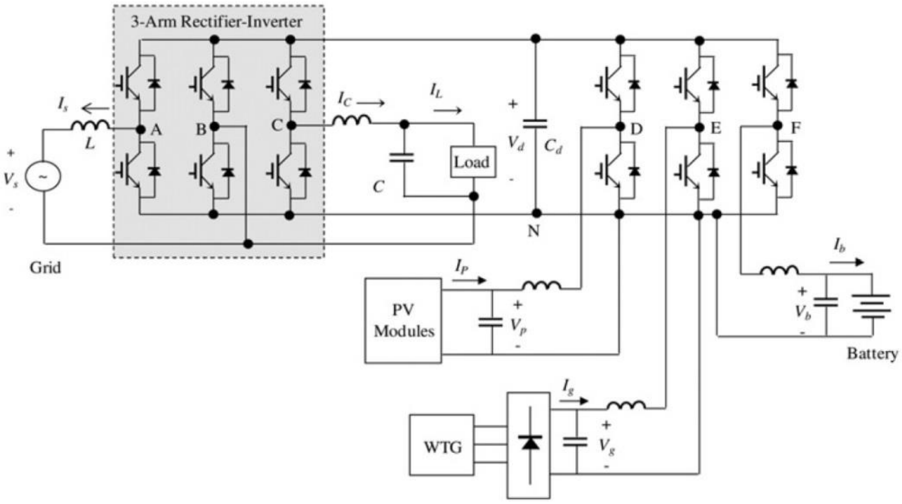

Figure 2.1. Proposed Block Diagram of Reference (Chiang et al. 2010).

Additionally, (Lamb et al. 2017) use grid connected cascaded H-bridge multilevel converter for regenerative power flow by investigating pq plane analysis. This can be an example of one of the regenerative circuit topologies. Also, (Bauman et al. 2011) designs regenerative snubber for DC-DC boost converter. Moreover, there are some regenerative circuit topologies with using LCL filter in literature (Liserre et al. 2004) and (Swamy 2018).

In recent years, RPS is used in electric vehicle (EV) applications because of practical feasibility. In literature, lots of RPS studies can be found about EV applications. But when these similar RPSs are used in high voltage renewable energy systems, they give effective results for industrial, commercial and residental applications. It should not be forgotten that efficient production is only possible from nature. Thus, as it is similar to this high voltage RPS, it is necessary to give a few examples from EV applications.

In reference (Zulauf et al. 2015) uses battery packs, bidirectional DC-DC converter and inverter for conserving grid energy, reducing test system cost and space requirements. The proposed topology is shown in Figure 2.2.

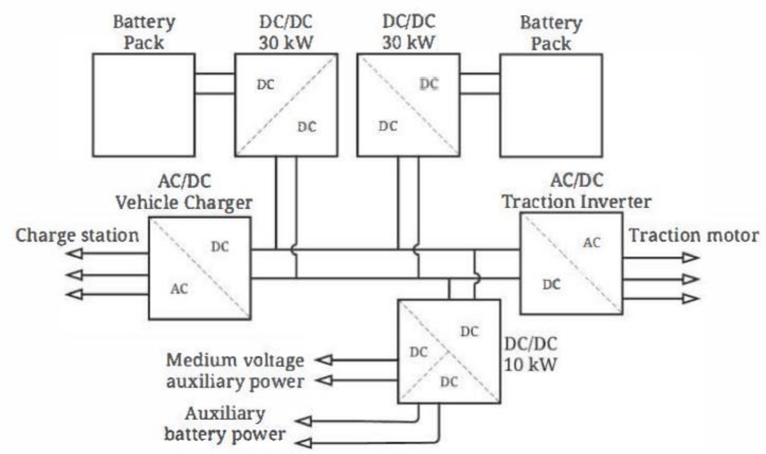

Figure 2.2. Proposed block diagram in Reference (Zulauf et al. 2015).

A common dc link is used for charging or recharging for batteries and traction inverter is used for operating traction motor. These units provide significant power savings for facilities and a 30 kW converter will require a 30 kW electronic load and a 30 kW power supply in test system. Additionally, Adaptive Power Converter (APC) and Auxiliary Power Unit (APU) are used for converting DC voltages.

The adaptive power converter (APC) is a 30 kW, 0-1000 V, fully bidirectional, interleaved three-phase DC/DC converter and this converter is shown in Figure 2.3.

The auxiliary power converter, or APU, is also used in this study. It is 10 kW, and it has two output busses, one designed for medium voltage accessories in the 200-400 V DC range (*Vout,mv*) and one designed specifically to recharge the 12 V vehicle auxiliary battery (*Vout,12v*). This converter is shown in Figure 2.4. and 2.5.

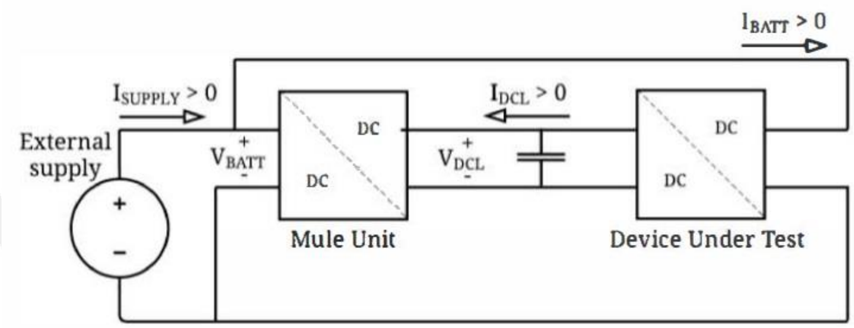

Figure 2.3. Simplified APC test setup schematic. Both DC/DC converters shown are APCs in this implementation of the regenerative test setup in Reference (Zulauf et al. 2015).

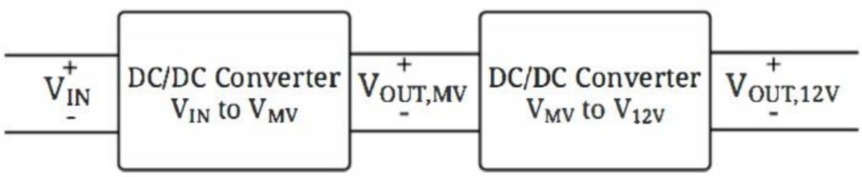

Figure 2.4. Auxiliary Power Unit (APU) Shematic in Reference (Zulauf et al. 2015).

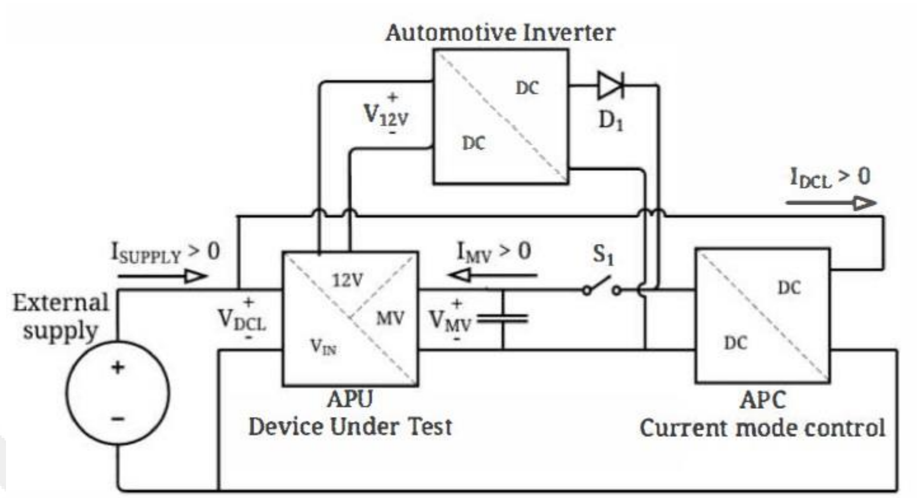

Figure 2.5. APU test setup simplified schematic. The switch is open for 12 V regenerative testing and closed for medium-voltage regenerative testing in Reference (Zulauf et al. 2015).

In Figure-2.5, S1 and D1 protect the inverter from high voltage values during the normal operation. During the medium-voltage test, when S1 is closed and Dl operates at reverse blocking mode, protecting the inverter. During the 12 V test, S1 is open and Dl conducts in forward mode.

Reference (Del Moral et. al. 2015) is according to improve performance of the buck converter in regenerative power system (RPS). RPS is used in HEV to support FC to provide more energy in this system. In addition, the dynamic performance of the converter in accordance with the load demands is very important and Figure 2.6. demonstrates the block diagram of the proposed system.

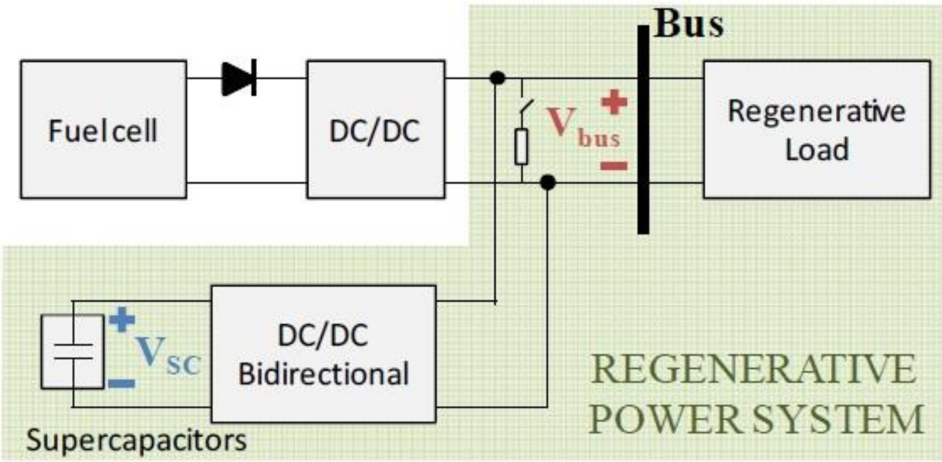

Figure 2.6. Block diagram of HEV Power System in Reference (Del Moral et. al. 2015)

In reference (Itani et al. 2016) presents the regenerative braking design control and simulation of a hybrid energy storage system (HESS) for an electric vehicle (EV). The EV is operated by two 30 kW permanent magnet synchronous motors. The HESS contains a Li-Ion battery and an Ultra-Capacitor (UC) sources.

Between several configurations (Cao et al. 2012), they used a bi-directional 3-Level DC/DC converter interfacing the UC, lowering the UC voltage with respect to the DC bus voltage enabling the UC voltage to be used over a wide range. Logical circuit controls the IGBT switch located downstream the braking resistor. It will permit the switching between the Ultra-capacitor and the battery in braking mode (Figure 2.7.).

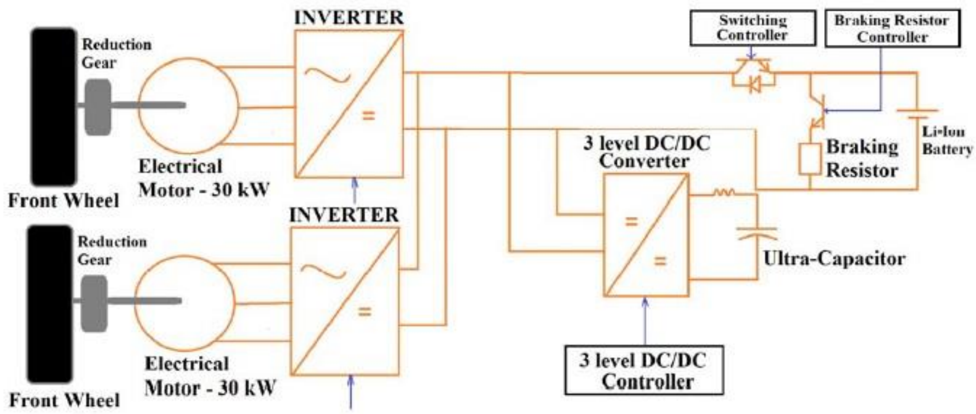

Figure 2.7. Block diagram of the proposed topology in Reference (Itani et al. 2016).

Moreover, (Tehrani et al. 2018) studies about electrical motorcycles, (Xu et al. 2019) and (Zhang et al. 2021) investigates the regenerative power flow effect on HEVs' regenerative braking system and motor driver systems on EVs respectively.

In addition, especially in 2015 and later, there are lots of studies on regenerative power flow in the literature, these papers about electrical railway systems for high speed trains (Kumagai et al. 2015; Hayashiya et al. 2017; Hayashiya et al. 2019; Cui et al. 2019; Chengpeng et al. 2020; Yu et al. 2020 and Krim et al. 2020). Also, there are other studies about aircrafts and illumination systems for examining regenerative power flow respectively (Heinrich et al. 2015) and (Veerappan et al. 2014).

Eventhough, it can be given lots of examples about literature survey of RPS at EV and other transportation facilities applications, it should be given large scale photovoltaic (PV) applications. Because these above papers are not relevant with PV systems exceptional (Chengpeng et al. 2020). This thesis work is related to adaptation of RPS to medium and large scale PV systems. Thus, literature survey part should be continued with large scale PV systems and their equipment design.

It is possible to say that lots of PV systems according to different types of converters and their control methods can be found, although it is not hardly ever found regenerative types of these systems in literature.

Large scale PV systems and their high-gain multilevel or multiphase DC-DC converter topologies are studied in (Choi et al. 2012a; Choi et al. 2012b; Zhao et al. 2012; Agamy et al. 2012). Additionally, these topologies used Maximum Power Point Tracking (MPPT) method for obtaining maximum efficiency. But in literature, Partical Swarm Optimization based MPPT method gives higher performance than simple MPPT method. Thus, if it is used PSO based MPPT for PV panels, it will give high efficiency results.

Moreover, cascaded multilevel H-bridge isolated DC-DC converter is suitable for adjusting output voltage and transferring output power to load unit. In this way, the approprate DC-DC converter topology is proposed in reference (Zhao et al. 2012) that is shown in Figure 2.8.

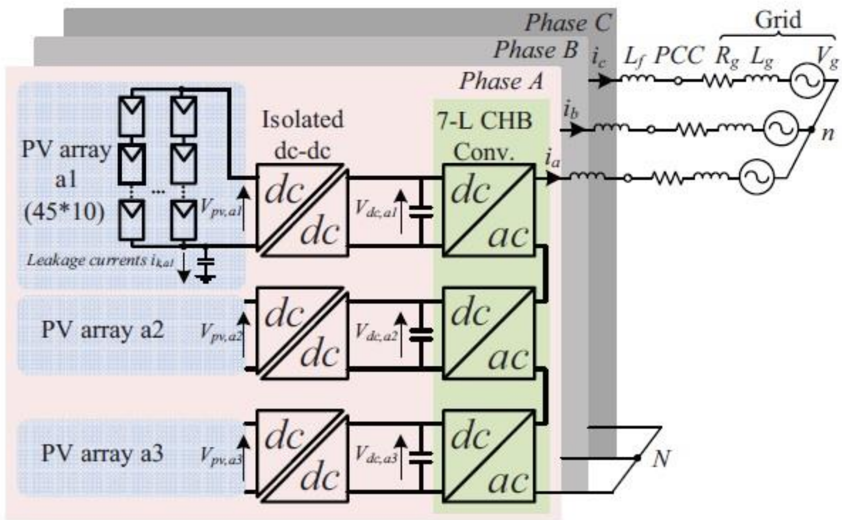

Figure 2.8. Proposed system configuration of the CHB multilevel converter integrating large-scale PV featuring the isolated DC-DC stage in reference (Zhao et al. 2012).

7 level DC-AC inverter topology is series connected to 7 level DC-DC converter topology and this configuration is valid for each phases while tranferring to grid or load unit. Also, single phase-shifted PWM method is used for triggering signals of IGBTs.

Generally, large scale PV systems are medium watt levels. But, if it does not give high efficiency results, it can be established low power levels by using a few PV panels. That is to say, while simple design architecture is used for low voltage systems, complex design architectures can be useful for large-scale PV systems and these systems are summarized in (Choi et al. 2012a).

1 MW PV system is simulated for Figure 2.9 (c) topology in MATLAB and conventional MPPT method, PI for dc voltage controller and reactive power controller. Additionally, dq transformation are used in order to obtain gate signals in this paper as it is shown in Figure-2.10. Controllers will be detaily told and calculations will be given for each component at other sections.

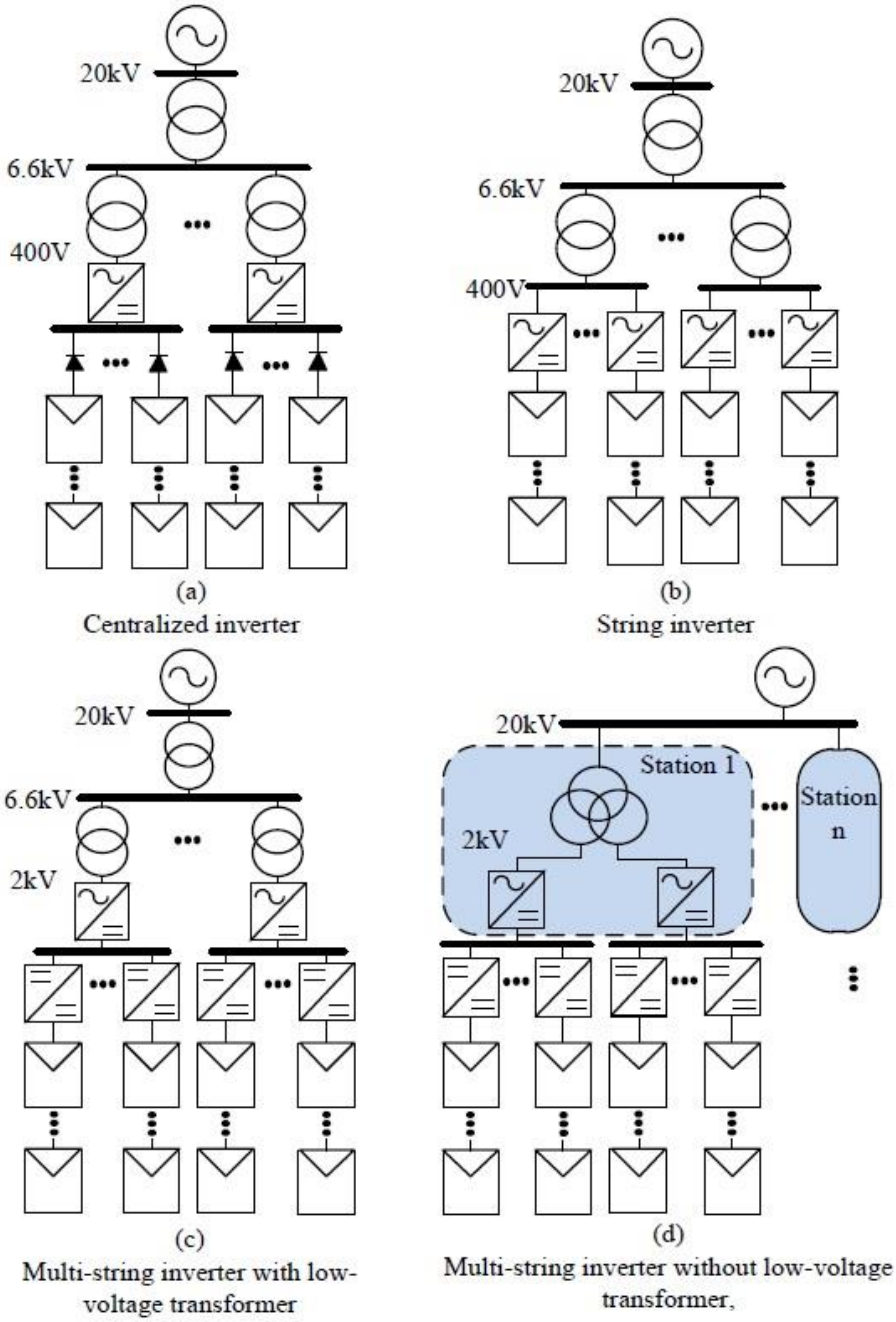

Figure 2.9. Large Scale PV System Architectures in (Choi et al. 2012a).

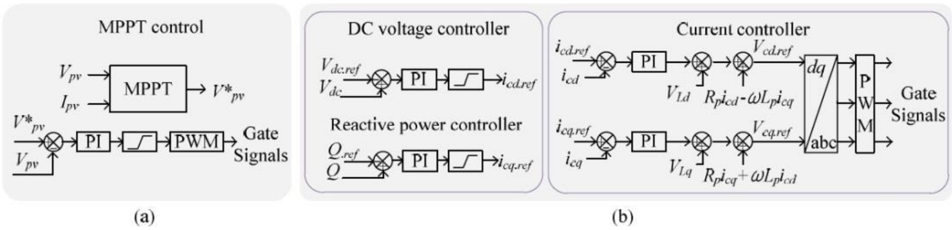

Figure 2.10. Control diagram of the proposed PV system in (Choi et al. 2012a). a) control of the DC/DC converter b) control of the VSC.

The control diagram of the proposed PV system based on the high gain DC/DC converter is shown in Figure 2.10. and it consists of two control blocks controlling the DC/DC converter and the VSC.

The DC/DC converter maintains the DC voltage of the PV array at the Maximum Power Point (MPP) using an MPPT based on the incremental conductance method (Figure 2.10. (a)). The incremental conductance method adjusts the PV array terminal voltage to MPP voltage by measuring the incremental and instantaneous array conductance (dI/dV and I/V, respectively) (Esram et al. 2007). The classical synchronous reference frame technique has been used to control the VSC (Kazmierkowski et al. 2002). The currents on the dq axis are controlled using standard PI controllers. The DC voltage controller presented in Figure 2.10. (b) maintains the output voltage of the DC/DC converter at the required level for the operation of the VSC. The reactive power is regulated using a PI controller.

These multilevel converter topologies can achieve high voltage operation and make it possible to connect to medium and high-voltage electricity grids using low ratio transformers. Moreover these converter topologies offer improved power quality, such as low current and voltage THD and smaller dv/dt. Among multilevel topologies, cascaded H-bridge (CHB) converter proves to be of interest for PV applications (Daher et al. 2008; Alonso et al 2003; Villanueva). H-bridges fitted with PV arrays act as isolated DC sources, making possible the independent voltage control and individual maximum power point tracking (MPPT) and enabling great flexibility in system expansion. Furthermore, the inherent improved power quality of multilevel converter allows lower switching frequency and thus smaller size of filters, leading to higher system's total efficiency. In spite of all these advantages, the CHB topology has a major drawback when associated with PV applications, which is the leakage currents issue caused by the stray capacitances between the PV panels and the earth and thus can damage the panels and/or pose safety problems (Calais et al. 1999). In (Rivera et al. 2011), a flyback converter was considered for the large-scale PV grid integration with the CHB converter to avoid hazard condition caused by leakage current issue. However, despite its simplicity, the flyback converter is typically used for low power ratings (Sangsun et al. 2002).

By using isolated DC/DC converters, the major issue regarding the leakage current can be overcome. Providing galvanic isolation between the PV panels and the CHB converter, the leakage current problem and the safety concern are completely removed from proposed topology in (Choi et al. 2012b) and demonstrated in Figure 2.11. and 2.12.

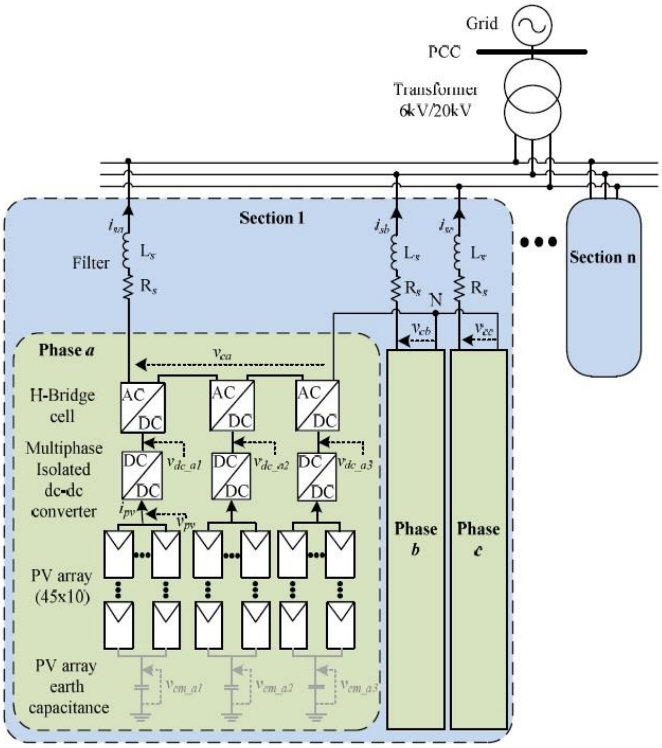

Figure 2.3. General structure of large-scale PV system with proposed topology according to (Choi et al. 2012b).

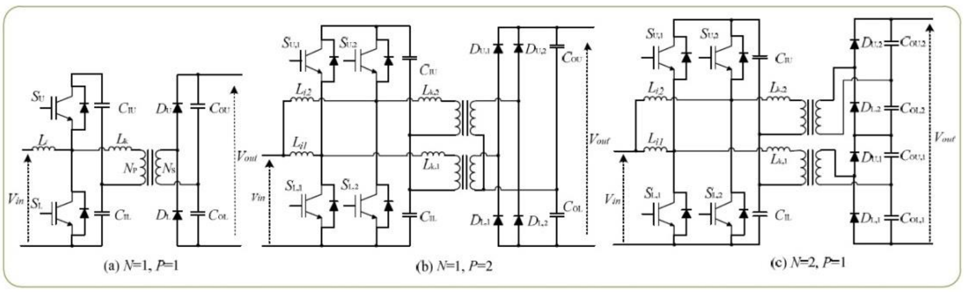

Figure 2.4. Multiphase isolated DC/DC converter; basic cell and examples of multiphase configurations in (Choi et al. 2012b)

The multiphase isolated DC/DC converter implemented in this study was introduced in (Yoon et al. 2011). The converter has advantages such as zero voltage switching (ZVS) of switches, zero current switching (ZCS) of diodes, and low input current ripple. When comparing to the standard flyback topology, which is the simplest and most common isolated DC/DC converter type, the main advantage of this converter is its higher power rating which can be achieved by using the multiphase configuration.

Besides all these examples about large scale PV systems, partial shading investigation is studied in (Katerchi et al. 2014). Partial shading applications are important for obtaining maximum efficiency from the PV system. In this study, each 200KW PV panels are connected to one Voltage Source Inverter (VSI) with LCL filter and AC grid at 1MW power. Also, Voltage Oriented Control and conventional MPPT method are used in this paper. Control sheme of this grid connected topology is shown in Figure 2.13.

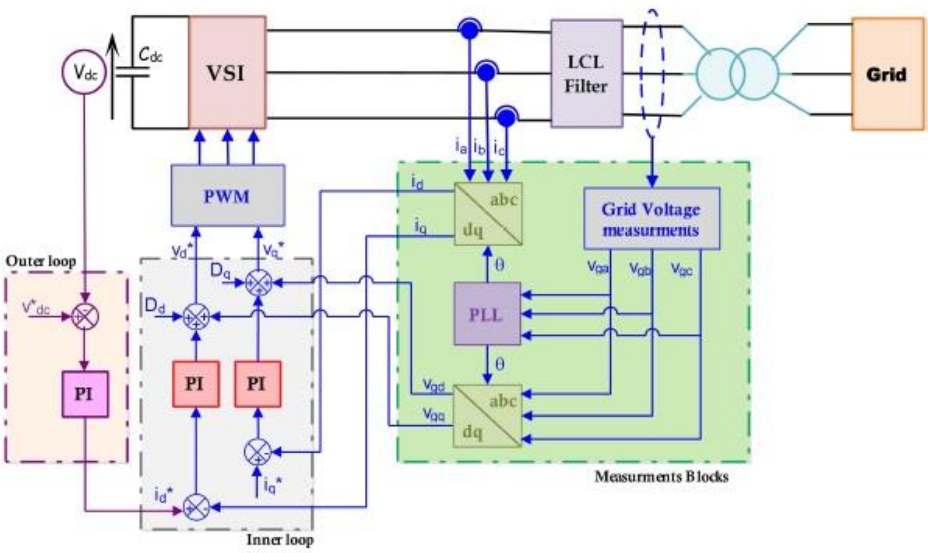

Figure 2.5. VOC control for the VSI in (Katerchi et al. 2014).

Simulation results are taken at standard weather conditions. (STC: G=1000W/m2, T=25ºC). Also it is composed of 1001 modules of 200 kW connected in series parallel configuration (Ns = 13;Np = 77).

The first case, Figure 2.14.(a), consider a shading of a string in a 200 kW sub-array, i.e. 1.3% of used modules; the shading of few modules has no important impact on the system. While the second case, Figure 2.14.(b), presents a shading for three groups disposed as following: G1 (13x2); G2 (6x3); G3 (3x2).

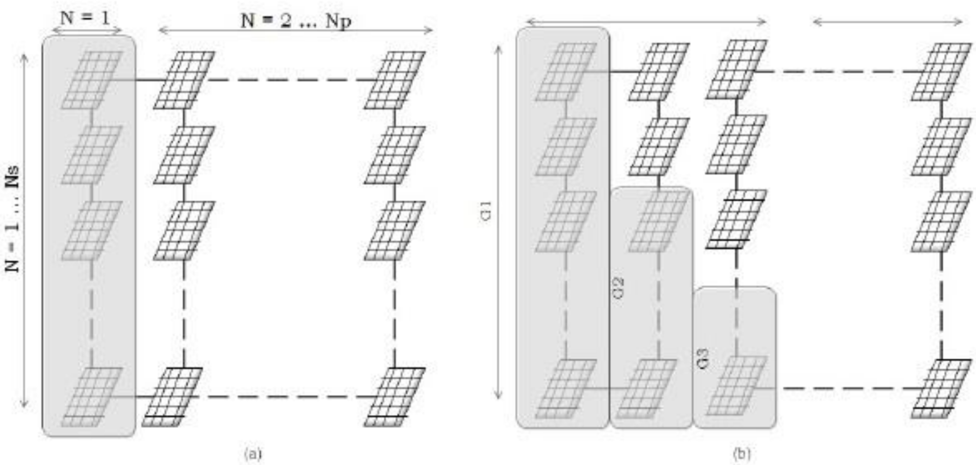

Figure 2.6. Shading Test (Katerchi et al. 2014).

Figure 2.15. shows the output characteristics of the shaded system. The number of shaded modules is equal to 50; i.e. 5% of the total number of modules used in the sub-array. As a result, the power generated by the shaded sub-array is equal to 190 kW. Since string modules are not equally illuminated, they are short-circuited through bypass diode, then the output voltage of the sub-array drops when shading is introduced in the simulation at the instant t=2s and the current is kept constant.

The DC link voltage is well maintained equal to its reference despite the PV voltage decrease and this is due to the conventional MPPT control implemented in the boost converter.

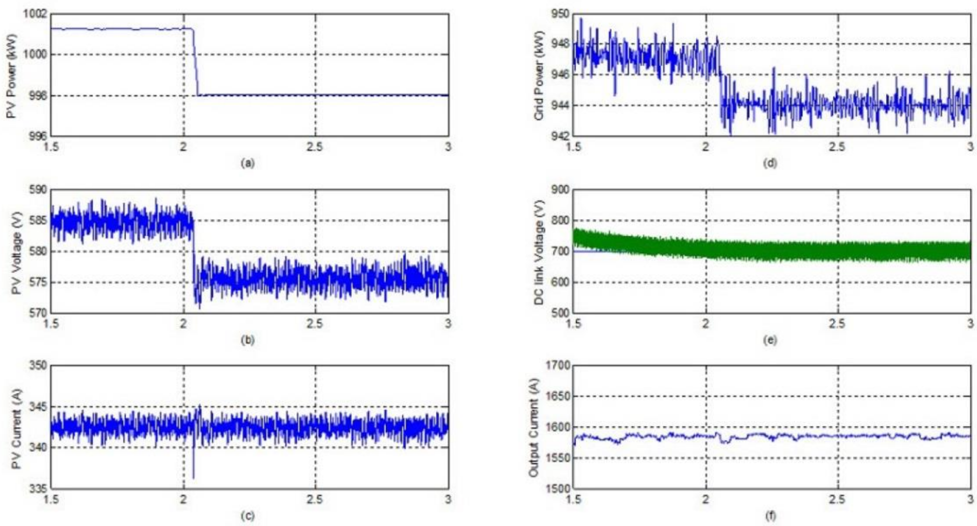

Figure 2.7. System Characteristic under Shading in (Katerchi et al. 2014).

2.2. Literature Review of Energy Management Systems

In recent years, energy efficiency studies and more environmentally friendly renewable energy systems have gained importance due to the decreasing fossil fuel power systems and their harmful effects on the environment. For this reason, various types of Energy Management Systems (EMSs) are created so that renewable energy systems can work together with high efficiency. These EMSs should be created properly according to the their power systems. Only in this way healthy power flows can be established between the power system equipments. Additionally, these EMSs are used with various topologies such as EVs, smart home systems, larger or smaller solar PV, batteries, wind turbines and grid connected power systems. There are various restrictions perform EMSs in these different topological structures. They are demand response, capacity of Energy Storage System (ESS), reliability, energy balance, reactive power support, high cost, capacities of renewable and conventional energy sources. In this section, rather than in which areas EMSs are used, how they work and their types are mentioned. When we look at the literature, the most common used type of EMSs are the rule-based ones (Gangatharan et al. 2020, Peng et al. 2017, Zhang et al. 2016, Tabari et al. 2016, Tehrani et al. 2018, Merabet et al. 2016, Hong et al. 2019, Boynueğri et al. 2013, Venayagamoorthy et al. 2016, Madaci et al. 2016, Rani et al. 2013, Hassan et al. 2016, Pippia et al. 2020, Riffonneau et al. 2011, Sorour et al. 2021). These EMS studies use different optimization techniques to perform their power systems efficiently. However, some of them have some deficiencies such as incomplete creation of the EMS according to the proposed power system topology, lack of some power flow scenarios, lack of cost calculations and realistic design of irradiation and temperature spectrum graphics. These subtitles are detaily explained below. Especially advantages and disadvantages of these EMSs can be compared at Table-2.1.

In the literature, we can say that the general operating algorithms of EMSs depend on the power balance, the state of charge of the batteries and how they will work in the most efficient way, regardless of the temperature and radiation values. In order to increase efficiency, fuzzy-logic EMS systems are also used in various applications (Wu et al. 2015, Valencia et al. 2016, Nair et al. 2020, Sorour et al. 2021), based on the power balance in the system, since they are more difficult to model but more controllable in terms of operation. Thus, they complicate the design of the EMS. Moreover, some studies create a predictive controller for their systems. Predictive type controllers may vary according to usage areas. (Rana et. al. 2017) controls bidirectional voltage source converter and its predictive controller method is compared with conventional PI controller. (Lashab et al. 2018) used predictive controller in Maximum Power Point Tracking (MPPT) method for PV application. (Zhou et al. 2019) investigated the performance analysis of their predictive controller on hybrid batteries power system. Also predictive-based dynamic model EMS is studied by (Falahi et al. 2013) for distributed generators in distribution systems. Apart from these, stochastic optimal EMS is modelled and operated for smart homes with plug-in EV at (Wu et al. 2018).

As a result, in all EMS applications, it is aimed adaptation of the system to different situations and to have high efficiency. However, some studies in the EMS literature lack some aspects. Before mentioning these, it is necessary to look at the articles that make the EMS literature review (Bukar et al. 2020, Bryne et al. 2018 and Alam et al. 2019).

The proposed EMS in this thesis study is compared with the other EMS studies in the literature. Although the rule-based EMS algorithms in the literature are compatible with renewable energy systems, they are not very sufficient in terms of increasing efficiency. Because the limit values (voltage or power limits or reference values) in these algorithms are fixed and can be changed according to the characteristics (batteries total power, demand power of loads and PV or wind powers) of the power system, higher efficiency results can be seen. The limit values of the proposed EMS algorithm can be configurable or changeable by users. It allows better adaptation to the characteristics of the connected power system and operates more efficiently. The features in this power system are the parameters taken as reference or limit values in the EMS, such as the grid power, the total power produced from the PV panels or wind turbines, the maximum demand power of AC and DC loads and the total power of the batteries. This power balance should be analyzed very well for regenerative power systems and it should be operated with an appropriate EMS. Only in this way, savings can be achieved by increasing the regenerative effect.

We can collect some of the shortcomings of EMS studies in the literature under sub-titles;

Importance of power flow scenario number 1:

This power flow scenario represents power flow from grid to batteries and loads in the thesis. For example, in the EMS algorithm proposed in the study numbered (Sassi et al. 2017), it is stated that when the SoC is less than 40% and the power can not be transferred to the loads with renewable energy sources, there is no charge or discharge on the batteries. Not charging the batteries when their state of charge is low is a factor that reduces the regenerative effect and efficiency. If there is no problem in the grid, power can be drawn from the grid to charge the batteries and feed the loads. The power flow scenario 1 in the proposed EMS shows that this is happening. However, if there is a problem in the network, the power flow scenario number 7 can be used in this case to feed the loads.

Importance of power flow scenario number 7:

Power flow scenario 7 represents load feeding by batteries and PV panels without grid in this thesis. In the EMS algorithms of the studies (Hassan et al. 2016; Chakir et al. 2019), conditioning according to the power taken from the PV panels is higher or less than the power demanded by the critical loads cause a loss of efficiency in power systems. Since the maximum power demanded by the critical load is known, the load can be fed without power from the grid by using the batteries and PV panel systems. Therefore, in the designed EMS, even if the power of PV panels is low, that is, less than the critical load power, it should be able to feed the load with slightly charged batteries, as in the power flow scenario 7. This scenario provides to mitigate purchasing power from the grid. If the power in grid is interrupted or the harmonics are high, especially the power flow scenario 7 can be usable.

The importance of the topological structure to make a suitable EMS:

In the power system topology proposed in the study (Kebede et al. 2021), the ability of PV panels to transfer power by connecting to the batteries necessitates that the load can only be fed from the grid in case of a problem that may occur in the batteries. In other words, it is very difficult to make an efficient energy management system on the power system topology proposed in this study. For this reason, it is very dangerous for critical loads to design EMS in accordance with the topology suggested here.

In the study numbered (Hong et al. 2019), the batteries and PV panels were connected with an integrated converter in multi-port structure, and the transition to DC-Link and DC load was achieved. In the power topology proposed here, the transitions between the power flow scenarios described are not shown, and each scenario is run alone. However, the full performance of the designed converter could be demonstrated by switching between power flow scenarios by operating with the proposed energy management system.

Realistic design of radiation and temperature spectrum graphics:

In the study (Bouharchouche et al. 2013), the radiation graph was designed according to the daytime and the EMS does not consider the situations when PV panels power is less. The radiation and temperature graphics are prepared by using realistic data and also night operation status of the whole system was investigated in this thesis work.

Table-2.1. Advantage and Disadvantage Table of other popular EMS studies in literature

Authors	Aims	Energy Sources	Advantage	Disadvantage	Year
A. Elgammal et al.	Decreasing operational cost	PV, FC	Fast and efficient data flow	Complex computational time	2018
N. Anglani et al.	Reducing operating cost and supply power to critical load system	PV	SoC, life time and total cost are studied	Lack of operating times for proper planning	2017
M. Ban et al.	Develop the system resilience, reliability and cost	PV	High flexibility capabilities	Needs cost division	2019
M. Nasr et al.	Develop life time of batteries	Wind, PV	MPPTs are designed for PV panels and wind turbines together	Does not contain demand response	2019
M. Jafari et al.	Develop MG performance	PV, FC	Independently operation of islanded mode	Lack of dynamic response of proposed MG	2019

A. Sorour et al.	Decreasing energy cost and improving battery life time	PV	Comparing operational cost and SoH of the battery	Creating lots of rules are difficult	2021
U. R. Nair et al.	Improve utilization of renewable generation and operational efficiency	PV, FC	Develop autonomous islanded microgrid, increased utilization of PV Power	Creating lots of rules are difficult	2020
F. Valencia et al.	Investigate non-linear dynamic behavior	Wind	Comparison of operating costs between REMS and EMS	Increased operating cost and has complex calculations	2016
Shilei Lu et al.	Reducing operational cost of proposed system	PV	Defining solution for resource shortage	Explaining energy storage system	2018
C. Dou et al.	Mitigating operational cost and line losses at distribution system	Not defin ed	Emphasizing economic and environmental benefits	Has complex calculations	2013
Mousa Marzband et al.	Increasing efficiency and decreasing total cost	Wind, PV	Creating an algorithm for energy sharing between sources	Power losses are ignored	2013
C.A. Sepulveda Rangel et al.	Decreasing cost and power losses	Wind, PV	Decreasing reverse power flow at grid	Does not contain cost related to ESS	2017
L. Han et al.	Minimize energy cost	PV	Central control for decreasing energy cost	Has complex calculations	2019
Mousa Marzband et al.	Reducing system operational cost	Wind, PV	Effective using of ESS	Lack of Deformation cost of batteries	2016
A. Sassi et al.	Creating central EMS for homes	Wind, PV	Satisfy load demand and optimize batteries utilization	Inadequate power flow scenario number	2017
S.Z. Hassan et al.	Emphasizing dynamic performance of the system	PV	Shows stability and voltage regulation	Inadequate power flow scenario number	2016
A. Chakir et al.	Effective operation	PV	Minimize operational energy losses of a household	Inadequate power flow scenario number	2019

3. DESIGN AND MODELING OF PROPOSED HYBRID REGENERATIVE POWER SYSTEM

In this section, converters are modelled with 3 minor topics as grid connected inverter, batteries connected isolated full-bridge bidirectional DC-DC converter and PV panels connected isolated full-bridge unidirectional DC-DC converter. Additionally, modelling of grid connected inverter chapter includes LCL filter design and all of the controller types of the converters are explained in these minor topics.

In literature, there are lots of topologies about renewable energy applications and control methods as in the previous parts. In the light of these studies, it was targeted maximum efficiency and minimum components. Because, overall hybrid regenerative power system has a considerable complexity. Figure 3.1. is simple representation of all system. It demonstrates the proposed topology of grid combined hybrid regenerative power system with solar energy and energy management system. Figure 3.2. shows all equipments and connections each other belong to proposed all hybrid power system.

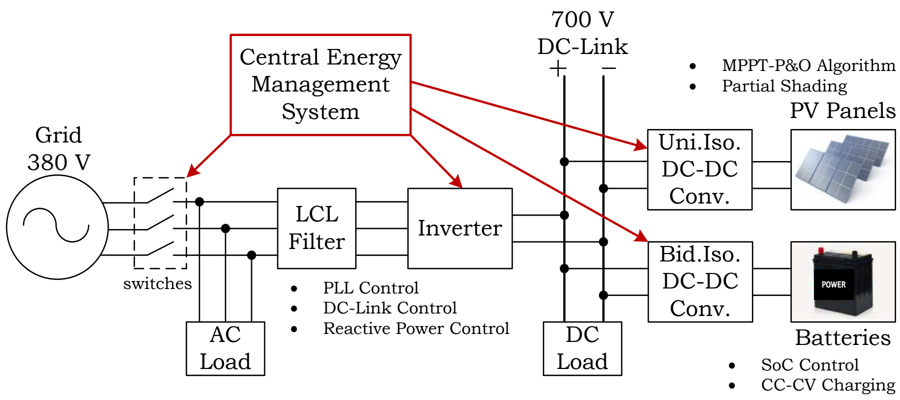

Figure 3.1. Simple Representation of Grid Combined Hybrid Regenerative Power System with Solar Energy and Energy Management System on the Proposed Components

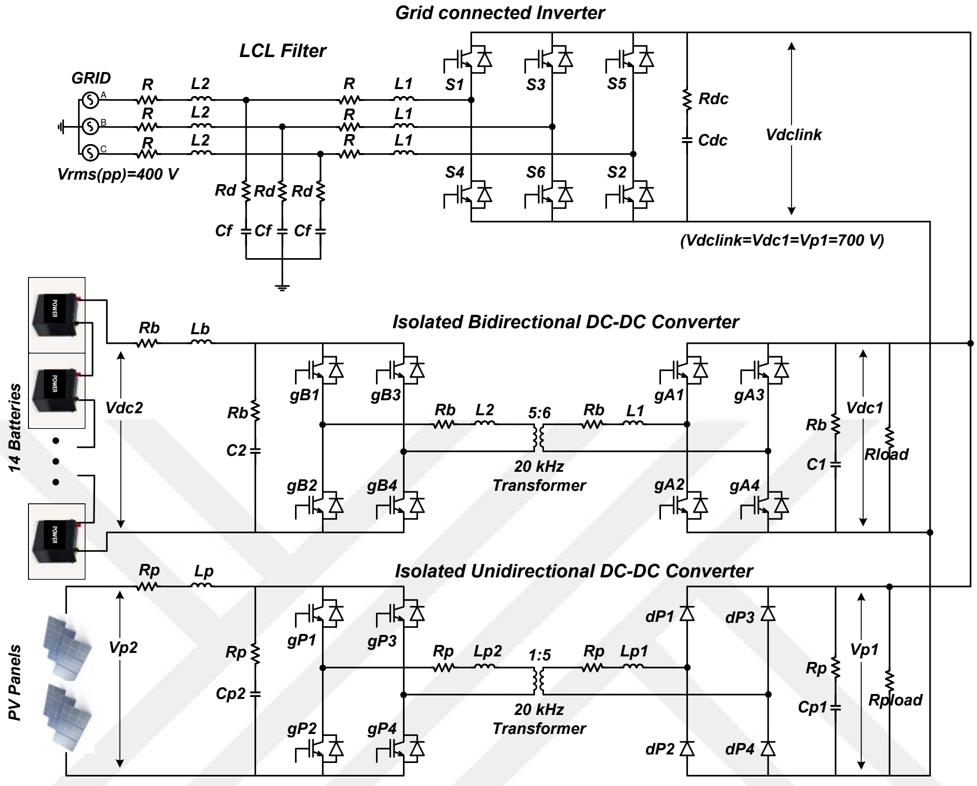

Figure 3.2. Proposed Grid Combined Hybrid Regenerative Power System with Solar Energy

3.1. Modeling of Grid Connected Inverter

In this study, grid connected 2-level inverter is modelled for connecting 700 V DC link voltage to 380 V AC grid voltage in MATLAB/SIMULINK. In literature, there are lots of inverter topologies that have lots of triggering signals such as (Okyere et al. 2006, Ahmed et al. 2013; Hang et al. 2017; Humayun et al. 2017a; Humayun et al. 2017b). But 5-level or more level Neutral Point Clamped (NPC) inverters are generally used at high power high voltage applications. These inverter topologies provide bidirectional power flow. In this way, it takes necessary power from grid and if the grid has more harmonics, it can transfer the power to grid and

AC load by using the produced voltage from batteries and PV panels. In this study, 2 level inverter is used because of the DC-Link voltage is 700 V and these inverter types are generally used at low power applications (Mnati et al. 2018; Wang et al. 2015; Krishna et al. 2015; Chandini et al. 2016; Vinod et al. 2016). Totally 6 IGBTs are used and each leg has 2 IGBTs at 2-level inverter. Moreover LCL filter circuit is connected to grid side of the inverter for mitigating fluctuations on the grid voltage waveform. Thus, measuring Total Harmonic Distortion (THD) is important for us.

First of all, control method of 2 level inverter and its circuit description with operation principles are defined at first chapter. Secondly, Phase Locked Loop (PLL) operation is explained for connecting inverter to grid with Clarke and Park transformations. Then LCL filter parameters are calculated for mitigating harmonics at the fifth chapter.

3.1.1. Circuit Description, Operation Principles And Control Methods Of 2-Level Grid Connected Inverter

Grid connected 2-level inverter is operated with grid to DC-Link voltage (Power Flow 1, PF1) and DC-Link voltage to grid (Power Flow 2, PF2) by using DC-Link voltage control method and reactive power control method respectively. But these control methods are necessary when the inverter connected to grid. Thus, firstly we should investigate the operation principle of the inverter alone and proposed inverter topology is shown at Figure 3.3.

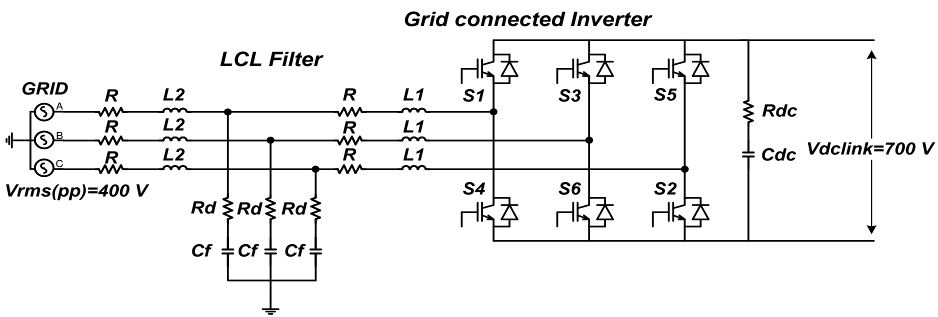

Figure 3.3. Proposed Grid connected 2-Level Inverter with LCL Filter

2-level inverter has simple control algorithm. It needs 3 sinusoidal waveforms that have 120 degrees between them which are produced output of PLL operation and 1 carrier signal in order to produce triggering signals. Sinusoidal signals has 50 Hz frequency and each sinus waveform should be compared with 5000 Hz carrier signal for each legs of the inverter. Fig. 3.4. shows the comparison of sinus-carrier signals for 3 legs of the inverter and total control algorithm is demonstrated with Simulink tool boxes. The result of this comparison, S1, S3 and S5 switches have different phases and these phases are changes during the process. Moreover, S4, S6 and S2 switches are opposite signals of S1, S3, S5 respectively. These signal waveforms are shown at simulation results section.

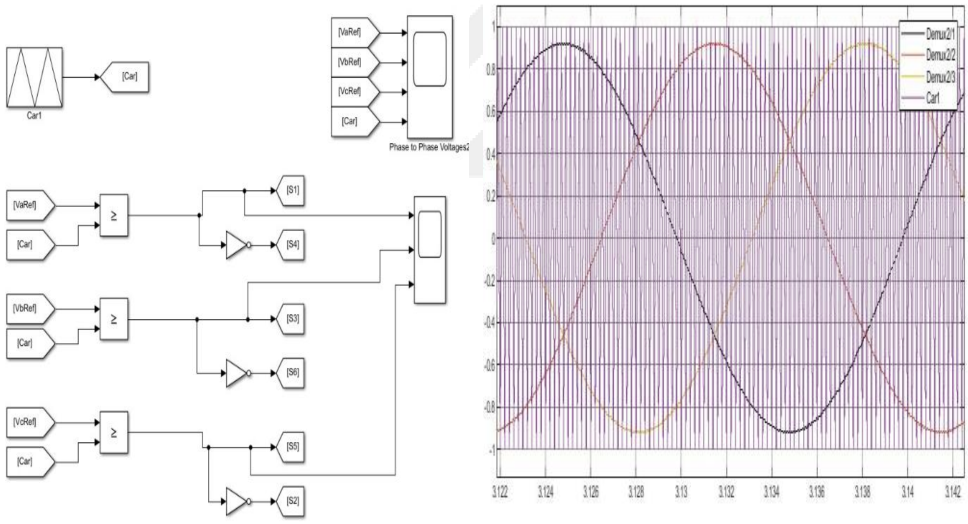

(a) (b)

Figure 3.4. Proposed Grid connected 2-Level Inverter switching signals control (a) Toolboxes (b) Graphic

3.1.2. Phase Locked Loop (PLL) Operation

Phase Locked Loop (PLL) is a feedback system combining a Voltage Controlled Oscillator (VCO) and a phase comparator so connected that the oscillator maintains a constant phase angle relative to a reference signal. Thus, it is necessary for increasing speed of the circuit. PLL can be used, for example, to generate stable output high frequency signals from a fixed low-frequency signal. But VCO can not produce stable high frequency carrier and VCO is affected by temperature and noise. We need a reference with stable frequency and we should force VCO to follow the reference. When VCO is connected reference oscillator, frequency of reference oscillator is stable, but VCO has unstable reference. Therefore, if we define reference oscillator is master and VCO is slave and connect a frequency divider feedback mechanism for decreasing output frequency to input side, output signal will have stable frequency. Additionally, low pass filter (LPF) should be connected between reference oscillator and VCO. If amplitude of frequency at LPF is low, frequency of VCO will be low or vice versa.

Briefly, PLL operation is shown at Fig. 3.5. with block diagrams, features of components are defined and its 3 states are explained below;

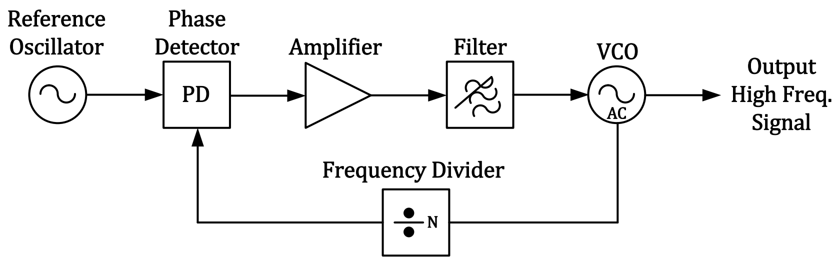

Figure 3.5. Block Diagram of PLL

Phase Detector:

- Compares input and output frequency
- The output of the phase detector is proportional to phase difference between input and feedback frequency

- Output of phase detector is DC or minumum frequency signal. Thus, it is reflected as the error voltage.

Filter:

- It removes high frequency noise
- It produces DC signal
- It can be active low pass filter or passive low pass filter.

VCO:

- It generates high frequency signal
- The instantaneous VCO frequency is controlled by its input voltage
- The frequency of VCO is directly controlled by DC input voltage.

PLL operation shows 3 states;

Free running:

- If no input voltage is applied, PLL operates free running state.

Capture:

- Once input voltage is applied, frequency of VCO starts to change and PLL is said to be capture mode and it is refered as “frequency pull in”.

Phase lock:

- When input frequency and freuency of VCO are equal, it is refered as phase lock state.

3.1.3. Clarke And Park Transformations

3.1.3.a. Clarke Transform (three phase to αβ transform)

Clarke transform is used for transforming three phase a, b, c lines to stationary α, β, 0 values. It provides converting the time-domain components of a three-phase system. Where, a, b and c are the components of the three-phase system in the abc reference frame. α and β are the components of the two-axis system in the stationary reference frame. 0 is the zero component of the two-axis system in the stationary reference frame. Fig. 3.6. shows the transformation according to the axis and mathematical expression is given below.

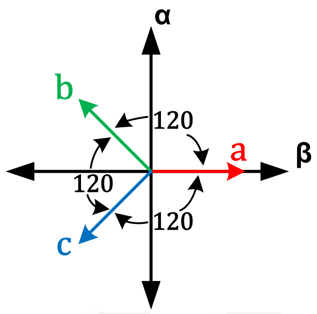

Figure 3.6. Clarke Transformation

$$\begin{bmatrix}\alpha\\ \beta\\ 0\end{bmatrix}=\frac{2}{3}\begin{bmatrix}1 & -\frac{1}{2} & -\frac{1}{2}\\ 0 & \frac{\sqrt{3}}{2} & -\frac{\sqrt{3}}{2}\\ \frac{1}{2} & \frac{1}{2} & \frac{1}{2}\end{bmatrix}\begin{bmatrix}a\\ b\\ c\end{bmatrix}$$

3.1.3.b. Park Transform (αβ to dq transform)

Park transform is used for transforming three phase a, b, c lines to stationary d, q, 0 values. It provides converting the time-domain components of a three-phase system. Where, a, b and c are the components of the three-phase system in the abc reference frame. d and q are the components of the two-axis system in the rotationary reference frame. 0 is the zero component of the two-axis system in the rotationary reference frame. Ɵ is the angle between a and q axis alignment or the angle between a and d axes for the d-axis alignment. ω is the rotational speed of the d-q reference frame Fig. 3.7. shows the transformation according to the axis and mathematical expression is given below. Additionally, mathematical expression of transformation is defined below for a q-axis alignment.

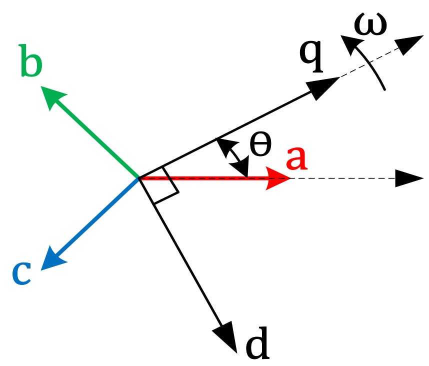

Figure 3.7. Park Transformation

$$\begin{bmatrix} d \\ q \\ 0 \end{bmatrix} = \frac{2}{3}\begin{bmatrix} \sin(\Theta) & \sin(\Theta - \frac{2\pi}{3}) & \sin(\Theta + \frac{2\pi}{3}) \\ \cos(\Theta) & \cos(\Theta - \frac{2\pi}{3}) & \cos(\Theta + \frac{2\pi}{3}) \\ \frac{1}{2} & \frac{1}{2} & \frac{1}{2} \end{bmatrix}\begin{bmatrix} a \\ b \\ c \end{bmatrix}$$

3.1.4. SRF-PLL Operation, Reactive Power And DC-Link Voltage Controllers

PLL is generally used in grid connected converter topologies for synchronizating to grid voltage and Synchronous Reference Frame – Phase Locked Loop (SRF-PLL) is commonly used three phase PLL in grid connected power converters. This technique estimates the frequency and phase of the grid voltage by using clarke and park transformations. Fig. 3.8. demonstrates SRF-PLL block diagram.

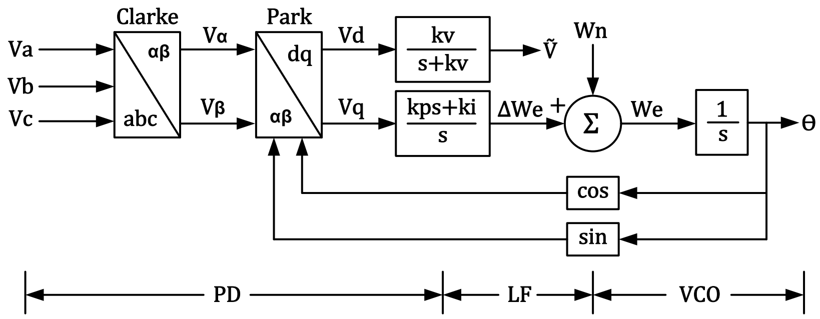

Figure 3.8. Block Diagram of SRF-PLL

In this figure;

PD, LF, VCO: Phase Detector, Loop Filter, Voltage Controlled Oscillator

Ṽ, We, Θ, Wn: Amplitude, Estimated Frequency, Phase Angle, Nominal Frequency

kp and ki: proportional and integral gains of LF

kv: cut off frequency of low pass filter used fort he amplitude estimation.

In this study, grid connected 2 level inverter is operated with SRF-PLL method and its MATLAB implementation is shown at Fig. 3.9.

Moreover, we should add reactive power control and DC-Link voltage control to the below SRF-PLL method. In this way, the system needs more PI controllers and defining *Kp-Ki* parameters. Fig. 3.10. and 3.11. demonstrate these control methods according to reactive power control and DC-Link voltage control respectively. Only we can change the power flow at Fig. 3.3. by using Fig. 3.11. instead of Fig. 3.10.(b) and Fig. 3.10.(c) while creating a DC-Link voltage control.

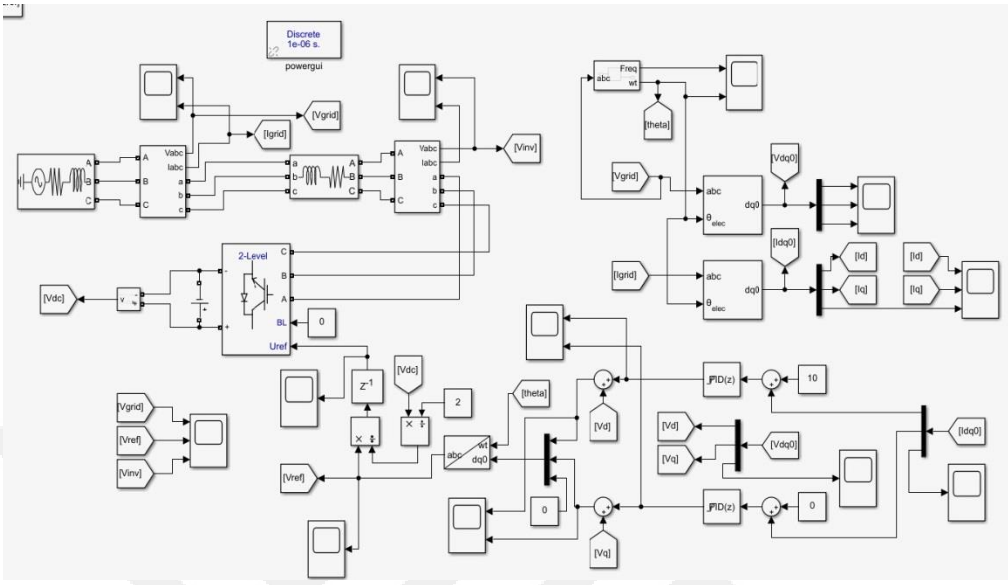

Figure 3.9. MATLAB Implementation of SRF-PLL

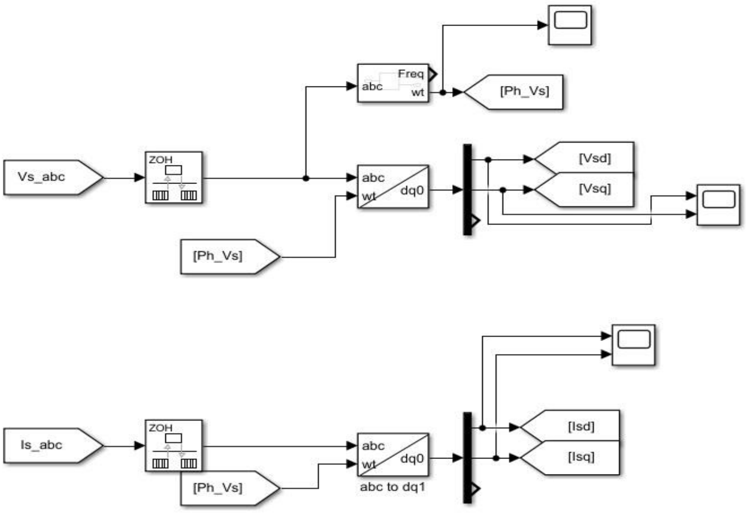

(a)

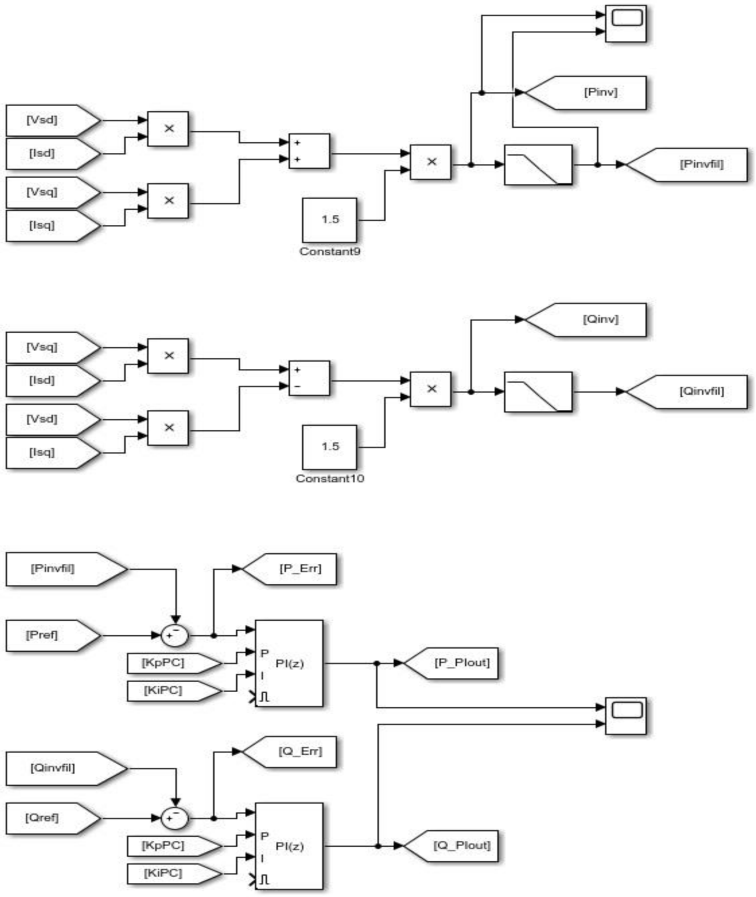
[Vsd]
[Isd]
[Vsq]
[Isq]
1.5
Constant9
[Pinv]
[Pinvfil]
[Vsq]
[Isd]
[Vsd]
[Isq]
1.5
Constant10
[Qinv]
[Qinvfil]
[Pinvfil]
[Pref]
[P_Err]
[KpPC]
[KiPC]
PI(z)
[P_PIout]
[Qinvfil]
[Qref]
[Q_Err]
[KpPC]
[KiPC]
PI(z)
[Q_PIout]

(b)

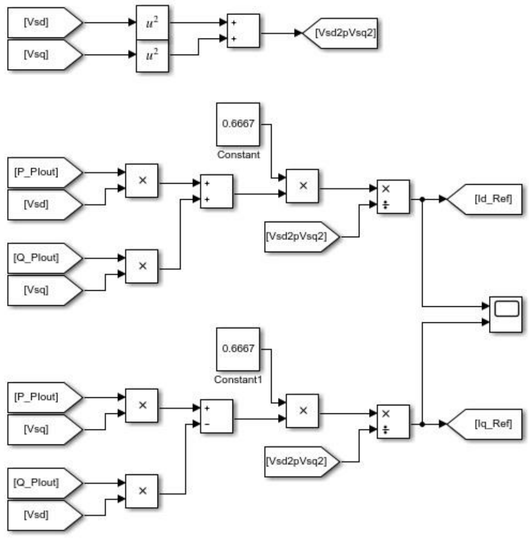

(c)

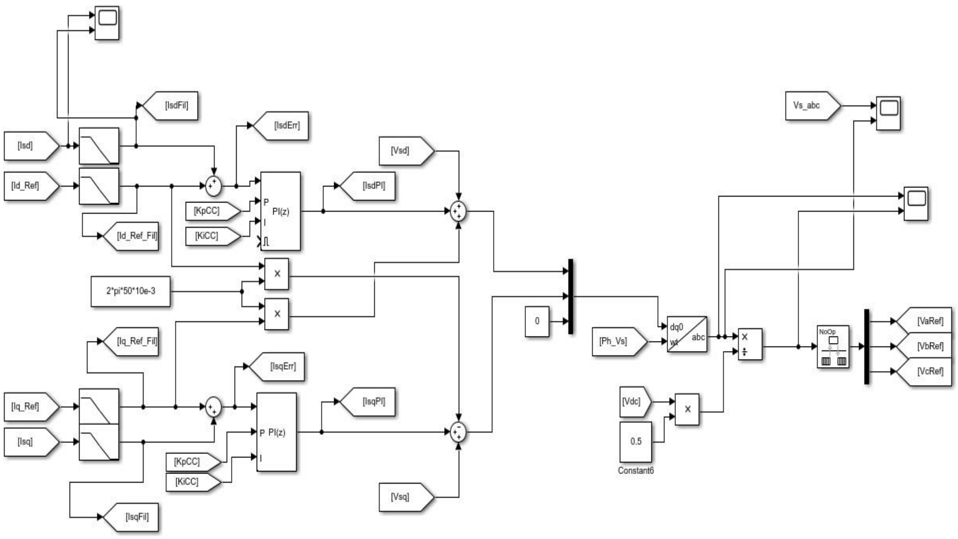

(d)

Figure 3.10. Reactive Power Control of Grid connected 2-Level Inverter

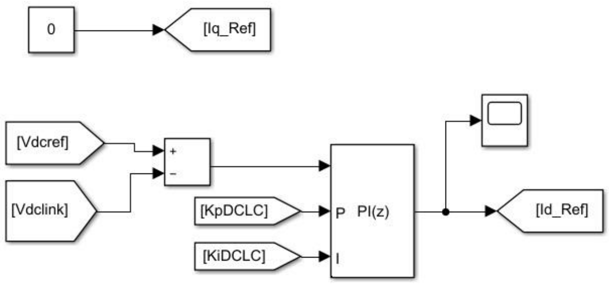

Figure 3.11. Changable part with Fig. 3.10.(b) and (c) for DC-Link Voltage Control

Firstly, voltage and current values are evaluated from grid side of the inverter and Vsd, Vsq, Isd and Isq values are obtained by using abc to dq transformation. After some mathematical calculations as Fig 3.10.(b), Pinv_fil and Qinv_fil are obtained. These 2 filtered powers can be evaluated with reference active and reactive powers with PI controllers. Then P_PIout and Q_PIout parameters are used as Fig. 3.10.(c) in order to obtain Id_Ref and Iq_Ref. After these operations Isd-Id_Ref and Isq-Iq_Ref are used in current control PI method. Thus, we use extra *Kp* and *Ki* parameters for current control. Finally, VaRef, VbRef and VcRef values can be usable for producing triggering signals of the inverter at reactive power control. In this way our inverter operates from DC-Link to grid (AC side).

When we use DC-Link voltage control method instead of reactive power control, our power flow should be grid to DC-Link voltage. Actually, they use similar controller but its Iq_Ref value is always “0 (zero)” and we can use the Fig. 3.3., PI based DC-Link voltage control instead of Fig. 3.10.(b) and Fig. 3.10.(c).

3.1.5. Design of LCL Filter for Grid Connected 2-Level Inverter

LCL filters are generally used for mitigating the harmonics at voltage waveforms on grid side of the inverters and these filters are investigated detaily by different authors in literature (Liserre et al. 2005; Wang et al. 2019; Sahoo et al. 2014; Reznik et al. 2014; Giacomini et al. 2017; Twining et al. 2003; Teoderescu et al. 2003; Karshenas et al. 2006). They are very effective than L and LC type filters at low power applications. Therefore, its parameters should be calculated correctly in order to obtain low THD values.

In this study, LCL parameters are calculated firstly with below equations and after the combination of filter and grid connected inverter, system parameters are shown at Table-2.

First of all, we should know the below parameters for designing LCL filter.

$E_n = 400\ V = V_{LL(rms)}$	$P_n = 10\ kW$	$f_g = 50\ Hz$
$V_{ph} = 400\ V/\sqrt{3} = 230.94\ V$	$V_{DC} = 700\ V$	$f_{sw} = 10\ kHz$

Base impedance can be calculated as (3.1);

$$Z_b = \frac{{E_n}^2}{P_n} = \frac{400^2}{10000} = 16 \tag{3.1}$$

Base capacitance can be calculated as (3.2);

$$C_b = \frac{1}{w_g Z_b} = \frac{1}{2 \times \pi \times 50 \times 16} = 198\ \mu F \tag{3.2}$$

And base inductance can be calculated as (3.3);

$$L_b = \frac{Z_b}{2\pi f_g} = \frac{16}{2 \times \pi \times 50} = 0.05\ H \tag{3.3}$$

%5 of reactive power absorbed, x=0.05. Then,

$$C_f = x\ C_b = 0.05 \times 198 \times 10^{-6} = 9.9\ \mu F \tag{3.4}$$

If C_b is equal to 1 pu, C_f will be 0.05 pu (%5).

In our LCL filter C_f capacitors are Y connected. But if they will be connected Δ type;

$$C_f/3 = 3.3\ \mu F$$

Then, maximum current ripple;

$$\Delta I_{Lmax} = \frac{2V_{DC}}{3L_1}(1-m)(m)T_{sw} = \frac{V_{DC}}{6 f_{sw} L_1}\ or\ \Delta I_{Lmax} = (0.1) \times I_{max} \tag{3.5}$$

L_1 is inverter side inductor and m is inverter modulation factor (typical m=0.1) at (3.5).

$$I_{max} = \frac{P_n\sqrt{2}}{3V_{ph}} = \frac{10000 \times \sqrt{2}}{3 \times (400/\sqrt{3})} = 20.412\,A \tag{3.6}$$

$$\Delta I_{Lmax} = (0.1) \times I_{max} = 2.041\,A$$

After calculation of maximum current I_{max}, L_1 can be calculated by using (3.7);

$$L_1 = \frac{3V_{DC}}{50 f_{sw} \Delta I_{Lmax}} = \frac{3 \times 700}{50 \times 10000 \times 2.041} = 2.057\,mH \tag{3.7}$$

If L_b is equal to 1 pu, L_1 will be 0.041 pu (%4.1).

Harmonic attenuation at the switching frequency, k_a is equal to (3.8);

$$\frac{i_g(h_{sw})}{i(h_{sw})} = k_a = \frac{1}{|1 + r(1 - a \cdot x)|} = \frac{1}{|1 + r(1 - L_1 \cdot C_b \cdot {w_{sw}}^2 \cdot x)|} \tag{3.8}$$

r is current ripple on the converter side and it is selected 0.1545 A at equation (3.8).

And, $a = [2.057 \times 10^{-3} \times 198 \times 10^{-6} \times (2 \times \pi \times 10000)^2] = 1607.9$

According to equation (3.8);

$$\frac{i_g(h_{sw})}{i(h_{sw})} = k_a = \frac{1}{|1 + 0.1545 \times (1 - 1607.9 \times 0.05)|} = 0.08876$$

For calculating grid side inductor "L_2";

$$L_2 = \frac{\sqrt{\frac{1}{{k_a}^2} + 1}}{C_f {w_{sw}}^2} = \frac{\sqrt{\frac{1}{{k_a}^2} + 1}}{C_f \times (2 \times \pi \times f_{sw})^2} = 0.3138\,mH \tag{3.9}$$

If L_b is equal to 1 pu, L_2 will be 0.006 pu (%0.6) and $r = L_2/L_1 = 0.1525\ validated.$

For the cut-off frequency;

$$f_{cutoff} = \frac{1}{\pi\sqrt{L_{total} C_f}} = \frac{1}{\pi\sqrt{(L_1 + L_2) C_f}} = 2078\,Hz \tag{3.10}$$

Resonance frequency "f_{res}" should be higher than 10 times of grid frequency and should be lower than half of the switching frequency. It can be calculated as equation (3.11);

$$w_{res} = 2\pi f_{res} = \sqrt{\frac{L_1 + L_2}{L_1 L_2 C_f}} = 19251.94 \; and \; f_{res} = 3064 \; Hz \tag{3.11}$$

$$\therefore It \; should \; be \; \left(10 \cdot f_g < f_{res} < 0.5 \cdot f_{sw}\right) \; and \; (500 < 3064 \; Hz < 5000) \; validated.$$

Then, equation (3.12) should be used for calculating damping resistances "R_d".

$$R_d = \frac{1}{3 w_{res} C_f} = 1.749 \; \Omega \; (Y - connection) \tag{3.12}$$

If damping resistances connection is Δ type, this result should be product with 3,

$$1.749 \times 3 = 5.246 \; \Omega \; (\Delta - connection)$$

In this way, these resistances can be calculated by using the impedance of the filter capacitor at resonance frequency with divided by 3. $R_d = X_c/3$

Moreover, we can calculate the *b* value in order to calculate *k* value.

$$b = \frac{1}{w_{sw}\sqrt{C_b L_2}} = 0.063 \tag{3.13}$$

Additionally, k value expresses how far the switching frequency that is calculated by equation (3.14).

$$k = b\sqrt{\frac{1 + r}{r \cdot x}} = 0.063 \cdot \sqrt{\frac{1 + 0.1545}{0.1545 \times 0.05}} = 0.77 \tag{3.14}$$

And equation (3.15) shows the power losses of damping resistors;

$$P_d = 3 \cdot R_d \cdot \sum_h \left[i(h) - i_g(h)\right]^2 = 47.25 \; W \tag{3.15}$$

Damping ratio of LCL filter; (f_r=f_{res} and f_s=f_g at equation (3.16))

$$\xi = \frac{\left[2\cos\left(2\pi \cdot \frac{f_r}{f_s}\right) - 1\right] \cdot 2\pi \cdot f_r \cdot L_1}{\sin\left(2\pi \cdot \frac{f_r}{f_s}\right)} = 76.146 \tag{3.16}$$

After these calculations, equivalent circuit, block diagram of LCL filter and its transfer function are shown below.

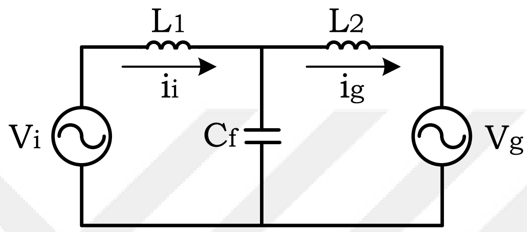

Figure 3.12. Equivalent circuit of LCL Filter

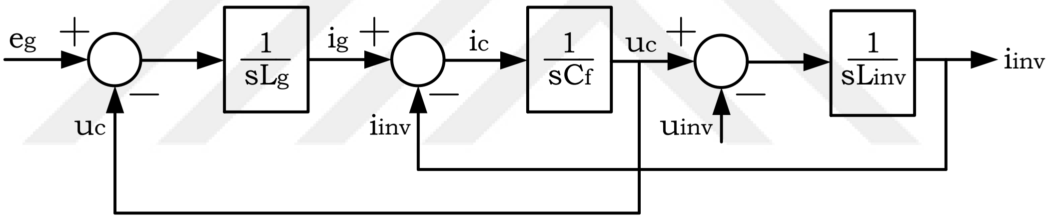

Figure 3.13. Block Diagram of LCL Filter (L_g=L_2 and L_{inv}=L_1)

For drawing bode diagram, transfer function of the designed LCL filter should be occured by the below calculations.

According to equivalent circuit of LCL filter at Fig. 3.12.;

$$TF_{LCL} = \frac{i_g(s)}{V_i(s)} = \frac{1}{sL_1 + \frac{sL_2/sC_f}{sL_2 + \frac{1}{sC_f}}} \times \frac{1/sC_f}{sL_2 + (1/sC_f)} \tag{3.17}$$

$$= \frac{1}{sL_1(1 + s^2L_2C_f) + sL_2} = \frac{1}{s^3L_1L_2C_f + s(L_1 + L_2)}$$

When found L_1, L_2 and C_f values are written in the above equation, transfer function of the proposed LCL filter will be;

$$TF_{LCL} = \frac{1}{6.39 \times 10^{-12}s^3 + 2.3708 \times 10^{-3}s}$$

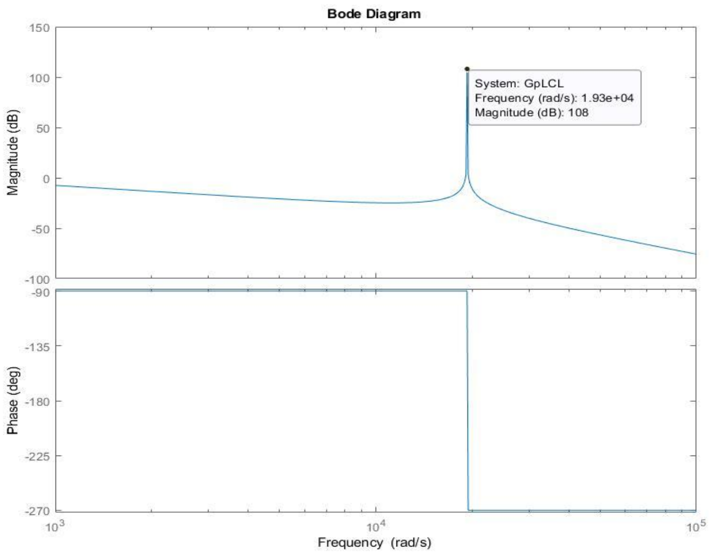

Figure 3.14. Bode Plot Diagram of The Proposed LCL Filter

When we look at the resonance frequency value of the graphic at Figure 3.14., it is shown $f_{res} = 1.93 \times 10^4\ rad/s$ and if the below relationship is used for transforming f_{res} from rad/s to Hz;

$$1\ Hz = 2\pi\ rad/s = 6.283\ rad/s$$

$$1\ rad/s = 1/2\pi\ Hz = 0.1592\ Hz$$

In this way, $1.93 \times 10^4 \times 0.1592 = 3072.56\ Hz\ (validated\ with\ eq. 3.11)$

Passive damping transfer function is also calculated with the below (3.18) formulla and its graphic is given at Fig. 3.15. and Fig. 3.16. shows bode plot of these two transfer functions together.

$$\frac{V_c(s)}{V_i(s)} = \frac{(sL_2)(1 + R_d C_f s)}{s(L_1 + L_2)(1 + R_d C_f s + L_p C_f s^2)}$$

$$L_p = L_1 \; is \; parallel \; with \; L_2 \tag{3.18}$$

$$\frac{V_c(s)}{V_i(s)} = \frac{s^2 L_2 R_d C_f + sL_2}{s^3\left(L_1 L_p C_f\right) + s^2\left(L_1 R_d C_f + L_2 R_d C_f\right) + s(L_1 + L_2)}$$

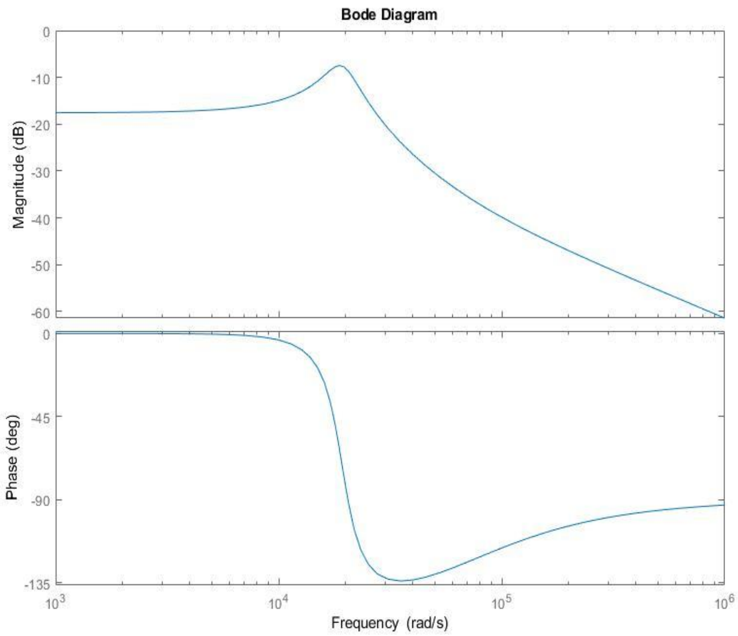

Figure 3.15. Passive damping transfer function graphic of proposed LCL filter

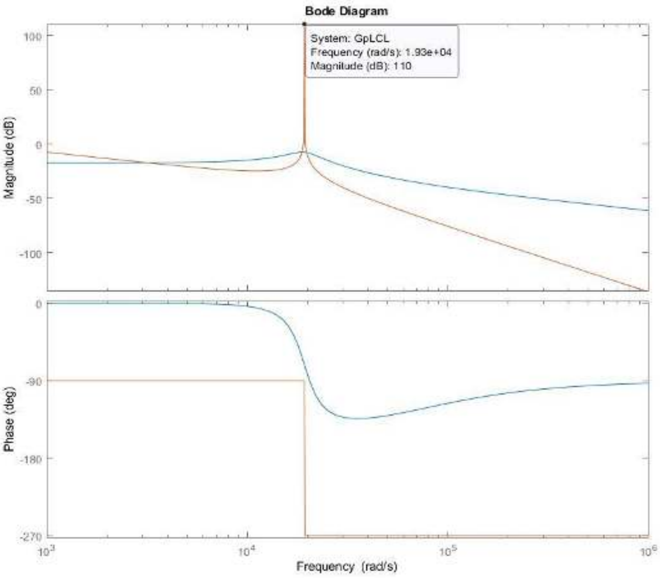

Figure 3.16. Bode Plot of Two Transfer Functions together

In addition to these, THD measurement values are included at the simulation and results section to show the effect of the proposed LCL filter.

Moreover, DC-Link capacitor of the grid connected 2-level inverter can be calculated by using the below equations (3.19, 3.20 and 3.21) respectively.

$$I_{phase} = 20\,A = \sqrt{2} \times I_{ph(rms)} \rightarrow I_{ph(rms)} = 14.142\,A \quad (3.19)$$

$$I_{cap(rms)} = I_{ph(rms)} \times \sqrt{\left[2M\left\{\frac{\sqrt{3}}{4\pi} + \left(\frac{\sqrt{3}}{\pi} - \frac{9M}{16}\right) cos\varphi^2\right\}\right]} \quad (3.20)$$

Firstly, $I_{ph(rms)}$ value should be found by using the I_{phase} current of the inverter (3.19) and I_{phase} is the begining stable value while the system is operated. Then $I_{cap(rms)}$ is calculated by equation (3.20). M is a modulation index and Φ is angle value that can change the ratio of $I_{cap(rms)}$ / $I_{ph(rms)}$. In this way, M=0.5 and Φ=45° are selected for finding the optimum $I_{cap(rms)}$.

When the above parameters are placed into equation (3.20), $I_{cap(rms)} = 7.387\ A$.

Then finally $C_{DC(min)}$ is calculated by equation (3.21) below.

$$C_{DC(\min)} = \frac{I_{cap(rms)}}{V_{ripple} \times 2\pi f_{sw}} = \frac{7.387\ A}{0.01 \times 2 \times \pi \times 10000} = 11.75\ mF \qquad (3.21)$$

Consequently, we can choose 2 times of the calculated C_{DC} for reducing DC-Link voltage ripples. Thus, we used 23.5 mF. All of the parameters are given at the below Table-3.1.

Table-3.1. Simulation Parameters of Proposed 2-level Grid connected Inverter with LCL Filter

DC-Link Voltage	V_{dclink}	700 V
Grid Voltage	$V_{rms(pp)}$	400 V
Inverter side Inductor	L_1	2.057 mH
Grid side Inductor	L_2	0.314 mH
Filter Capacitor	C_f	9.9 μF
DC-Link Capacitor	C_{dc}	23.5 mF
Damping Resistors	R_d	1.75 Ω
DC-Link Resistor	R_{dc}	0.001 Ω
Internal Resistors of Inductors	R	0.11 Ω
Grid Frequency	f_{grid}	50 Hz
Switching Frequency	f_{sw}	10 kHz
PI Parameters for Power Flow 1 (from DC-Link to Grid);	P_{ref}	-10 kW
	Q_{ref}	-1 kVAR
	Kp_{PC}	0.1
	Ki_{PC}	0.001
	Kp_{CC}	0.7
	Ki_{CC}	0.02

PI Parameters for Power Flow 2 (From Grid to DC-Link);	V_{dcref}	700 V
	Kp_{DCLC}	1.3
	Ki_{DCLC}	0
	Kp_{CC}	0.05
	Ki_{CC}	0

3.2. Modeling of Isolated Bidirectional DC-DC Converter for Batteries

Isolated Bidirectional DC-DC Converters (IBDCs) are generaly used for combining batteries and DC link voltages. In literature, there are different types of IBDC topologies to meet our needs. This topology can be changed input-output voltages and its powers. Thus, they can be 3 or 8 levels that are called modules and each module has same converter type. But, these topologies can be used for high power applications. Especially these papers used modular multilevel topology (Todorčević et al. 2013a; Todorčević et al. 2013b; Filsoof et al. 2013; Costa et al. 2013) and the modular multilevel topology is used for obtaining different voltage levels from output side of the converter. In fact, it can be easily executable by choosing buck or boost modes in order to control different voltage values. Moreover, (Todorčević et al. 2013a; Todorčević et al. 2013b; Filsoof et al. 2013; Costa et al. 2013; Feng et al. 2014; Zhao et al. 2012; Song et al. 2017; Inoue et al. 2007; Kumar et al. 2017) use their own bidirectional dc-dc power converters in medium voltage applications. Additionally, three phase IBDCs can be usable for high power applications such as (Fei et al. 2018; Kim et al. 2011).

The recommended IBDC is designed based on Dual Active Bridge (DAB) or H-Bridge topology because of convenient feasibility among the other isolated BDC topologies and it is similar with (Kayaalp et al. 2015; Walter et al. 2003; Krismer et al. 2006; Mi et al. 2008; Segaran et al. 2008; Haneda et al. 2020; Jalbrzykowski et al. 2009; Moghaddam et al. 2012; Yazdani et al. 2017).

In this chapter, IBDC is operated by applying Dual Phase-Shift (DPS) control method on all of the triggering elements because of providing harder control mechanism but gives better efficiency results than the other phase shift control methods such as Single Phase-Shift (SPS) (Song et al. 2017) and Extended Phase-Shift (EPS) (Zhao et al. 2012). In literature, SPS is commonly used as far as EPS and DPS because of more simple mathematical algorith (Song et al. 2017). However DPS has more complex algorithm, it gives higher efficiency performance results than the others. In the light of these information, isolated BDC parameters are calculated according to DPS requirements such as compatibleness of input-output dc link voltages and phase-shift angles. Additionally, main dc link capacitor and resistive load are defined for obtaining maximum efficiency and minimum settling times of dc link voltages. Thus, this study discusses effect of DPS control method on IBDC for buck and boost modes by operating both power flow directions. This case will be explained by switching signal graphics.

The recommended IBDC system topology is given in first section with its parameters. The second part defines the dual phase shift control method and third section contains batteries features and finally, the fourth section tells Constant-Current Constant-Voltage (CC-CV) control method.

3.2.1. Circuit Description And Operation Principles

The IBDC is designed based on H-Bridge converter and it contains 8 switches with isolated high frequency transformer. Converter can be operated with regard to intended voltage levels respectively. Figure 3.17. shows the proposed IBDC topology and if output side of the converter is wherever chosen, dc-link capacitor C_1 and resistive load R_{load} should be connected there for the reliable operation of buck-boost modes.

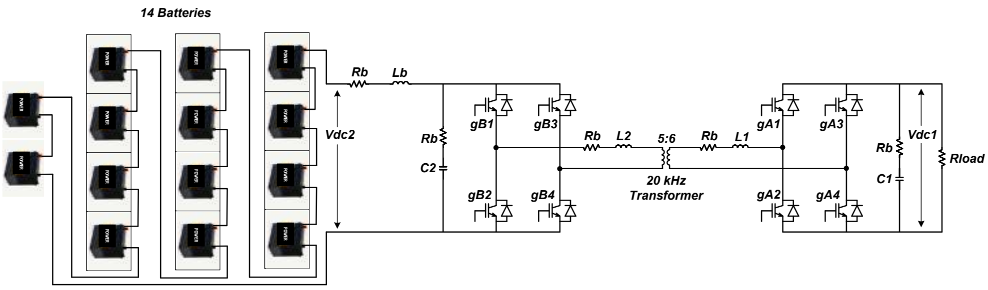

Figure 3.17. Circuit Topology of proposed Isolated Bidirectional DC-DC Converter

The circuit topology of IBDC is H-bridge buck-boost DC-DC converter that is also called dual active bridge circuit, see in Fig.3.17. First of all, DC link capacitors "C_{input}, C_{output} or C_2, C_1" and auxiliary inductors "L_1 and L_2" are calculated by taking into consideration with dual phase-shift angle σ or ϕ and input-output voltages V_{dc1}, V_{dc2} respectively. These two dc-link capacitors are used for limiting of inrush current, achieving to zero voltage switching (ZVS) and zero current switching (ZCS). In this 10 kW converter model, efficiencies of dual phase-shift control method are measured by without using snubber capacitors in order to provide cost & size reduction and clearly understand effect of phase-shift on bidirectional converter topology. Converter is operated by power flow 1 (PF1) and power flow 2 (PF2) and simulation results are obtained both of the two directions. PF1 represents discharging of batteries to 700 V DC-Link voltage and PF2 represents charging of batteries from the DC-Link voltage.

First of all auxiliary inductors and dc-link capacitors are calculated according to buck and boost phase-shift angles.

$$P = \frac{V_1 V_2 N}{\omega L}\left(\sigma - \frac{\sigma^2}{\pi}\right) \tag{3.22}$$

$$C_{input} = \frac{\Delta I_L T_{sw}}{8\Delta V_0} \tag{3.23}$$

$$C_{output} = \frac{I_0 D T_{sw}}{\Delta V_0} \tag{3.24}$$

In equation (3.22) should be $V_2 > V_1$ and dual phase shift angle δ is used for calculating auxiliary inductances L_1 and L_2 ($L = L_{trans} + L_1 + L_2$ and L_{trans} is the inductance of high frequency transformer. If it is too small, it can be ignored while making the calculations. All of the inductances can be equally chosen if input and output voltages are close values each other.) based on power of the converter *P*, turn ratio *N* and $\omega = 2\pi f$ by considering buck and boost modes (Inoue et al. 2007).

Equations (3.23) and (3.24) provide to calculate dc-link capacitors. Where ΔVo is peak-to-peak voltage ripple of the buck mode of the converter output (1 to 2% of the output voltage) for (3.23) and f_s is 20 kHz switching frequency, T_{sw} is $1/f_s$. Moreover, ΔIL is the peak-to-peak current ripple (124 A). At equation (3.24), *D* is duty cycle (0.5) and ΔVo is peak-to-peak voltage ripple of the boost mode of the converter output (0.6 V). Other parameters are the same as (3.23). Moreover, L_b is used for mitigating the current ripple and it is important for charging and decharging health of the batteries. Another formulla is given at (3.25) for calculation of the total inductance value at the converter.

$$P = \left(\frac{NV_1}{2 f_s L}\right)^2 D^2 (1-D)^2 R_{load} \tag{3.25}$$

If we calculate our *L* value by using the above equation;

$$10000 = \left(\frac{0.2 \times 96}{2 \times 20000 \times L}\right)^2 \times (0.5)^2 \times (1-0.5)^2 \times 100$$

$$L = 12\ \mu H$$

And *L* is seperated to $L_1 = 11\ \mu H$ and $L_2 = 1\ \mu H$.

Because charging current of batteries should be high for fast charging.

$V_1 = 336\ V$ because of 14 batteries are series used and each of them is 24 V.

$$C_{input} = C_2 = \frac{124}{8 \times 0.6 \times 20000} = 1.29\ mF$$

$$C_{output} = C_1 = \frac{7 \times 0.5}{0.6 \times 20000} = 0.29\ mF$$

Generally, calculated capacitor values can be usable but they should be increased in order to mitigate ripple voltage of DC-Link and total voltage ripple of batteries. Thus, they are chosen high values (*C_1=23.5 mF and C_2=40 mF*).

Table-3.2. Circuit & Simulation Parameters of the Proposed IBDC

IBDC Parameters		Boost (PF1)	Buck (PF2)
		For DPS Control Method;	
Input-Output IBDC Voltages	V_{dc1}, V_{dc2}	700 V, 336 V	700 V, 336 V
DC-Link Capacitors	C_1, C_2	23.5 mF, 40 mF	23.5 mF, 40 mF
Auxiliary Inductors	L_1, L_2	11 μH, 1 μH	11 μH, 1 μH
Transformers Turn Ratio	N	5:6	5:6
Output DC-Link Resistors	R_b	0.001 Ω	0.001 Ω
Inductor of Batteries side	L_b	0.2 mH	0.2 mH
Proportional Gain	Kp	0.02	0.2
Integral Gain	Ki	0.1	0.1
Switching Frequency	f_{sw}	20 kHz	20 kHz
Load	R_{load}	100 Ω	100 Ω

The rated DC voltage values are selected asunder to each other. Its reason is batteries total voltage is 336 V and transformer turn ratio "N" is selected 5:6 in order to hold suitable operating range.

Moreover, C_1, C_2 are more dominant parameters from inductances to reduce DC link settling times. Thus, C_1 and C_2 values are tried to reduce more than inductances. Additionally, K_p is different values at PF1 and PF2. When the batteries decharge, IBDC uses DC-Link voltage control method and if batteries are charge condition, K_p should be increased at PI operation of Constant Current Constant Voltage (CC-CV) control.

3.2.2. Dual Phase-Shift Control Method

DPS control method is rarely used at isolated BDC applications. This method has different types and these types are presented as lots of studies in the literature. (Cheng et al. 2017; Akagi et al. 2011; Wang et al. 2012) are used DPS control method. Reference (Song et al. 2017) used SPS control for eliminating reactive power and obtaining available system efficiency. Reference (Kumar et al. 2017) studied power characterization of SPS experimentally and lastly (Fei et al. 2018) includes current stress optimized switching strategy with mathematical equations experimentally. Consequently, all of these studies emphasize SPS control is more effective fisibility than other phase-shift control methods but DPS gives high efficiency performance than the others.

The current stress becomes higher values when the voltage range of two side of the transformer increase. This condition gives rise to use higher volt-ampere rating components and switching frequency must be increase in order to minimize the weight and size. Under this condition, increase of the current stress cause to switching losses and great reduction in efficiency. Therefore, requirement of good performance, DPS control method must be use instead of increasing switching frequency and 20 kHz is sufficient for optimum operation. DPS control has a little bit complex algorithm and its modelling is harder than the Extended Phase Shift

(EPS) and Single Phase Shift (SPS). Furthermore, the mathematical complexity of DPS control can be risen when the dead band effect is considered.

Two switching legs of primary and secondary side of the high frequency transformer has different phase shift angle at DPS control method. In other words, gA1, gA2, gA3, gA4 between gB1, gB2, gB3, gB4 switches have different angle each other. Also each leg of A and B sections has different angle. Their switching waveforms are given at simulation results section.

3.2.3. Batteries Features

Lithium-Ion 24 V, 10 Ah batteries are used and 14 of them are series connected to proposed IBDC. Thus, their total voltage value is 24x14=336 V. When the batteries parameters are defined at MATLAB, using real battery datasheet gives correct results. Thus, in this study benefitted from Ionic Batteries Company 24 V, 10 Ah lithium-ion battery (Model: IC-24V10-EP) datasheet by taken close or average values because of comparing the other 24 V, 10 Ah batteries (https://lithiumhub.com/wp-content/uploads/2019/06/24V-10Ah-specs-front.pdf).

Table-3.3. 24 V, 10 Ah Battery Parameters at MATLAB.

Nominal Voltage	24 V
Rated or Maximum Capacity	10 Ah
Cut-off Voltage	18 V
Fully Charged Voltage	29.9357 V
Nominal Discharged Current	4.3478 A
Internal Resistance	0.024 Ω
Capacity at Nominal Voltage	9.0435 Ah
Battery Response Time	30 s

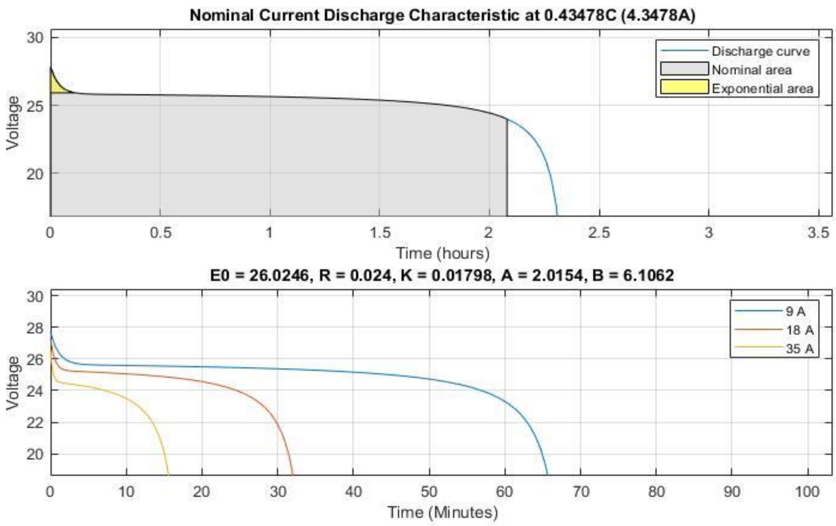

Figure 3.18. Discharge Times of 24 V / 10 Ah Battery at Different Current values.

Figure 3.18. demonstrates if discharge current increase, discharge time of the battery will be decreased.

3.2.4. Constant Current – Constant Voltage (CC-CV) Control

CC-CV control is used for charging of the batteries. Lots of studies are applied this control method because of more practical than the other charging algorithms (Dash et al. 2015; Bhattacharjee 2012; Duryea et al. 2001; Chen et al. 2006; Armstrong et al. 2008; Çolak et al. 2008; Lin et al. 2010; Dung et al. 2016; Thomson et al. 2018). This method partipates 2 section. At the first section, when charging current is stable and this is called bulk current, batteries voltage is increased. Then if increased voltage is higher or equal than open circuit voltage (threshold or preset voltage) of the battery, it continues stable and charging current will be decreased. Decreased current is reached a minimum value that is called float current at the second section. Figure 3.19., Figure 3.20. and Figure 3.21. show the CC-CV control strategy graphic, CC-CV algorithm and MATLAB implementation of the CC-CV control mechanism respectively.

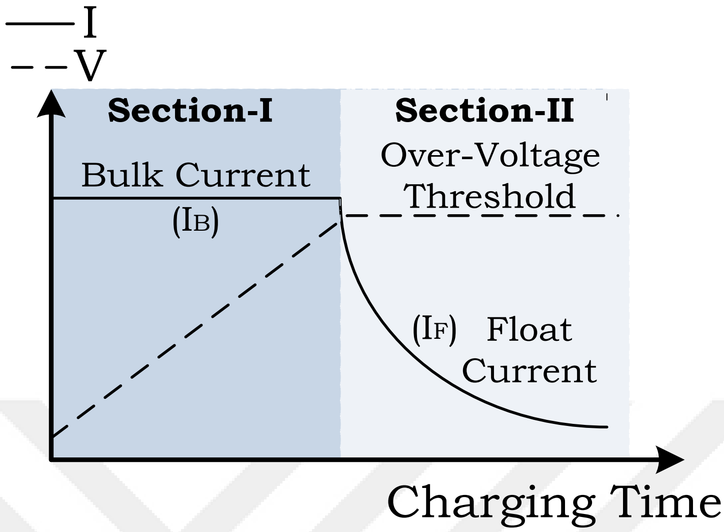

Figure 3.19. CC-CV Control Strategy Graphic

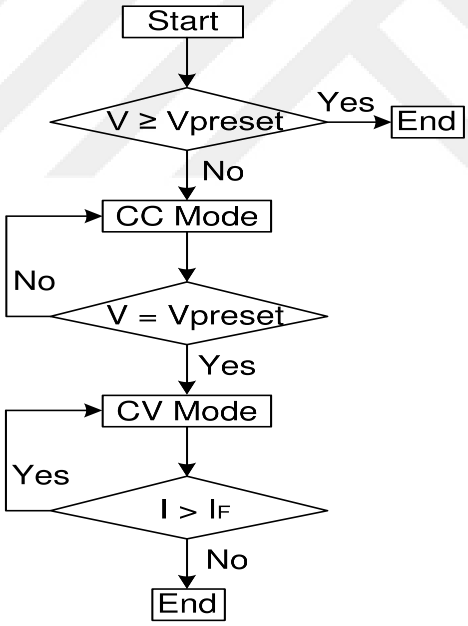

Figure 3.20. CC-CV Control Algorithm

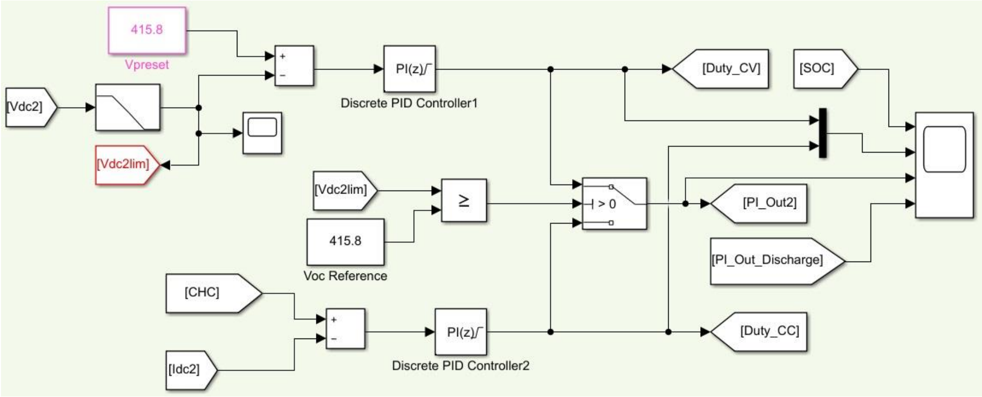

Figure 3.21. MATLAB Implementation of the CC-CV Control

In CC-CV control mechanism, voltage and current values of the batteries are used with V_{dc2} and I_{dc2} respectively. Figure 3.21. shows that bulk (charge) current is stable current of the 14 series connected batteries at section-I of the charging process. When V_{dc2} is equal to V_{oc} or higher than the V_{oc} (29.7 V x 14 = 415.8 V for 14 series connected batteries), section-II begins and current of the batteries decreases. Its minimum level called float current. Additionally, SoC reference should be chosen below of %85 because of if it is chosen close to %100 charging rate, high current levels can be harmful for batteries. Thus, defining of SoC reference, bulk and float currents are important for creating CC-CV control. Bulk current is defined by users but float current is defined by automatically and its calculation is given below. Generally, bulk current should be chosen by looking datasheet of the batteries. Also, float current should be equal to maximum capacity of the one battery is divided by 100 (3.26) so briefly it means that when maximum charging capacity reaches to %100, battery charging current decreases to float current value.

Float current (I_F);

$$I_F = \frac{10\ Ah}{100} = 0.1\ A \quad (3.26)$$

While the charging process continues, final output of PI_Out2 is used from the A type switches of the converter in order to make phase-shift angle. But when the discharging process occurs, the PI_Out2 value is not used. PI_Out value that is the output of DC-Link voltage control method is used to take 700 V at output of the IBDC. But, if the DC-Link Voltage control method is used at discharging process, discharge current is defined by automatically and this issue cause to define too high discharge current. Thus, current controller provides to define discharge current by batteries users. These DC-Link voltage controller and current controllers are shown at the below figures respectively for discharging process.

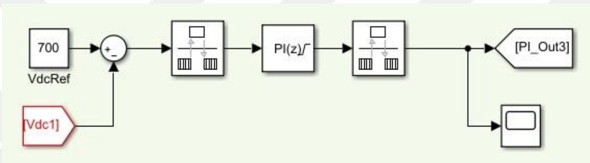

Figure 3.22. DC-Link Voltage Controller for discharging

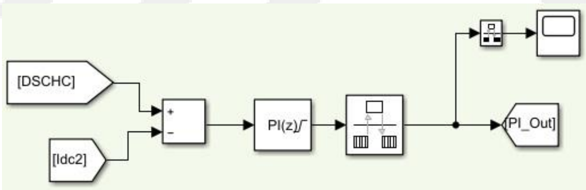

Figure 3.23. Current Controller for discharging

3.3. Modeling of Isolated Unidirectional DC-DC Converter for PV Panels

This chapter includes literature survey of DC-DC converter types, photovoltaic (PV) circuit and operating principle, features of PV panels, modelling of full bridge unidirectional DC-DC converter, Maximum Power Point Tracking (MPPT) technique, Perturb & Observe (P&O) algorithm, proposed topology description with controllers at MATLAB.

When we look at the literature, especially in recent years, there are many different types of new DC-DC converter topologies besides full-bridge and half-bridge topologies (Ahmed et al. 2015). Since these new topologies are non-isolated systems, they are often used in low-power applications such as EVs and HEVs. For this reason, although isolated converter topologies with transformers are disadvantegeous in terms of weight and cost, they can still maintain their currency due to their long life and being usable in higher power applications.

Moreover, in the literature, it is seen that PV panel connected power systems generally press power to the grid using boost converter and PLL method (Phanikumar et al. 2013; Li et al. 2019; Gupta et al. 2019; Femia et al. 2009). However, in these low power applications, fewer PV panels are used and the DC-DC converter is prone to breakdown, making the system unreliable.

In addition, it can be said that cascade topologies created by using boost converters together cause problems such as harmonic increase in the system, especially if they convert different voltage levels (Farivar et al. 2016; Zhao et al. 2012; Choi et al. 2014; Tafti et al. 2016; Mukundan et al. 2017; Wang et al. 2017).

For these reasons, the fact that isolated H-bridge or full-bridge converters that has transformers in their structure can be used in more robust and high power systems has been the reason for preference in this study.

3.3.1. Photovoltaic Circuit And Operating Principle

Photovoltaic (PV) circuit or PV cell is the basic unit of PV panels where the photovoltaic effect is utilised to produce electricity from light energy. Photons are formed when the sunlight hits the semiconductor surface and the electrons in the atom are released. Photons contain different amount of energy for each wavelength in the solar radiation spectrum. When photons come on to the solar cell, some of them are reflected exactly, some are absorbed by the solar cell and some pass through the solar cell. Photons absorbed by the solar cell generate electricity.

Sunlight is produced in different colors by the combination of low energy infrared photons, high energy ultraviolet photons and visible light photons. Photovoltaic material types respond to a narrow range of these energies, depending on their specific bandwidth. Thanks to the absorbed photons, the electron movement due to temperature and radiation creates a current in the PV cell "*Iph*". This resulting current passes through the shunt and series connected resistors "*Rsh* and *Rs*" of different semiconductor materials with different values, creates cell voltage "*Vpv*". The circuit below that is shown at Figure 3.24., is given precisely to show the generated voltage by the effect of temperature and irradiance. Additionally, the below formullas can be used for calculating output current "*Ipv*" of the PV cell. (Saiju et al. 2019; Khanam et al. 2018) references are usable for calculating these parameters according to different materials and climate changes. The following formulas are used to calculate these parameters.

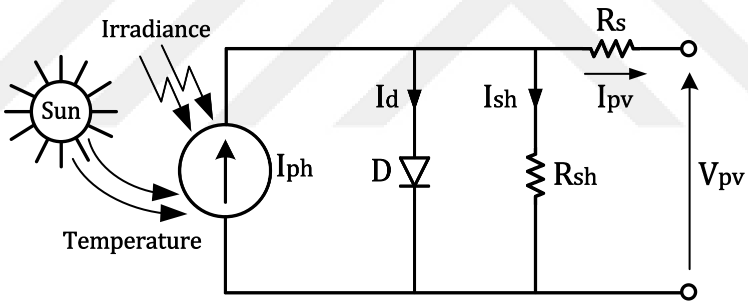

Figure 3.24. Photovoltaic Circuit

Photocurrent is dependent on short-circuit current, actual-reference temperatures and irradiation on the device surface (W/m^2).

$$I_{ph} = [I_{scr} + K_i(T_k - T_{ref})] \times \frac{\lambda}{1000} \tag{3.27}$$

$$I_{rs} = \frac{I_{scr}}{\left[exp\left(\frac{qV_{oc}}{N_s kAT}\right) - 1\right]} \tag{3.28}$$

$$I_0 = I_{rs} \times [T/T_r]^3 \times exp\left[\frac{q \times E_{g0}}{Ak} \times \left(\frac{1}{T_r} - \frac{1}{T}\right)\right] \quad (3.29)$$

$$I_{pv} = N_p \times I_{ph} - N_p \times I_0 \times \left[exp\left\{\frac{q \times (V_{pv} + I_{pv}R_s)}{N_s kAT}\right\} - 1\right] - V_{pv} + \frac{I_{pv}R_s}{R_{sh}} \quad (3.30)$$

Iph : Photocurrent (light generated current at the nominal condition (25°C and 1000W/m^2))

Iscr : Short-circuit current

Ki : Short-circuit current / temperature coefficient (0.0017 A/k)

Tk : Actual temperature

Tref : Reference temperature

λ : Irradiation on the device surface (W/m^2)

Irs : Reverse saturation current

q : Electron charge (1.6×10^{-19} C)

Voc : Open-circuit voltage varies with PV panel type

Ns : Number of cells connected in series

Np : Number of cells connected in parallel

A : Ideality factor (1.6)

k : Boltzman constant (1.3805×10^{-23} J/K)

Ipv : PV module output current at single diode model

Rs : Series resistance of PV module

Rsh : Parallel (shunt) resistance of PV module

3.3.2. Features of PV Panels

In this study, 1 Soltech 1STH-215-P type panels are used. They combined each other with 4 parallel strings and 12 series connected modules. Its module data and I-V, P-V characteristics of array are shown at Table-3.4. and Figure 3.25. respectively. All parameters are taken from MATLAB/Simulink program.

Table-3.4. Used Solar Panel Parameters at MATLAB

PV Panel Brand / Type & Parameters	1 Soltech 1STH-215-P
Maximum Power (W)	213.15
Open Circuit Voltage (V)	36.3
Voltage at Maximum Power Point Vmp (V)	29
Temperature Coefficient of Voc (% / deg.C)	-0.36099
Cells per module (Ncell)	60
Short-circuit current Isc (A)	7.84
Current at Maximum Power Point Imp (A)	7.35
Temperature Coefficient of Isc (% / deg.C)	0.102

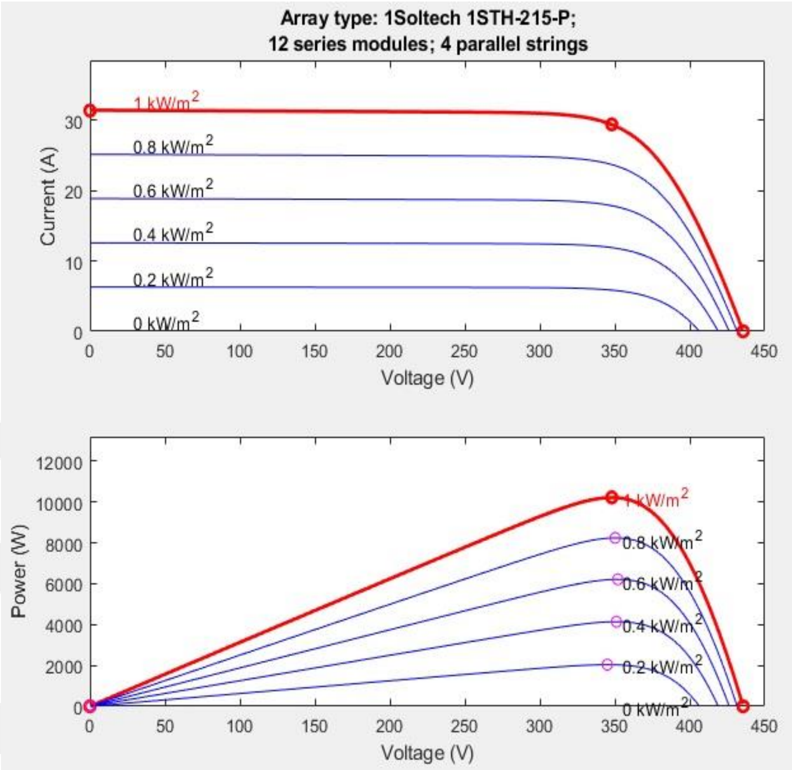

Figure 3.25. I-V and P-V curves of the used solar panels array according to different irradiance levels

3.3.3. Modeling of Unidirectional Full Bridge DC-DC Converter

Isolated unidirectional full-bridge DC-DC converter topology includes 4 IGBTs, 4 diodes, 1 transformer and 2 DC-link capacitors. Auxiliary inductors inside the converter can be connected in different ways and these inductors are usually connected to the input and output of the transformer. When calculating these two auxiliary inductors, first of all, the total value is found and the internal inductance value of the transformer is substracted and the remaining value is divided according to the smoothness of the voltage-current waveform at the output of the transformer. Equation 3.31 provides calculation of these auxiliary inductors. Additionally, C_{input} and C_{output} DC-Link capacitors can be calculated by using the Eq. 3.32 and 3.33. D is the duty value in these equations can be taken the average value of the MPPT-PI controller output according to different temperature and irradiance levels.

$$P = \frac{V_1 \times V_2 \times n}{W \times L} \times \left(\delta - \frac{\delta^2}{\pi}\right) \quad (3.31)$$

In this formulla, δ is phase-shift angle and n is transformer turn ratio. Then;

$$C_{input} = \frac{\Delta I_L \times T_{SW}}{8 \times \Delta V_o} \quad (3.32)$$

$$C_{output} = \frac{I_o \times D \times T_{SW}}{\Delta V_o} \quad (3.33)$$

Equation 3.31 depends on the phase shift angle and this angle changes with different duty values. When PV panels connected to full-bridge converter, different irradiance or temperature levels cause to different duty cycles. Therefore, δ value can be used with defining a range for accurate calculation. But this condition a little bit hard because of duty is output parameter of the PI controller also. In this way, another formullas (Equations 3.34 and 3.35) can be useful because of the necessary input-output voltage ratio.

$$\frac{V_o}{V_{in}} = \frac{2 \times n}{1 + \sqrt{1 + \frac{4k}{Dmax^2}}} \quad (3.34)$$

$$k = \frac{4 \times n^2 \times L_R}{R_o \times T_s} \quad (3.35)$$

In these formullas Dmax is maximum duty value, $L_R = L_1 + L_2$+Transformer internal inductor, R_o is load resistance and T_s=1/fs, fs is switching frequency.

L1 and *L2* calculation:

$$\frac{V_o}{V_{in}} = \frac{2 \times n}{1 + \sqrt{1 + \frac{4k}{Dmax^2}}} = \frac{758}{348} = \frac{2 \times 2.4}{1 + \sqrt{1 + \frac{4k}{0.95^2}}}$$

$$\mathrm{k} = 0.1014$$

$$L_R = \frac{0.1014 \times 100 \times 5 \times 10^{-5}}{4 \times 2.4^2} = 22\ \mu H = L_{tr} + L_1 + L_2$$

$$L_1 + L_2 = 22\ \mu H - 2\ \mu H = 20\ \mu H$$

Then, total auxiliary inductor value should be seperated for obtaining smooth seconder voltage of the transformer.

$$L_1 = 5\ \mu H \ and\ L_2 = 15\ \mu H$$

L3 calculation:

Extra series connected inductor should be used for mitigating the output current ripple at the proposed full-bridge converter. In this way, LC or CL filter types are useful when battery is connected to the load side of the converter. In this system, CL filter type is created for more reducing current ripples because of it depends on the input empedance and output empedance rates. The below formullas gives us the minimum *L3* value. But when all of the HRPS equipments are connected this inductor value is not necessary because of only resistors are used at DC-Link. If the load has only batteries, this inductor can be used for reducing charge current.

$$L_{min} = \frac{V_{L,max}}{\frac{I_{ripple} \times I_{L,max}}{t_{on}}} = \frac{\frac{N_2}{N_1} \times V_{in} - V_{out}}{\frac{I_{ripple} \times I_{L,max}}{t_{on}}} \tag{3.36}$$

$$V_{L,max} = \frac{24}{10} \times 352 - 700 = 144.8\ V$$

$$I_{L,max} = \frac{P_{o,max}}{V_{o,min}} = 4900/26.4 = 185.6\ A \ \ and\ t_{on} = 0.028\ sec., I_{ripple} = 1.1\ A$$

$$L_{min} = \frac{144.8}{\frac{1.1 \times 185.6}{0.028}} = 19.85\ mH \approx 20\ mH$$

3.3.4. Maximum Power Point Tracking System And Perturb & Observe Algorithm

Maximum Power Point Tracking (MPPT) is used for catching maximum operating power value of PV panels according to irradiance and temperature values. It is established by making different algorithms such as Perturb and Observe (P&O), Incremental Conductance (IC), etc… Moreover, these MPPT algorithms are compared at lots of studies in photovoltaic applications literature.

In this study, P&O algorithm is used because of its simple diagram and has easier implementation than the other techniques. Its flowchart is demonstrated at the Figure-120.

In simulation model, P&O and PV panel simulink blocks are used at input side of the isolated full-bridge DC-DC converter.

It is very important to determine the parameter values which are used in the algorithm, correctly while creating the P&O algorithm. At this point, knowing the maximum-minimum total voltage and current values of the PV panels used in open circuit will help to determine the limit parameters. Additionally, these limit parameters may vary depending on whether the MPPT system can operate according to voltage and current.

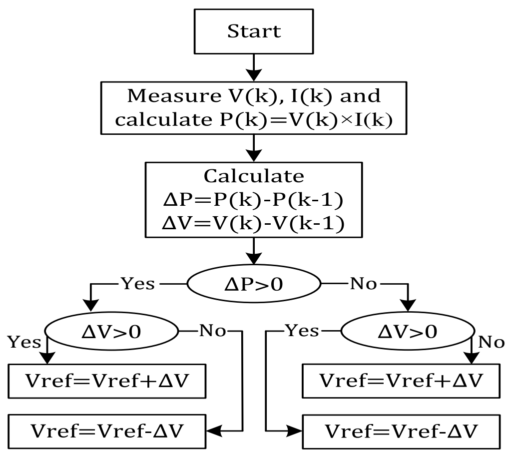

Figure 3.26. Perturb and Observe (P&O) algorithm flowchart

When we look at the P&O flowchart, total measured voltage and current values are utilized by calculating “Δ” values by substracting the previous values of total power and total voltage from instant values of them. Then, new Vref value is defined at every loop depending on whether these difference “Δ” values are greater or less than zero. Thus, the highest voltage and current values are captured by the MPPT algorithm and these voltage-current values are different at different temperature-irradiation conditions.

3.3.5. Proposed Topology Description With Its Controllers At Matlab

When we look at the literature, we see that boost converters are generally used with PV panels and one switching signal is easily used for obtaining required output voltage at these topologies. However, in this study, since there will be different power flow scenarios in the hybrid regenerative system, a longer-lasting reliable DC-DC converter is needed. Thus, full-bridge unidirectional isolated DC-DC converter is available for these operations. Proposed converter topology and its MPPT controller are taken from MATLAB/Simulink at Figure-3.27 and its parameters are shown at Table-3.5.

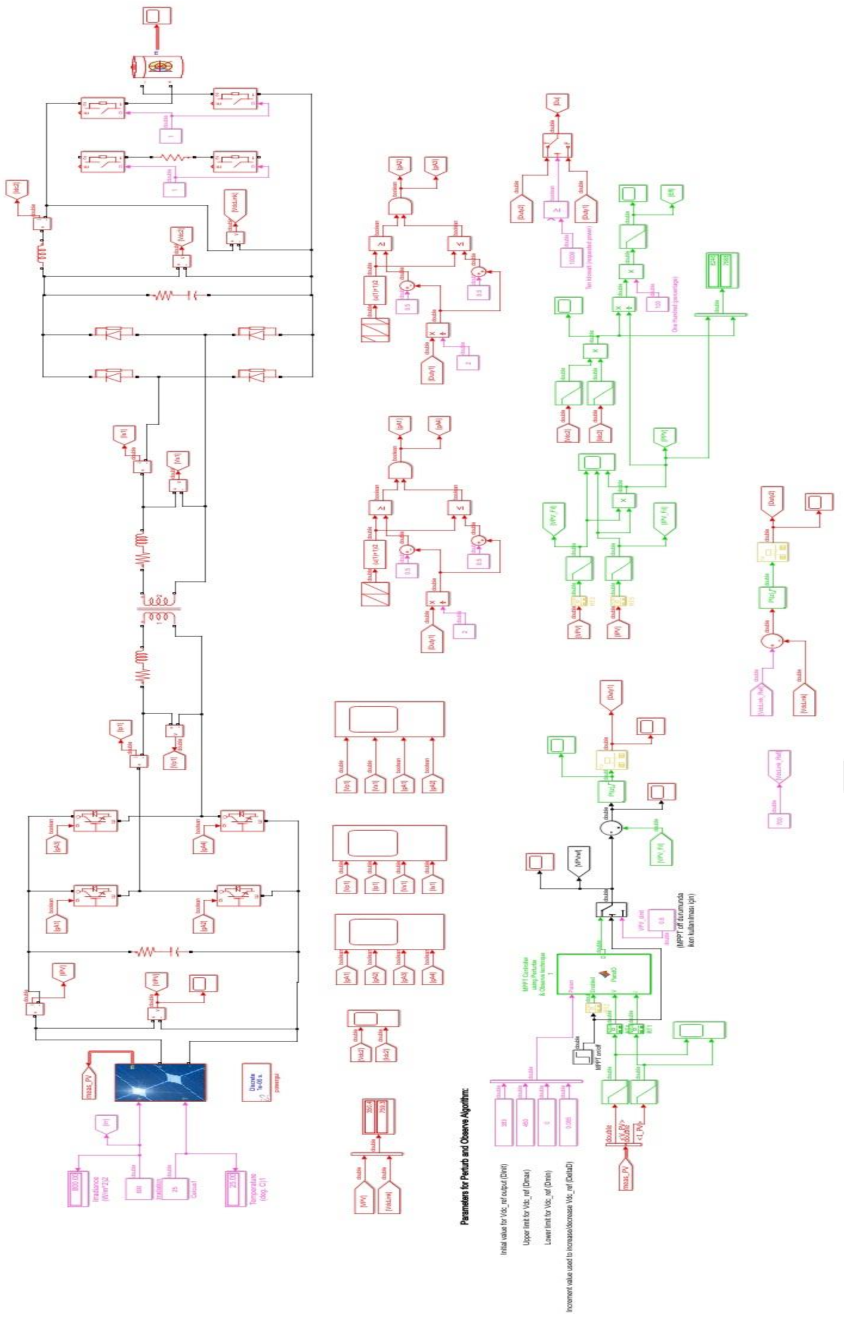

Figure 3.27. PV panels connected isolated full-bridge unidirectional DC-DC converter with MPPT controller at MATLAB/Simulink program.

In this topology, solar panels, 4 IGBTs, 20kHz transformer and 4 diodes are connected with auxiliary inductors and capacitors according to the Figure 3.27. These IGBTs are triggered with duty ratio that is produced from MPPT algorithm. gA1-gA4 and gA2-gA3 switches are same phase angle but these pairs are complimentary each other. Therefore, there is a 180 degree phase difference between the signal generators of these switch pairs.

Table-3.5. Isolated Full-Bridge Unidirectional DC-DC Converter Parameters

IUDC Parameters	Values
Solar panels side input capacitor (*C1*)	45 *mF*
DC-Link side output capacitor (*C2*)	23.5 *mF*
Transformer primary side inductor (*L1*)	5 *µH*
Transformer secondary side inductor (*L2*)	15 *µH*
Output auxiliary inductor (*L3*)	20 *mH*
Internal Resistances (*R*)	0.001 *Ω*
Transformer Turn Ratio (*n*)	5:12
Switching Frequency (*fsw*)	20 *kHz*

4. DESIGN AND MODELING OF PROPOSED CENTRAL ENERGY MANAGEMENT SYSTEM

Hybrid Regenerative Power System (HRPS) is created by combining grid connected inverter, PV panels connected isolated full-bridge unidirectional DC-DC converter, batteries connected isolated full-bridge bidirectional DC-DC converter and AC-DC loads.

In this chapter, power flow scenarios are only introduced on HRPS. Then, fifth chapter demonstrates operation of all of the power flow scenarios results with and without proposed Central Energy Management System (CEMS) and these scenarios are shown at Figure 4.1 with their names. In addition, Table-4.1 shows that controllers of system equipments are defined for each power flow scenario. And second part, proposed EMS and controllers of the system equipments are explained detaily in this chapter.

4.1. Operating Modes of Hybrid Regenerative Power System

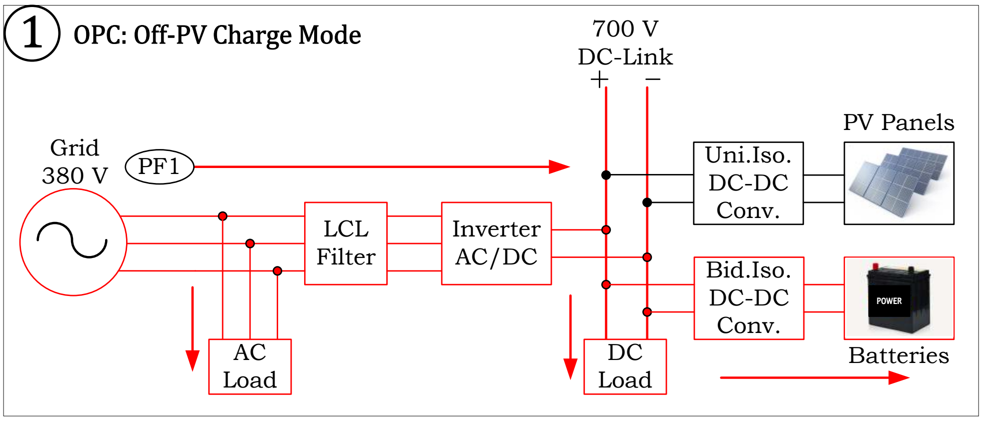

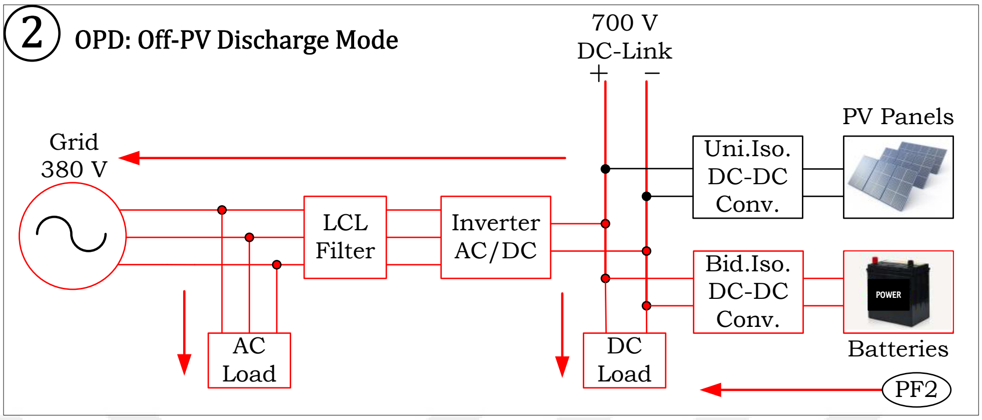
2
OPD: Off-PV Discharge Mode
700 V
DC-Link
+
−
Grid
380 V
PV Panels
Uni.Iso.
DC-DC
Conv.
LCL
Filter
Inverter
AC/DC
Bid.Iso.
DC-DC
Conv.
AC
Load
DC
Load
Batteries
PF2

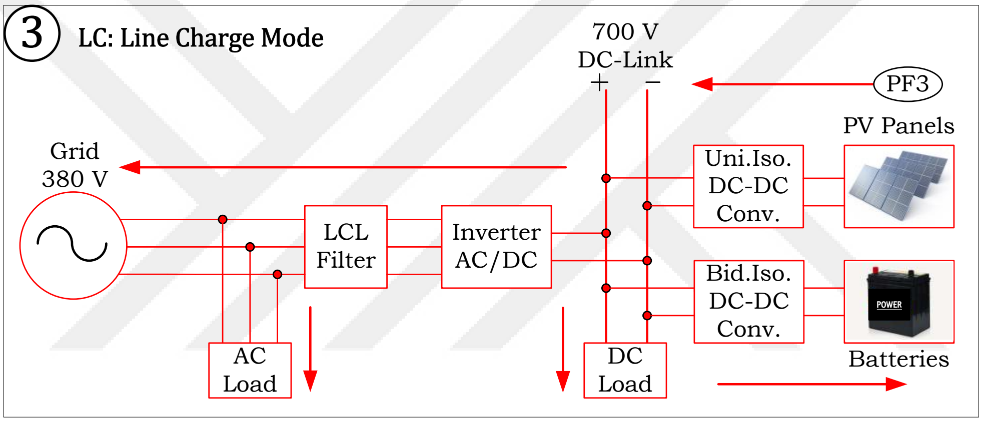
3
LC: Line Charge Mode
700 V
DC-Link
+
−
PF3
PV Panels
Grid
380 V
Uni.Iso.
DC-DC
Conv.
LCL
Filter
Inverter
AC/DC
Bid.Iso.
DC-DC
Conv.
AC
Load
DC
Load
Batteries

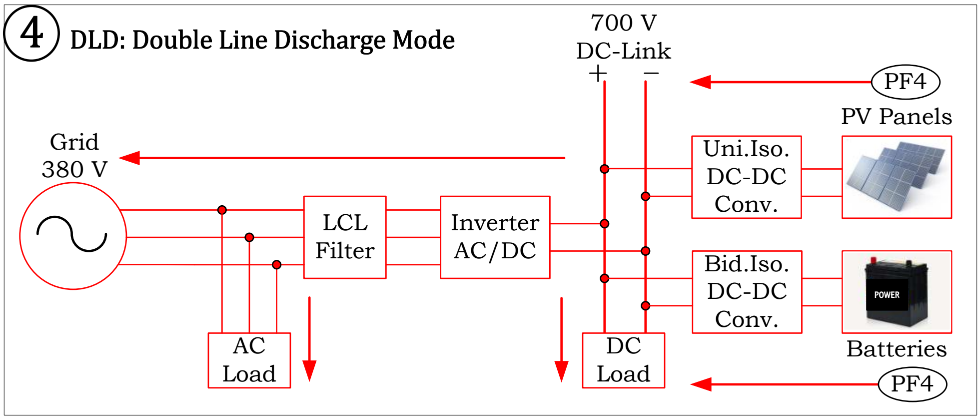
4
DLD: Double Line Discharge Mode
700 V
DC-Link
+
−
PF4
PV Panels
Grid
380 V
Uni.Iso.
DC-DC
Conv.
LCL
Filter
Inverter
AC/DC
Bid.Iso.
DC-DC
Conv.
AC
Load
DC
Load
Batteries
PF4

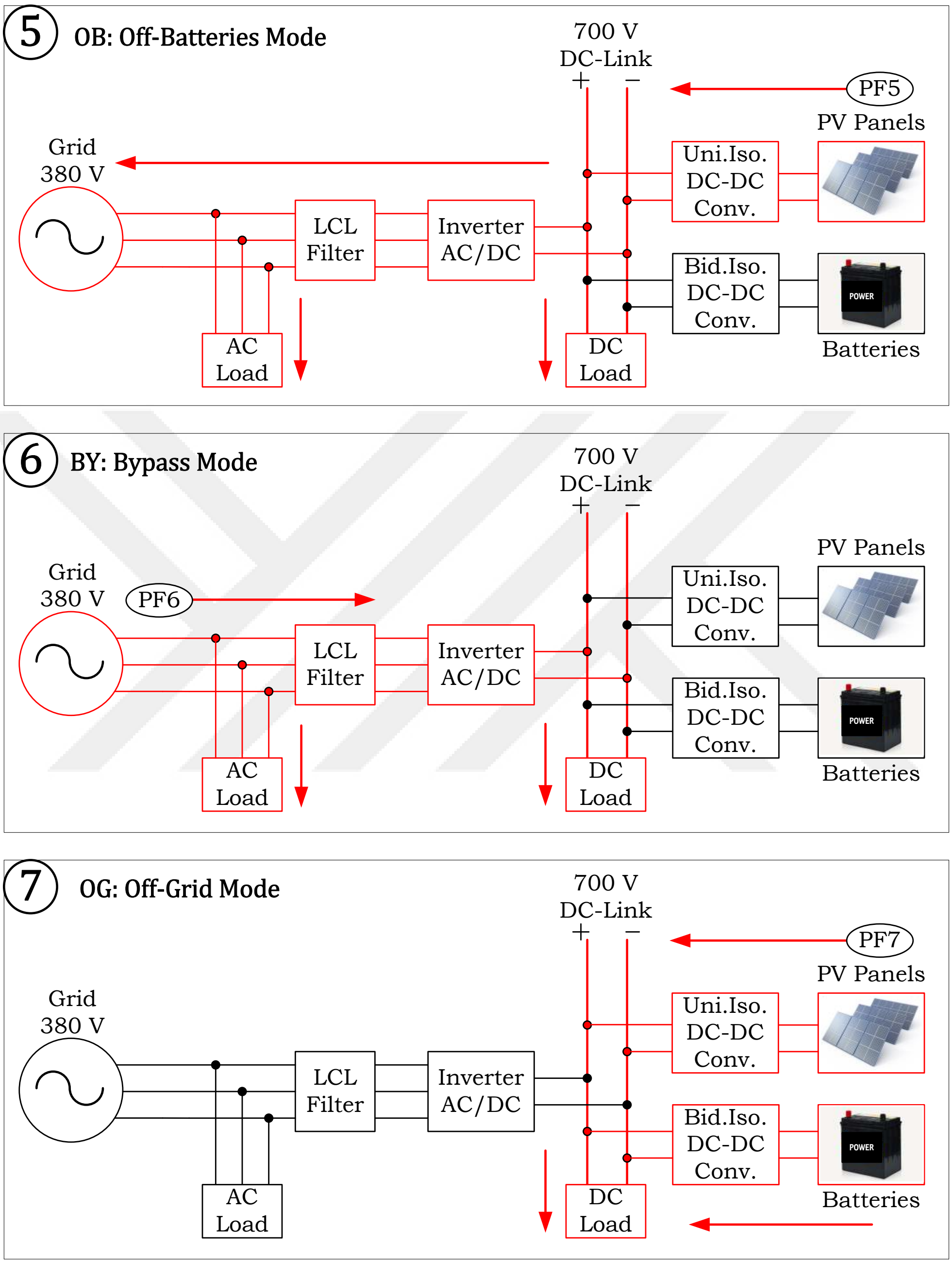

Figure 4.1. HRPS Power Flow Scenarios

Table-4.1. Controllers of HRPS components according to different Power Flow (PF) scenarios

Scenario Modes & HRPS Components	Grid	Inverter	Batteries + IBDC	PV Panels + IUDC
SC1 - OPC	Source Power	DC-Link Voltage Control	CC-CV Control	OFF
SC2a - OPD	Inject Power	DC-Link Voltage Control	Discharge Current Control	OFF
SC2b - OPD	Inject Power	Power Control	DC-Link Voltage Control	OFF
SC3 - LC	Inject Power	DC-Link Voltage Control	CC-CV Control	MPPT Control
SC4 - DLD	Inject Power	DC-Link Voltage Control	Discharge Current Control	MPPT Control
SC5 - OB	Inject Power	DC-Link Voltage Control	OFF	MPPT Control
SC6 - BY	Source Power	DC-Link Voltage Control	OFF	OFF
SC7 - OG	OFF	OFF	DC-Link Voltage Control	MPPT Control

4.2. Proposed Central Energy Management System

In this section, a new energy management system application to automatically operate the Hybrid Regenerative Power System (HRPS), which has been modeled before, according to the desired power flow scenarios and the results are obtained as a result of this application are explained in detail.

First of all, it is considered how the power flow scenarios that are operated alone on the created HRPS should work in harmony with each other, automatically and in a way that meets the system requirements. In this context, it is necessary to know exactly the power flow scenarios in the power system.

It is very important that all scenarios in this proposed power system work in a logical order. In order for the Central Energy Management System (CEMS) created to work properly, it is thought to be able to adapt to variable conditions. Chief among these is the difference in the power demanded from workplaces or residences under day-night difference and variable temperature conditions. We can say that this demanded power change is less during the night and slightly more during the day. We can see this situation in the graph below.

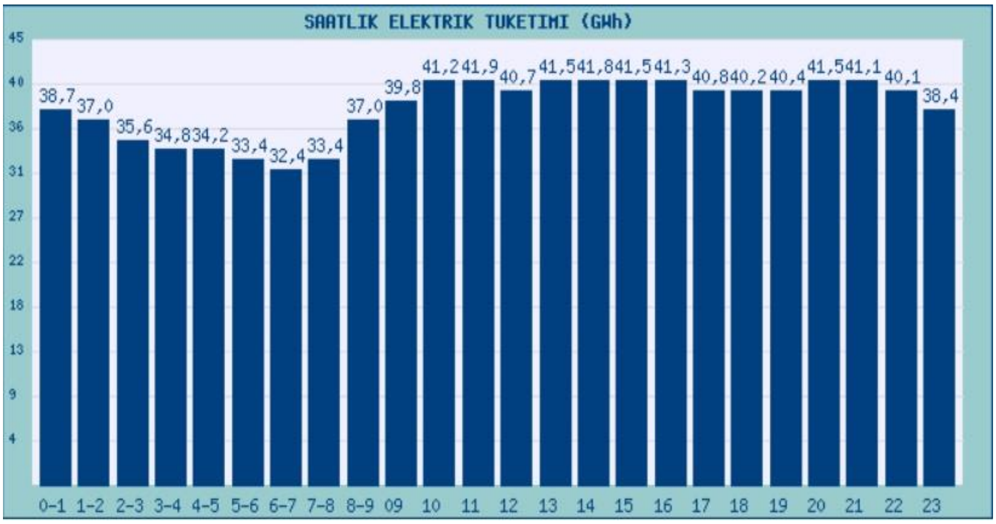

Figure 4.2. Average electricity consumption by hours in Turkey in 2018. [enerjiatlasi.com]

The hourly consumption in the figure above is not taken as a basis, since the power system created is not very high-powered and can supply more specific critical loads. The aim to be seen in the simulation study, the results of which are obtained; as stated above, it is possible to apply all power flow scenarios by creating a power balance according to variable light, temperature, load and charge states of the batteries. In addition, it is explained in the conclusion part of the thesis how effective the regenerative feature is in terms of both workplaces and residences by discharging the batteries and transferring the power produced from photovoltaic panels to the grid in the proposed system.

When we look at the energy management system literature before, we saw that such applications are mostly made at high power, while low power applications are especially studied on electric and hybrid electric vehicles. It is possible to say that this application, in which the regenerative effect that is called micro-grid related to critical loads, is seen, has an innovative feature with its working power and CEMS prepared in accordance with it, although not topologically in the literature.

The CEMS applied in the proposed HRPS are shown in Figure 4.3. below, and the power flow directions and control methods in the equipment used are indicated. How the power flow scenarios run on the power system can work in general is shown in this figure.

It is very important to choose the power values of the equipments in the power system specified in Figure 4.3. and in the proposed power system close to each other in order to increase the efficiency of the system. However, a smaller number of batteries were chosen as the cost of the entire system should be considered. This power balance should be well established on CEMS, which will ensure the operation of the system, and power flow scenarios should be selected accordingly. Therefore, theoretical analyzes have been made in general sub-titles related to the operation of the power system.

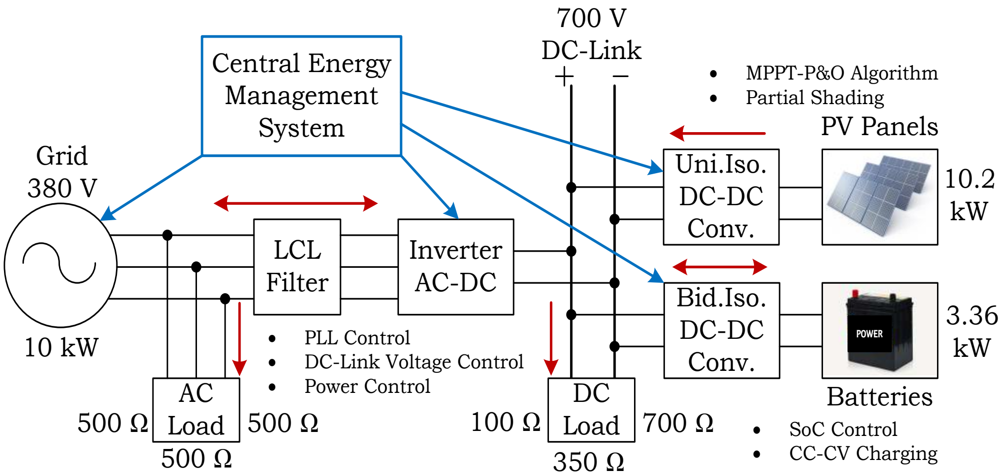

Figure 4.3. General Diagram of Proposed Hybrid Regenerative Power System and Central Energy Management System

4.2.1. Dynamic Analysis of Energy Storage System

While performing the dynamic analysis of the energy storage system, how much power can be stored or spent instantly in charge and discharge states can be found by processing according to small time intervals. In the formula below, we see the discharge and charge functions, respectively, depending on time. The $x_{st}(h)$ in the formula shows the energy level stored in the energy storage system according to time (h), $n_{c,st}$ and $n_{d,st}$ respectively, the charge and discharge efficiencies, $P_{st}(h)$ the power change in the h time, and T_s the sampling time interval (Pippia et al. 2020).

$$x_{st}(h+1) = \begin{cases} x_{st}(h) + \dfrac{T_s}{\eta_{d,st}} P_{st}(h), & P_{st}(h) < 0 \\ x_{st}(h) + T_s \eta_{c,st} P_{st}(h), & P_{st}(h) \geq 0 \end{cases} \quad (4.1)$$

4.2.2. State of Charge and State of Health (SoC & SoH)

Companies that manufacture batteries know that many different types of batteries have their own unique way of working. In other words, batteries can show different power values according to their percent charge status and currents, depending on whether the voltage value is low or high. At this point, it is important to determine the lower and upper limits when installing the energy management system, as the ability of the batteries to operate at the same power values will extend the life of the batteries (State of Health-SoH). The lower limit and upper limit values for the batteries are defined on the proposed CEMS.

While the state of charge of the batteries never falls below the determined lower limit during system operation, the defined upper limit is actually seen as a threshold value. This situation is explained in detail in the simulation results.

There are several methods in the literature to predict the state of charge of batteries. These are named as “recursive least squares method with variable forgetting factor”, “artificial neural network utilization method” and “Coulomb-count method”. In this report, “Coulomb-counting method” is explained in order to be more useful. If the charge state calculated according to the time intervals is considered from the beginning, the changing power on the battery over time is related to the current charge capacity of the battery divided by 1 and the two parameters multiplied (4.2). The ratio of the instantaneous charge capacity of the batteries to the nominal charge capacity shows us the state of health (SoH) of the batteries instantly (4.3). The charge capacity, which varies according to defined time intervals, is related to the charge or discharge current used in this interval, and the instantaneous charge capacity can be found by calculating from the formula (4.4) (Sorour et al. 2021).

$$SOC(t) = SOC(0) - \frac{1}{C_{ref}(t)} \int_0^t P_b(t)dt \tag{4.2}$$

$$SOH(t) = \frac{C_{ref}(t)}{C_{nom}} \tag{4.3}$$

$$C_{ref}(t) = \frac{1}{SOC(t_\alpha) - SOC(t_\beta)} \int_{t\alpha}^{t\beta} I(t)dt \tag{4.4}$$

4.2.3. Condition of AC and DC Loads

In this study, 3-phase loads with 500 Ω connected to the grid side and 700 Ω, 350 Ω and 100 Ω equivalent resistances connected to the DC-Link side are used. On the simulation, DC loads were switched on and off by connecting 7 700 Ω loads in parallel to each other and connecting switches at the beginning and end of each resistance value. Since the change in the loads will create the demanded power, these resistance values specified in the DC load show differences. In the load switch charts below, which switches are open or closed are indicated as an example. During the operation of HRPS with CEMS, the AC load and a single DC load of 700 Ω were constantly connected to the system (SWacL and SWdcL are ON condition all the time during the simulation period). The switch named SWdcL2 allows 1 of the DC loads connected in parallel to be connected. The name of the switch that connects the other 5 DC loads to the system is SWdcL3. Matlab implementation of DC and AC loads are shown at Figures 4.4. and 4.5. respectively. The open and closed states of these switches according to time are shown in Figures 4.6 and 4.7.

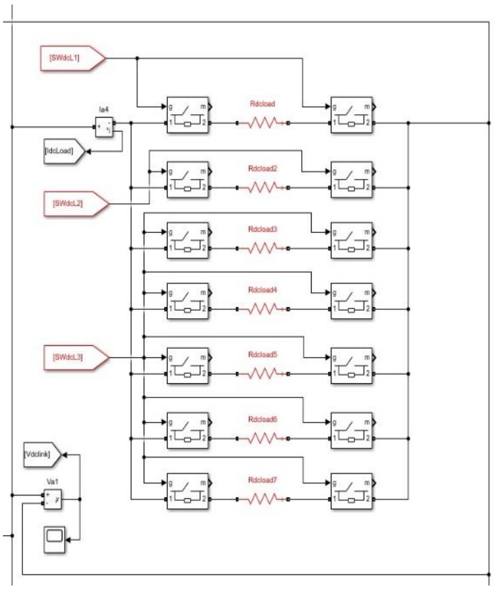

Figure 4.4. DC load resistances (each of them is 700 Ω)

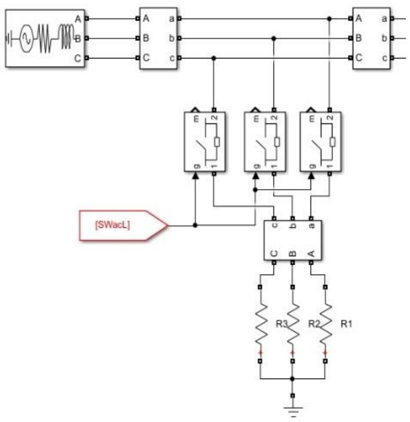

Figure 4.5. AC load resistances (each of them is 500 Ω, R_1=R_2=R_3)

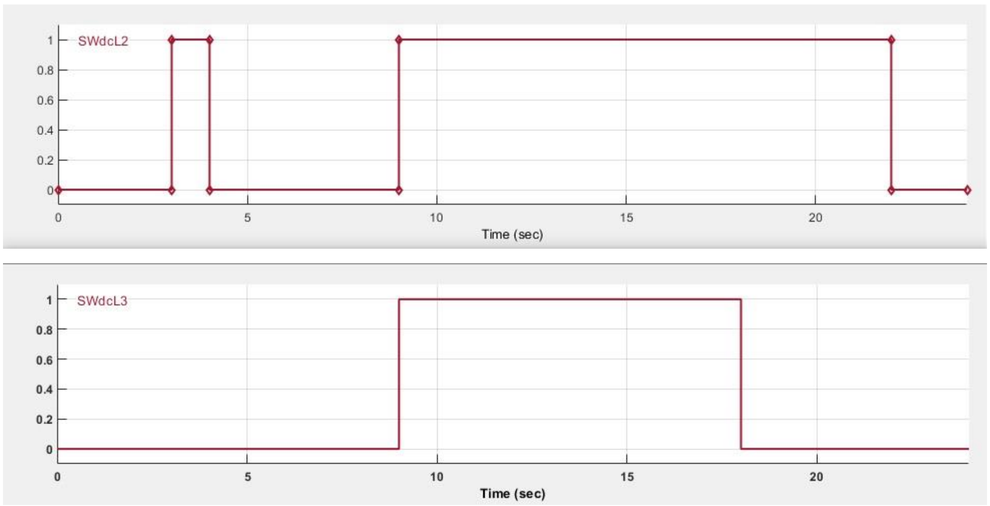

Figure 4.6. SWdcL2 and SWdcL3 DC loads switches conditions

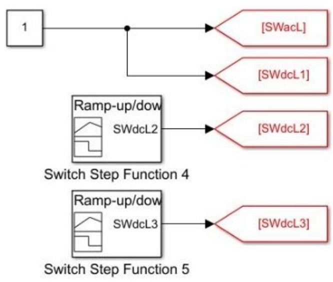

Figure 4.7. Switches conditions for DC and AC loads

4.2.4. Energy Prices and Profit Calculation Function

In our country, according to the national tariff for the period of 2021, the unit price of 1 kWh electricity is 0.4743 TL/kWh for residences and 0.7063 TL/kWh for workplaces. In the simulation results, the percentage profit status is shown by the ratio of the total power injected into the grid to the total power drawn from the grid. In this way, the difference of the two values is taken and the electricity consumption fee is also revealed. Again, it will be sufficient to use the formula (5) below in order to find out how many TL the price will come from our simulation study according to the power consumed and produced in unit time and to see how much efficiency it can work daily as a percentage.

$$\eta ECP = \frac{\left|\int_a^b P_{pro}(x)dx\right|}{\int_0^{24} P_{con}(x)dx} \times 100\% \qquad (5)$$

4.2.5. Irradiance and Temperature Spectrums

In this study, the radiation and temperature spectra obtained according to the date of 25.07.2021 were prepared and used. In the spectra used, each hour is shown as 1 second. Figures 4.8. and 4.9. show the radiation and temperature spectra, respectively.

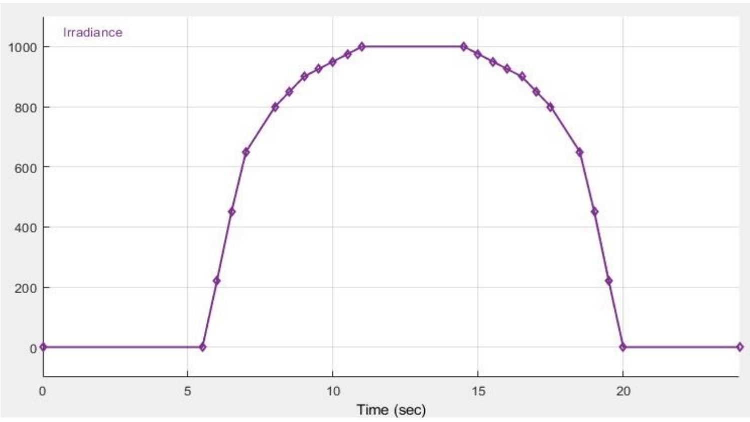

Figure 4.8. Irradiance Spectrum

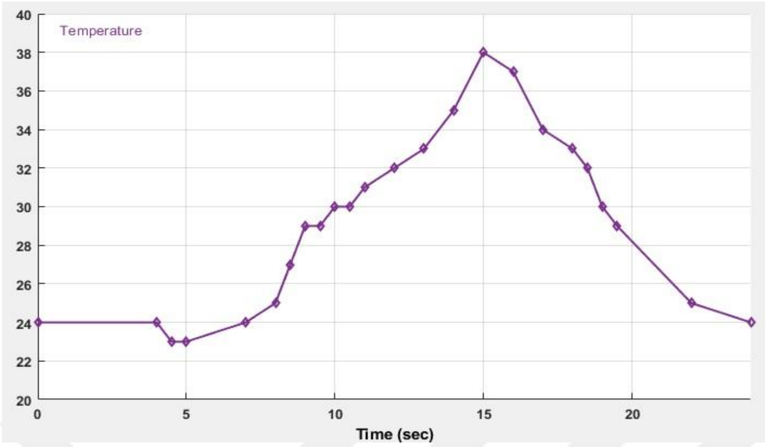

Figure 4.9. Temperature Spectrum

4.2.6. Modeling of Proposed Energy Management System

With the Central Energy Management System (CEMS) implemented on HRPS, it is aimed to run all power flow scenarios shown in Figure 4.1. In cases where the radiation and temperature spectrums created in this direction are different, some scenarios may work longer, while others may work for a shorter time. This difference is also due to the varying load states. It is very important that the scenarios run instantly change according to the power balance in the system, the power demanded from the load, the state of charge of the batteries and the amount of radiation received by the photovoltaic panels.

First of all, when we look at the general structure of our power system, if we think about which scenario can work and when; We can deduce that in scenarios 1, 2 and 6, PV panels can be disabled when there is no light at night, scenarios 3 and 5 must operate at noon depending on the light intensity, and scenarios 4 and 7 may differ according to the power balance. However, it should be kept in mind that CEMS must respond appropriately to the changing power demands in the load, no matter which scenario works momentarily.

The algorithm and MATLAB application of the proposed EMS are shown in Figures-4.10. and 4.11., respectively.

The working principles of the proposed EMS mechanism and the transitions between power flow scenarios are explained in terms of being an example thanks to the generated radiation and temperature spectrums and load changes. In other words, the designed EMS benefits from a very small amount of radiation effect, although not completely. The reason for this is to run the system more efficiently. So power flow scenarios involving PV panels at night without radiation are unnecessary to run. Likewise, if the power demands on the loads are met, it will be possible to inject more power into the entire power system with supporting of the radiant effect. In the light of all this information, the working principle of the EMS proposed in the study and the simulation results are explained together.

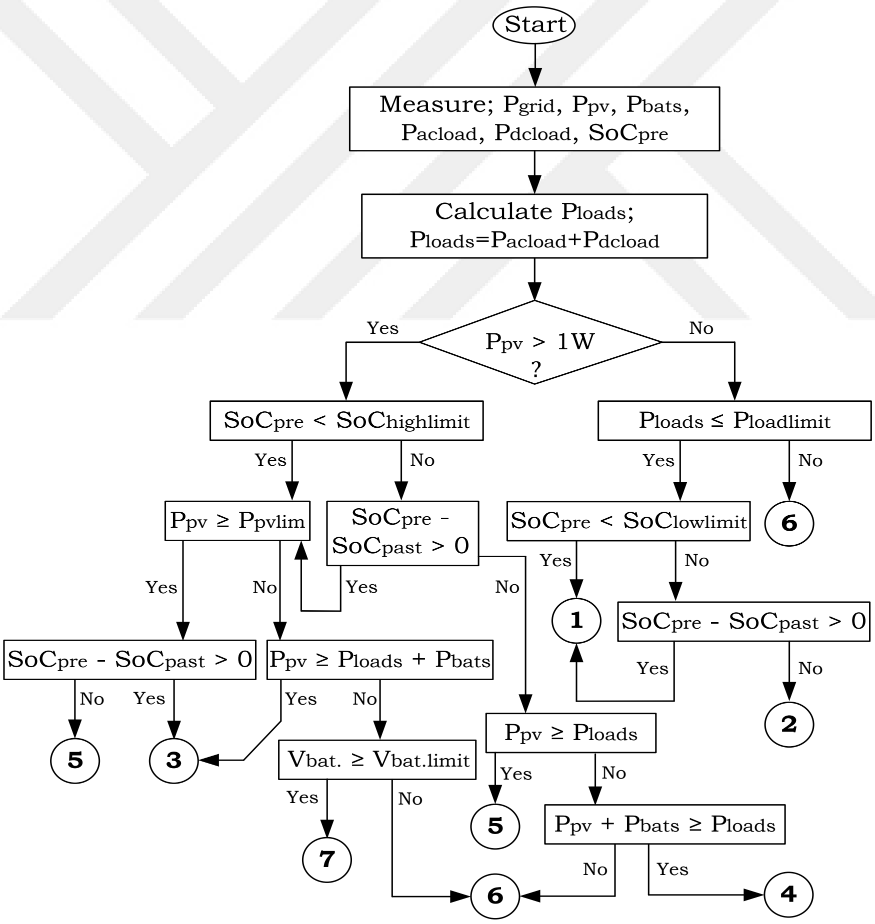

Figure 4.10. Proposed Central Energy Management System Algorithm

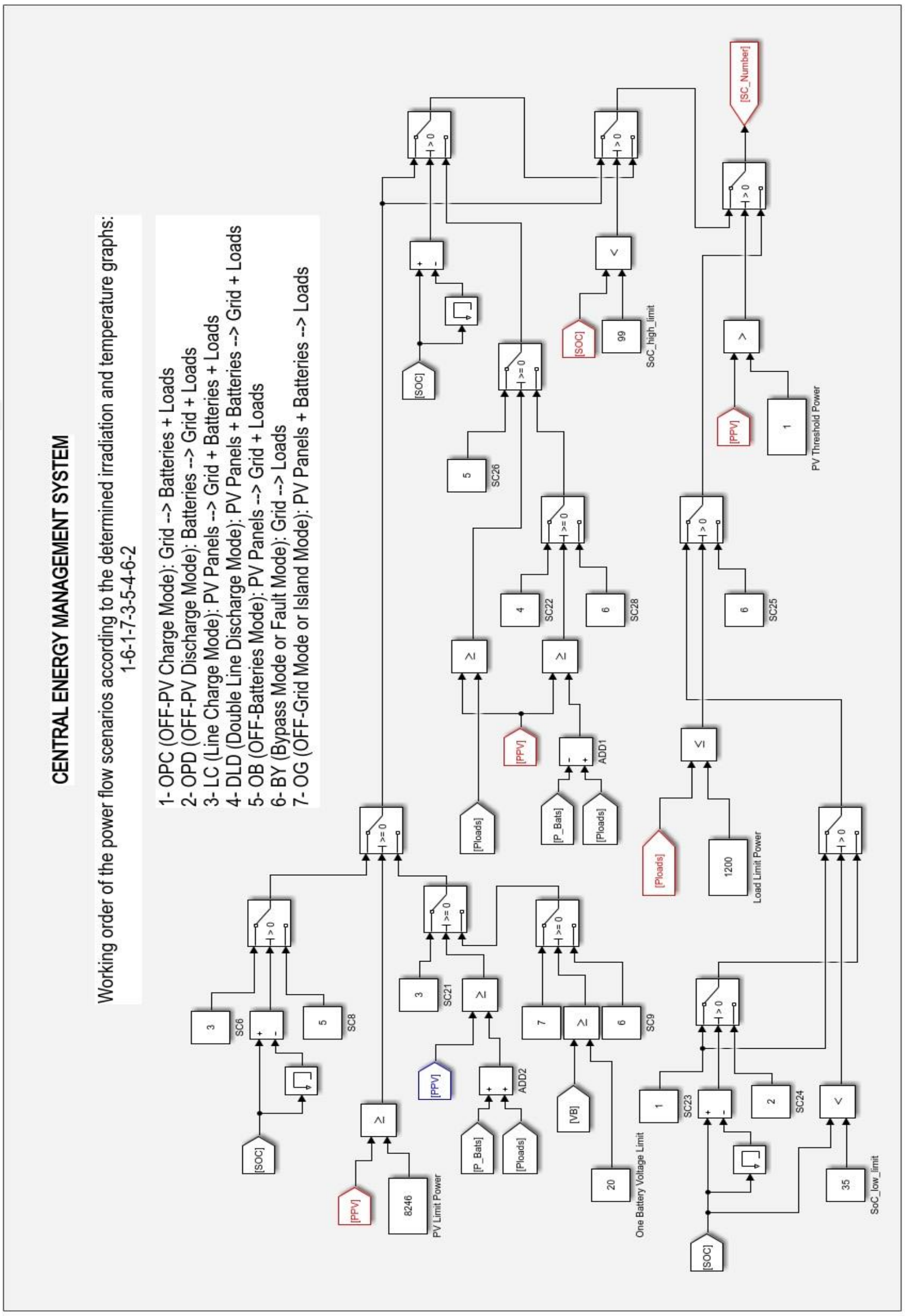

Figure 4.11. Proposed Central Energy Management System at MATLAB/Simulink

First of all, if we explain the operation of the EMS created according to Figures 4.10. and 4.11., we need to obtain instantaneous information about the power produced by the PV panels from the power system, the total power of the batteries, the total power that may occur in the loads and the instantaneous state of charge of the batteries. After receiving this information, we need to measure whether the power value received from the PV panels is more or less than the 1 W power value defined as the threshold, in order to understand whether the system works at night or during the day. According to the irradiance spectrum that is defined in Figure 4.8., the power value received from the PV panels is 0 W, since it coincides with 00:00 in the 0th second and the radiation value is 0 W/m^2.

The next thing is whether the grid power is more or less than the total power of the batteries and loads. The total power of the batteries is 3 kW against the grid power of 10 kW at the beginning, and the total power of the loads is 700+320=1020 W. But the important point here is what should happen when the power demanded from the loads increases? For this reason, scenario 6 will work in cases where the total power of the loads is more than the defined limited load power, and the difference of scenario 6 from scenario 1 is that the batteries are deactivated. Because the main thing here is not to be able to charge the batteries, but to be able to meet the demanded power even from the grid. In this case, since the total load power will be less than the limited load power at the beginning, the answer "yes" comes in the defined next if block.

Another question that follows, "Is the battery charge less than the defined lower limit of charge?" is in the form. Here, since the state of charge of all batteries is initially set to 0% and it is less than the defined 35% lower limit value. Then, the answer of this question is "yes", the power flow scenario number 1 starts working directly. Since the answer will be “no” even if the instantaneous charge state of the batteries goes above the defined lower limit while the scenario number 1 is running. the next question is “does a positive value emerge when the previous charge state is subtracted from the instantaneous charge state of the batteries?” in short, "Are the batteries in charge state?" comes the question. Since the batteries are charged in scenario 1, the answer of the question is "yes", so scenario 1 continues to work.

If the state of charge of the batteries is more than the defined lower limit during the first start of the system, scenario 2 starts to run first, and scenario 1 runs again when the state of charge of the discharged batteries is less than the defined lower limit of SoC in this power flow scenario.

As just explained, while scenario 1 is running, the DC load value was reduced from 700 Ω to 350 Ω in the 3rd second. In this case, the total load power demanded increased from 1020 W to 1720 W. In other words, since the total load power is more than the limited load power, the battery system circuit has been canceled and scenario 6 has started. Similarly, in the 4th second, the total load power was reduced back to 1020 W, and the scenario number 6 was returned to the number 1 scenario.

If the charge current of 1st scenario is high at the beginning and discharge current of the 6th sceneario is low, SoC will be higher than the SoC low limit. Then after the 6th scenario, when demand DC load power is lower than the load limit power, the question will be “does the SoC of the batteries lower than the SoC low limit?” and the answer could be “no”. Then the next question is “does the charging operation continue?” and the answer could be “no” because of the last scenario was 6th. Batteries are discharging at the 6th scenario. Thus, the next power flow scenario could be 2nd. Also batteries are discharging at the 2nd scenario. When the SoC is lower than the SoC low limit (35%), 1st scenario will be active. After the second activation of the 1st scenario, if SoC of the batteries is higher than the SoC low limit at 1st scenario, 1st scenario will be continue. Because, charging process continues. But these conditions are not shown in the simulation process. At this point, only it is desired to verify the EMS algorithm can provide continuity.

HRPS continued to operate in scenario 1 until the power value produced by the PV panels exceeded 1 W. In other words, after the sunrise at 05:30, the other side of the algorithm starts to work. Because the power produced by the PV panels has exceeded 1 W. In this case, since the answer is "yes", in the next question, it is checked whether the charge status of the instant batteries is below the defined upper limit. According to the results in the simulation, the state of charge of the batteries is less than the defined upper limit and the power produced by the PV panels is checked again. At this point, a threshold power is defined. Since the new PV panels have just started to produce power, a value below the defined limited power comes out. Since the answer is "no" here, this time, in another question, it is checked whether the power value received from the PV panels is more than the total power of the loads and the sum of the instantaneous power of the batteries. Here, the answer is "no" again. Then, a voltage value of the one battery should be controlled if it is higher or not than a defined voltage limit (20 V). Batteries are charged at 1^{st} scenario and their voltage values excess this voltage limit. Therefore, the answer is "yes" and 7^{th} scenario will be active. Then, total power of the PV panels or solar power becomes more than the sum of the instantaneous batteries total power and the demanded load power because of increasing irradiation. Hence, scenario 7 leaves its place to scenario 3.

Total DC load demand power was increased from 1020 W to 5220 W while power flow scenario 3 was running. After the increasing of load demand power, solar power excesses limit PV power (8246 W) because of increasing irradiation again. 8246 W is produced limit power of the PV panels and it is coincidence to 800 W/m^2 irradiation value. Then, the aswer will be "yes" and comes "does charging operation continue or not?" question. 3^{rd} power flow scenario provides to charge batteries and the answer will be "yes" again. Thus, 3^{rd} scenario continues its operation. Thanks to the above limit PV power or limit irradiance value, the network can be fed without waiting for the maximum irradiation. While the operation of 3^{rd} scenario, CC-CV transition is occurred at the batteries.

After the CC-CV transition at charge mode of the batteries, SoC does not lower than defined SoC high limit. Then, continue of the charging process cause to comes us comparing of total solar power and PV limit power. At this point, solar power is still higher than this limit power. Then, scenario 3 is operating because of charging batteries continues. After reaching 100% SoC at batteries at 3rd scenario, charging process is finished. So the next question is "solar power is higher than demand load power or not". Irradiance level for PV panels are still high at this time and total power of PV panels are higher than the demand load power. Thus, power flow scenario 5 starts.

The 5th scenario could be start if batteries are broken at 3rd scenario. When the batteries are charged at CC or CV mode, batteries can have more temperature depends on charging current. If charging process is terminated according to this heat effect, it will be logical that changing scenarios from 3rd to 5th. Because batteries are OFF condition at scenario 5.

After the starting of 5th scenario, irradiance level and solar PV power starts to decrease. When this solar power is not sufficient for meeting the demand power of loads, the answer will be "no". Then, it should be controlled sum of solar power and charged batteries power is higher than total demand load power or not. The answer comes "yes" and then 4th scenario is active.

SoC of batteries are 100% while scenarios 5th and 4th are starting to operate. Solar power is decreased to PV threshold power (1 W) when scenario 4 is active in the proposed EMS process. But, if discharging current is high and SoC of batteries can be lower than SoC high limit. At this condition, batteries does not charge and total solar power is lower than PV limit power. Then, PV power will be lower than the sum of batteries simultaneous power and total demand load power. Then, the answer comes "no" and compairing a voltage value of one of the batteries and one battery voltage limit. If discharging current is low value, voltage of the battery will be higher than the defined voltage limit (20 V). This condition causes to start 7th scenario. But, if discharge current is high value, the voltage of the battery can be lower than the defined voltage limit and it causes to start 6th power flow scenario. In this way, proposed EMS can operate continuosly and properly. These conditions can be possible according to the above explained situations.

When the 4th scenario is running, demand total load power is 1720 W. Then, total solar power is lower than 1 W because of sunset at 20:00. Thus, scenario 4 is terminated. After this case, 6th power flow scenario will be active again, because 1720 W demand load power is higher than the load limit power (1200 W). In this way, only grid feeds the load. As the hours pass, total demand load power is generally decreasing. When the clock is 22:00, demand load power is 1020 W again. Thus, when the question is “total demand power is lower than the limit power or not?”, the answer will be “yes” and SoC of the batteries is higher than the SoC low limit. It causes to comes this next question that is “charging operation continue or not?” Lastly, batteries are OFF condition at 6th scenario and the answer will be “no”. So, it causes to begin starting of 2nd power flow scenario.

The 2nd scenario continues to operate until the SoC value drops below the defined lower limit value (35%). When this decrease occurs, the power flow scenario 1 starts working again.

By determining the power flow scenarios according to the EMS, the equipments that will work in the power system should be activated or passive using a switching controller. In this case, the switch states of the equipment according to the power flow scenarios are shown in the Table-4.2. Figure 4.12. shows the modeling of this switch controller on MATLAB.

Additionally, charge and discharge currents of batteries at all of these power flow scenarios can be adjustable by the proposed EMS users and its related Figure 4.13. demonstrates how can change these current values.

4.2.7. Determination of Switch States according to Power Flow Scenarios

The control mechanism of the switches in Figure 4.12. works as described below.

After deciding which scenario will work in the first part of EMS, the question of which scenario SC_Number is equal to is asked for a total of 3 key names.

Table-4.2. Condition of equipment switches according to scenario types

Scenarios & Switch Names	Inverter Switches (SWinv)	IBDC Switches (SWbat)	IUDC Switches (SWpvp)
SC1 - OPC	1	1	0
SC2 - OPD	1	1	0
SC3 - LC	1	1	1
SC4 - DLD	1	1	1
SC5 - OB	1	0	1
SC6 - BY	1	0	0
SC7 - OG	0	1	1

For example, if SC_Number = scenario 3; For SWinv, it is first asked if SC_Number = 1, since the answer is "no", the value "0" is connected to the false part of the if tool box in SIMULINK workspace. This "0" value that comes later corresponds to the question of SC_Number = scenario 6 in the second if tool box. If the answer is still "no", the value 0 continues from the false part of the tool box. Then SC_Number = coincides with the question of scenario 2? If the answer is still "no", the value 0 continues from the false part of the tool box. Finally, in the if tool box number 3, SC_Number = scenario 3 is asked. Here the answer is “yes” and the value “1” comes from the true part of the tool box. It continues in this way and when asked if it is equal to other scenarios, the answer will be "no", so the false connected parts are continued and as a result of this process, it is understood that the inverter and the grid will be used in this scenario, with the SWinv switches being 1 in the 3rd scenario. The same logic, question, answer and similar connection types have been made in this mechanism for other switches in accordance with the scenarios.

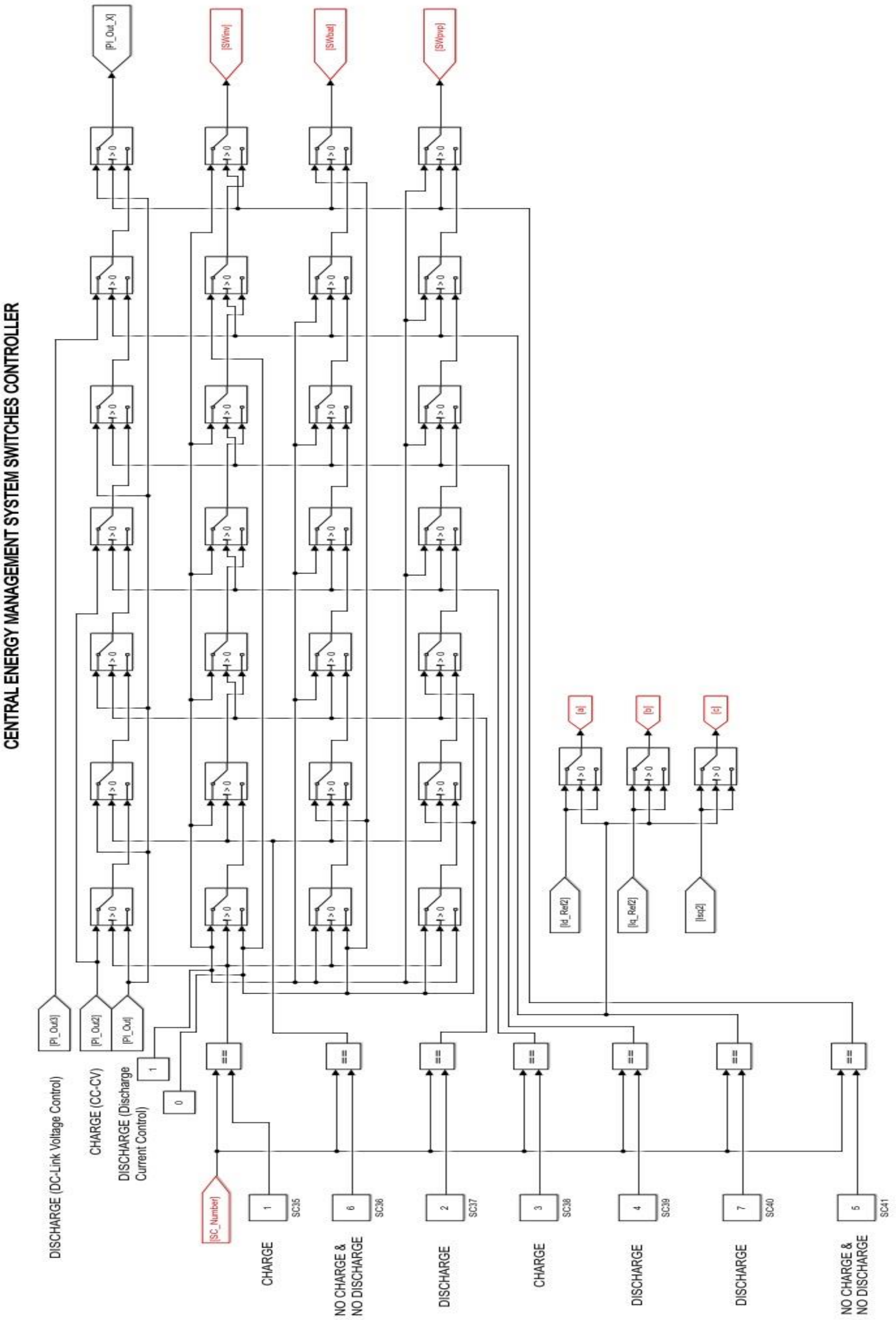

Figure 4.12. Selection of switch states according to power flow scenarios

4.2.8. Inverter Controller Mechanism according to Power Flow Scenarios

Since the DC-Link voltage controller is used in all scenarios for the inverter, the parameters of the DC-Link voltage controller will be used in the same way no matter which scenario the SC_Number value is equal to.

At this point, even though the Id_Ref2, Iq_Ref2 and Isq2 values are SC_Number = 1, and the answer is yes or no, the same values are connected to both the true and false parts of the tool boxes to ensure the same parameters in all scenarios.

4.2.9. Operation of Charge and Discharge Controller of Batteries according to Power Flow Scenarios

First of all, in order to decide the charge or discharge of the batteries, the status of the PI controller output values used while modulating the 4 IGBTs connected to the DC-Link side of the isolated bidirectional DC-DC converter is very important.

During the operation, a PI_Out2 value is calculated as an output in the CC-CV charge controller and the PI_Out value is calculated in the discharge current controller at the same time.

Which of these two values to use is decided according to which one is equal to PI_Out_X. So PI_Out_X value is used to control the trigger signals mentioned above.

For example, in scenario 4, the batteries are discharged and the PI output to be used should be PI_Out. So PI_Out_X must be PI_Out. For this, in the controller shown in Figure-4.12, it is first asked if SC_Number = 1, since the answer is "no", at this point the PI_Out value is connected to the false part of the first if tool box. Afterwards, it is asked if SC_Number is equal to scenarios 6, 2 and 3, respectively. Since the answers are still "no", the PI_Out value continues from the false part of the next if tool boxes. Then comes the question whether SC_Number is equal to scenario 4. The answer is “yes”, and at this point, since we want the batteries to discharge in scenario 4, the PI_Out value is connected to the true part of the next tool box this time. Since the SC_Number value is not equal to 7th and 5th scenarios, the answers will be "no", and the PI_Out value continuing from the false parts of the other if tool boxes will be equal to the PI_Out_X value and the discharge operation will be performed successfully.

In other power flow scenarios, charge and discharge states are determined by the same logic and similar connection types.

4.2.10. Operation of Controller in PV Panels according to Power Flow Scenarios

At this point, there is no need to make any energy management system. Because no matter what power flow scenario operation HRPS is in, the photovoltaic power system continues to work in the MPPT – P&O algorithm designed.

4.2.11. Charge-Discharge Current Controller according to Power Flow Scenarios

In the designed EMS, it is also aimed that the charge and discharge currents can be manually defined and controlled from outside. Because in this way, according to the closed or open state of the air or the SoC values of the batteries, we can power the charge and discharge currents at the desired value for the desired time and number of times, and we can charge our batteries as much as we want. In accordance with this situation, the charge-discharge current control mechanism, which is the 3rd part of the EMS shown in Figure 4.13., is used.

In the way this controller works, first of all, CHC and DSCHC parameters should be written instead of the current values entered through the charge and discharge controllers of the batteries. Then, for example, when the system is operating in scenario 1, the CHC charging current will be 12 A, and when the system is not operating in scenario 1, the CHC charging current will appear as 12 A in scenario 3. In these scenarios, charging currents was chosen same. By using the structure in Figure 4.13., current selections of both CHC and DSCHC can be made according to the scenarios and these values can be changed manually. For example, in scenario 2, DSCHC is defined as 7 A. In short, the way the system works is similar to the switching controllers. For other scenarios, similar comments can be made and performed on this controller.

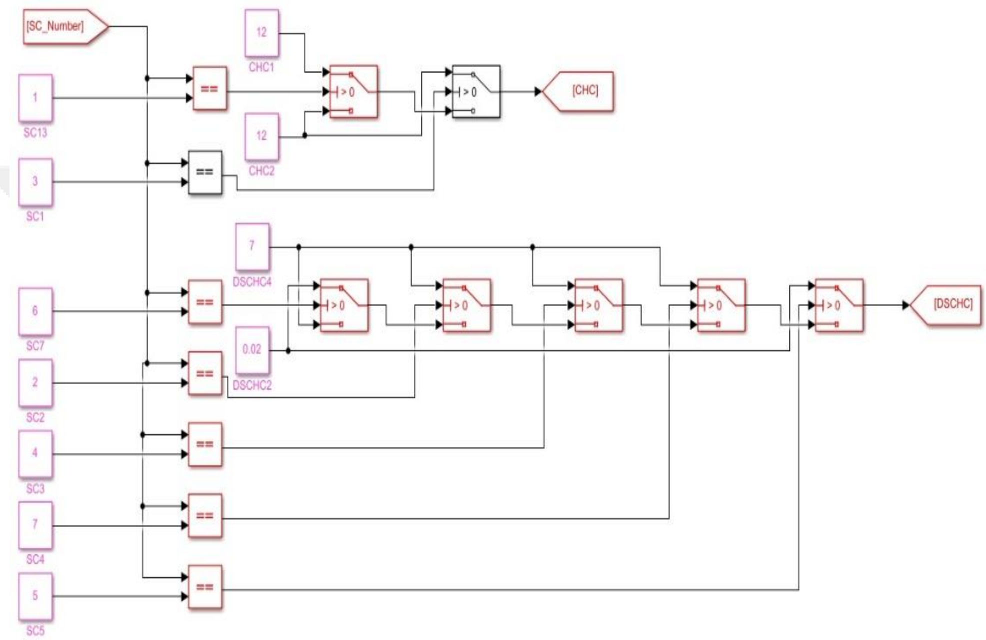

Figure 4.13. Charge-Discharge current control mechanism according to power flow scenarios

5. PERFORMANCE ANALYSIS OF PROPOSED HYBRID REGENERATIVE POWER SYSTEM AND EMS

This topic includes manuel operation results of power flow scenarios without the proposed EMS on HRPS at first 7 chapter and 8th part results are obtained by operating these power flow scenarios with the proposed rule-based EMS. After the simulation results efficiency calculations are shown for each power flow scenario. But these efficiency results can not be compared each other because of they are executed at different load levels. Only information can be obtained about how efficient the power flow scenarios are according to these given load levels. Finally, cost efficiency results are given at 9th chapter.

5.1. Results of OFF-PV Charge Mode (Scenario-1)

- Grid connected inverter operates with DC-Link voltage control for holding DC-Link voltage to 700 V.
- Batteries are charged by 10 A with CC-CV control at IBDC topology.
- All of the related graphics of power system components are given at next figures with OPC power flow scenario.
- DC Load is 350 Ω at this simulation and different load values can be defined at this scenario.

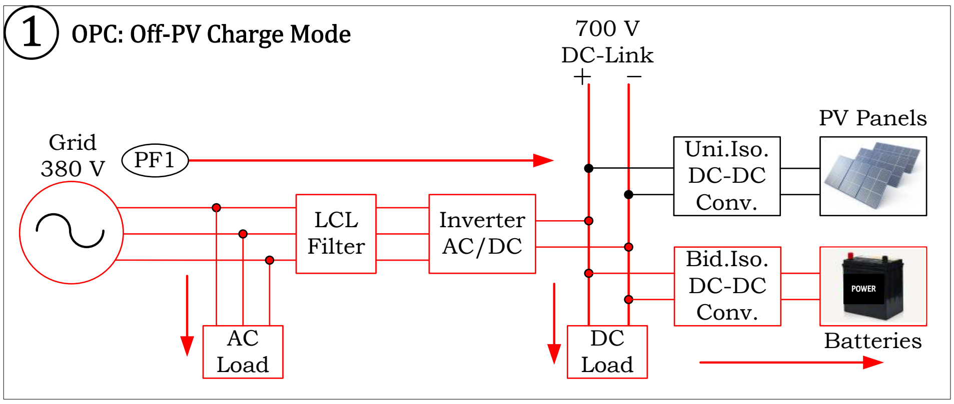

Figure 5.1. OFF-PV Charge Mode (Scenario-1)

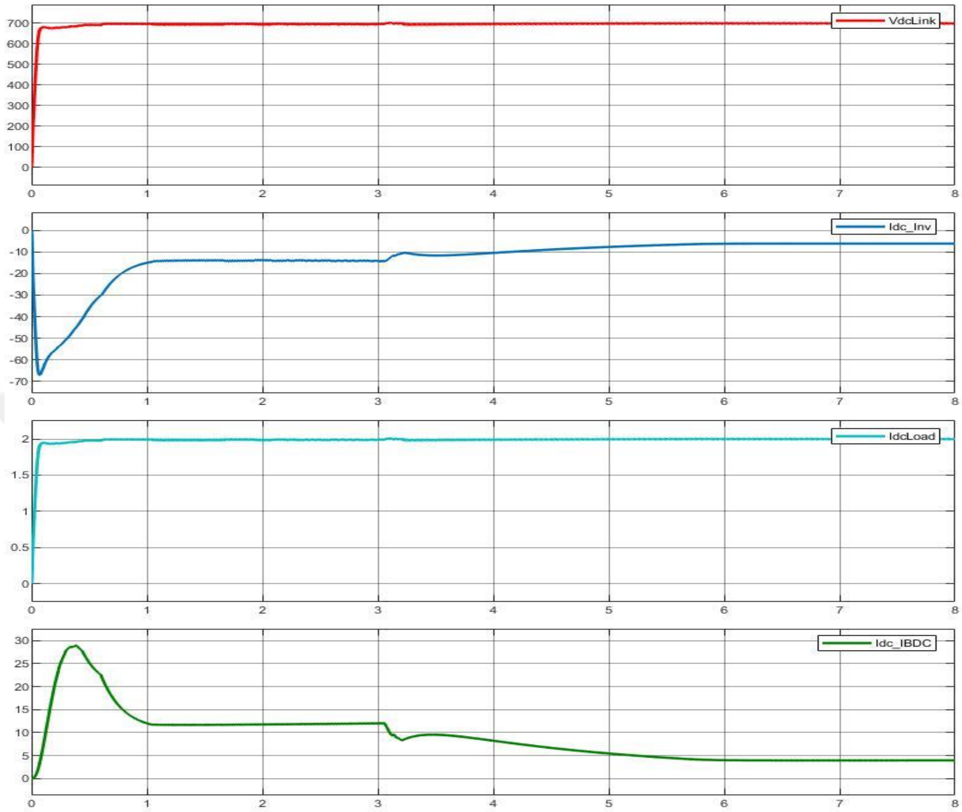

Figure 5.2. DC-Link Voltage, Inverter output current, DC-Load current and input current of IBDC respectively.

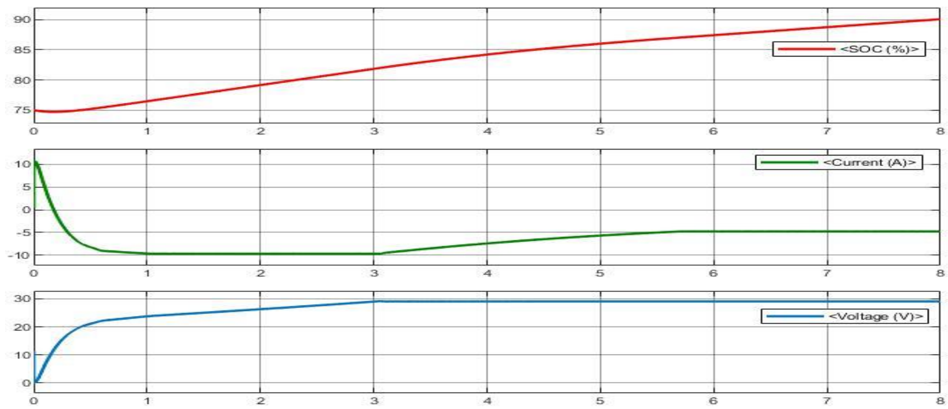

Figure 5.3. SoC, current and voltage values of one battery.

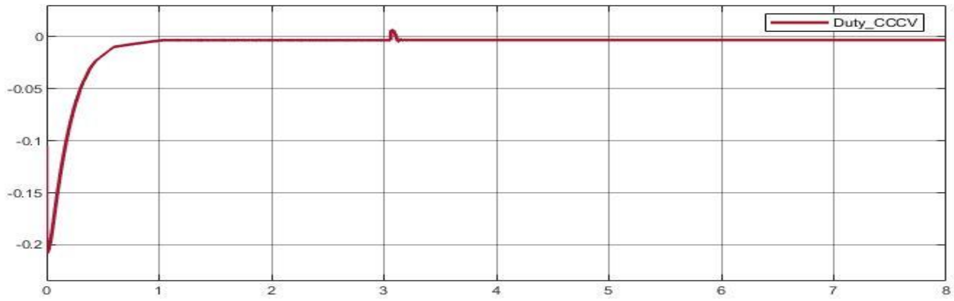

Figure 5.4. Duty value of CC-CV control for batteries.

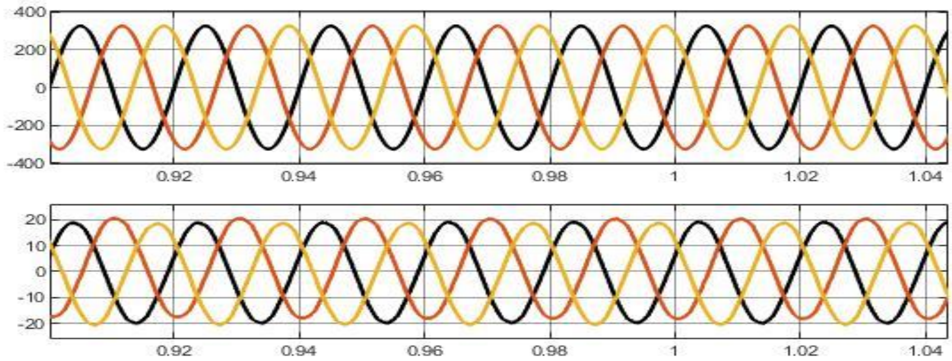

Figure 5.5. Grid voltage and current waveforms at CC condition.

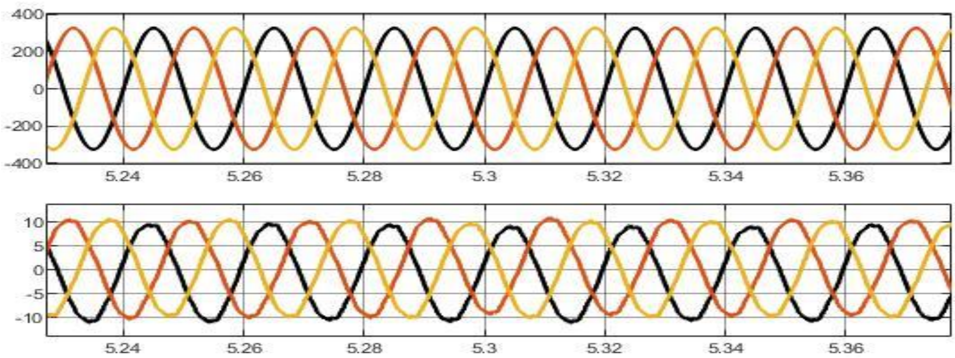

Figure 5.6. Grid voltage and current waveforms at CV condition.

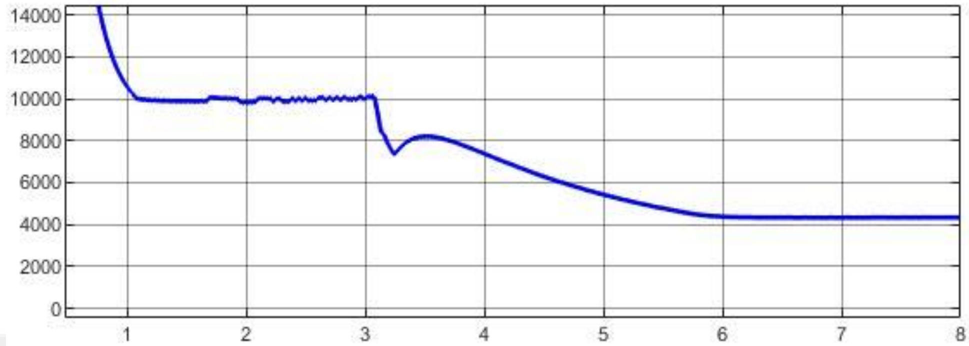

Figure 5.7. Supply power from grid.

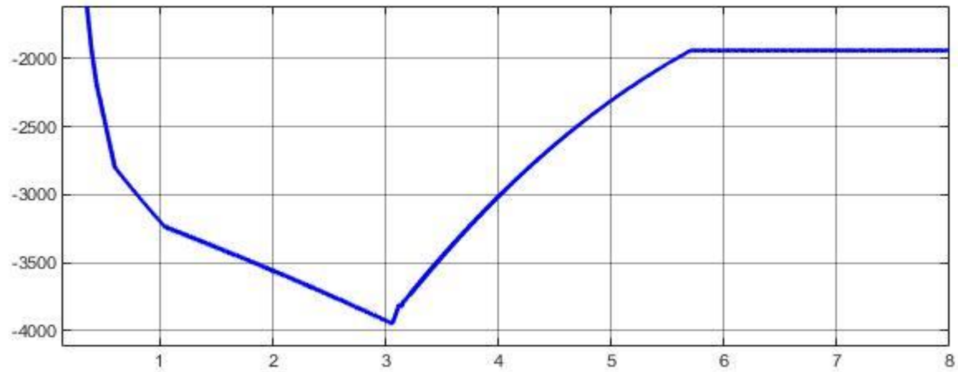

Figure 5.8. Batteries total charge power.

Power Balance and System Efficiency Calculations:

Between 6 – 8 seconds;

Input Power (from Grid) = 4080 W

DC Load Power = (700 / 350) x 700 = 1400 W

Batteries Charge Power = 4.8 A x 29.4 V x 14 = 1976 W

Power Loss of the System = 4080 – 1400 – 1976 = 704 W

Efficiency = ((4080 – 704) / 4080) x 100 = % 82.75

5.2. Results of OFF-PV Discharge Mode (Scenario-2)

- Grid connected inverter operates with DC-Link voltage control for holding DC-Link voltage to 700 V.
- Batteries are discharged by 4 A with discharge current control at batteries connected IBDC topology.
- All of the related graphics of power system components are given at next figures with OPD power flow scenario.
- This scenario can be also accomplished by defining available DC and AC loads. These results are taken for no-load condition.

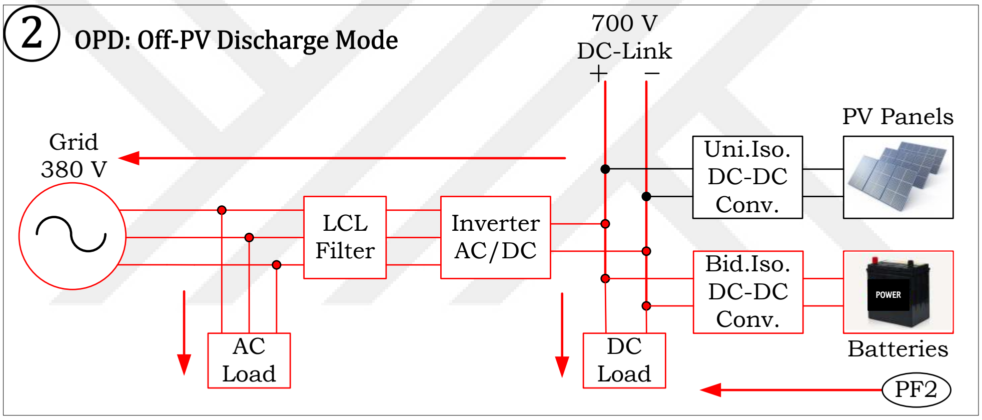

Figure 5.9. OFF-PV Discharge Mode (Scenario-2)

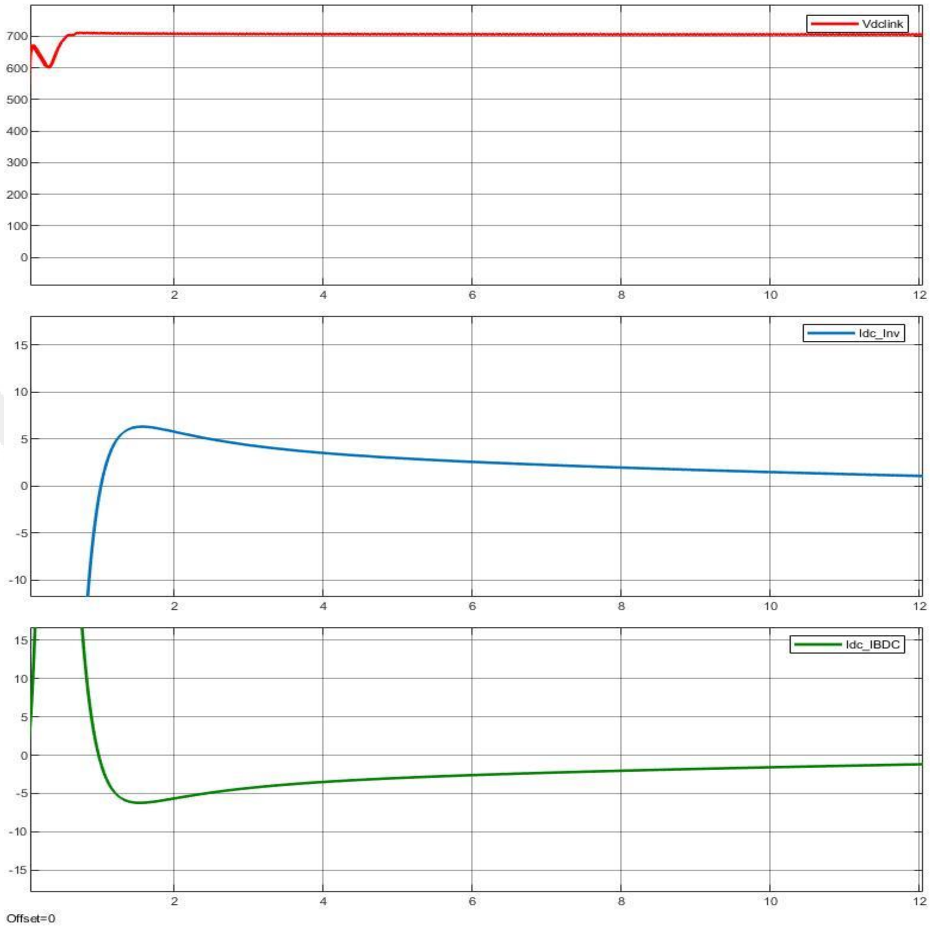

Figure 5.10. DC-Link Voltage, inverter input current and IBDC output current

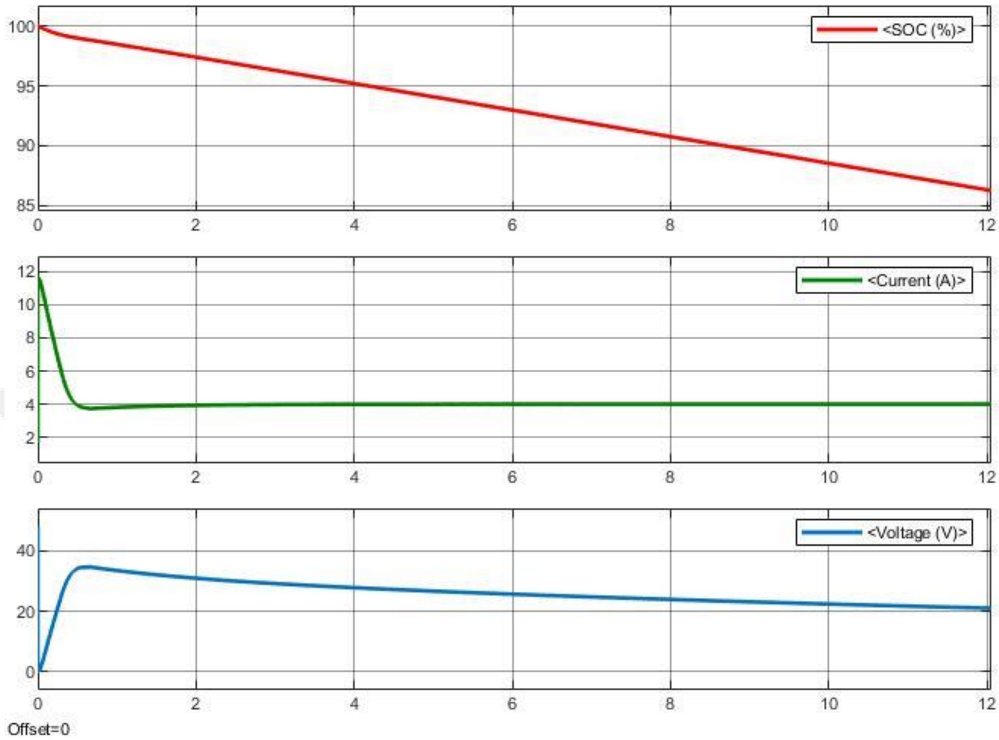

Figure 5.11. SoC, current and voltage values of one battery.

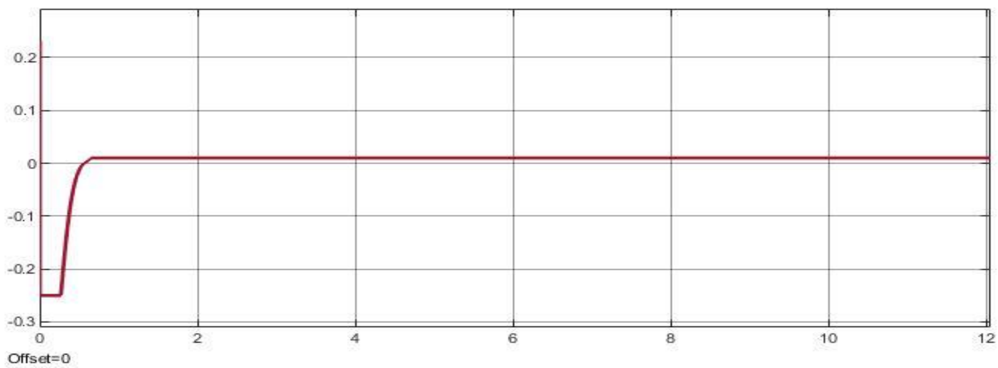

Figure 5.12. Discharge Current Control Duty value.

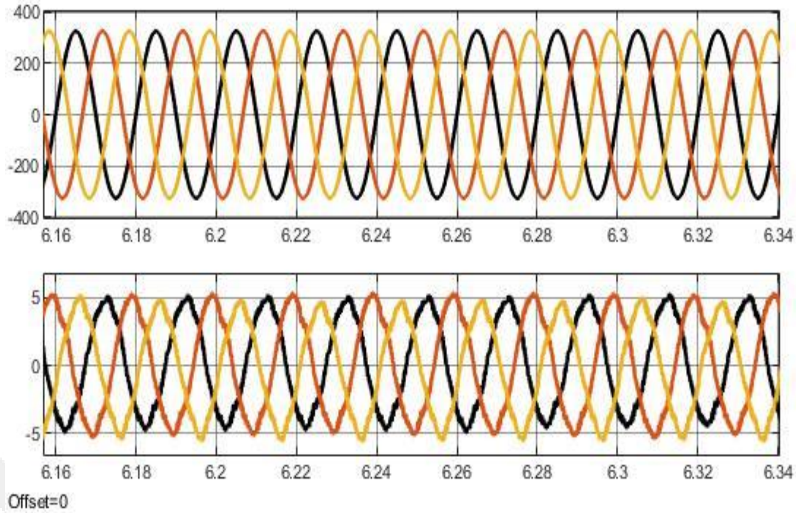

Figure 5.13. Grid voltage and current waveforms

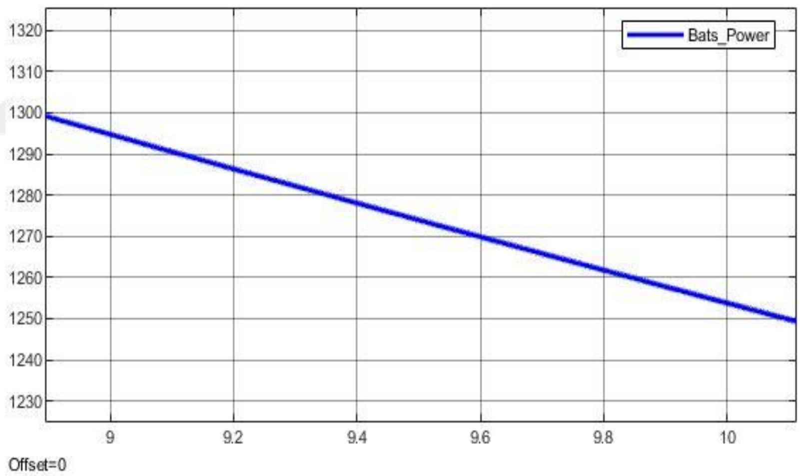

Figure 5.14. Batteries Total Source Power

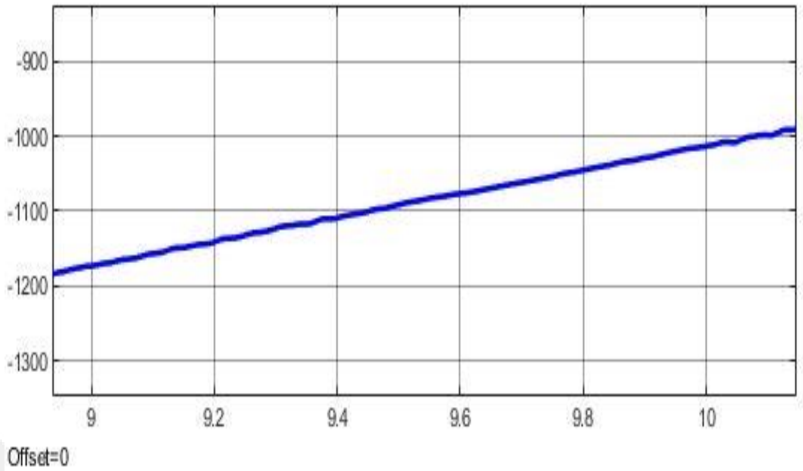

Figure 5.15. Injected Grid Power

Power Balance and System Efficiency Calculations:

For average value at 9.5 second;

Input Power (from Batteries discharge power) = 1275 W

Injected Grid Power = 1120 W

Power Loss of the System = 1275 – 1120 = 155 W

Efficiency = ((1275 – 155) / 1275) x 100 = % 87.84

5.3. Results of Line Charge Mode (Scenario-3)

- Grid connected inverter operates with DC-Link voltage control for holding the DC-Link voltage to 700 V.
- Batteries are charged by 10 A with CC-CV control at batteries connected IBDC topology.
- PV panels connected UDC operates with MPPT-P&O algorithm at 1000 W/m^2 irradiance and 25 $°C$ temperature.
- All of the related graphics of power system components are given at next figures with LC power flow scenario.

- DC Load = 350 Ω and AC Loads = 500 Ω in the simulation. Different load values, different irradiance – temperature levels and charge current can be adjusted in this scenario.

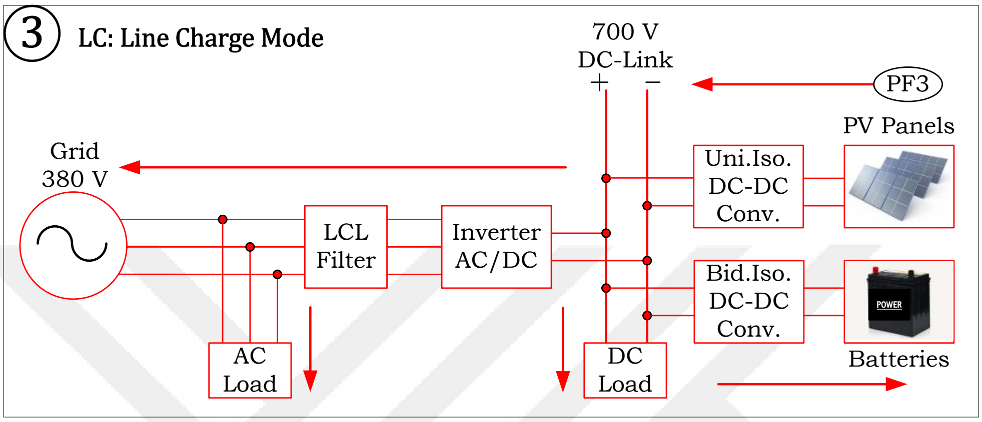

Figure 5.16. Line Charge Mode (Scenario-3)

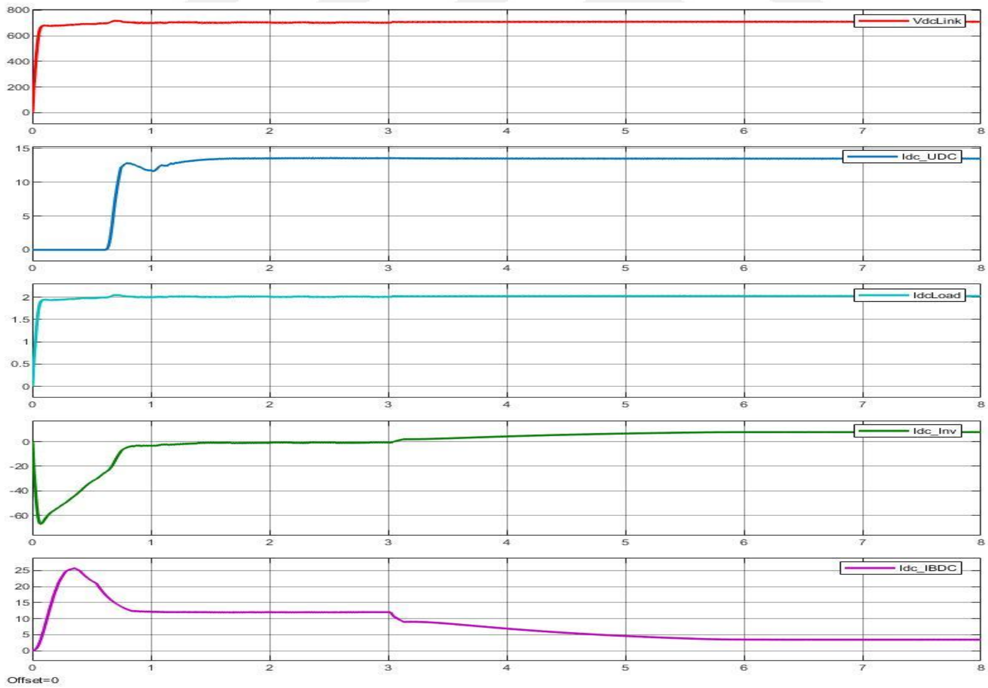

Figure 5.17. DC-Link voltage, UDC output current, DC Load current, Inverter input current and IBDC input current

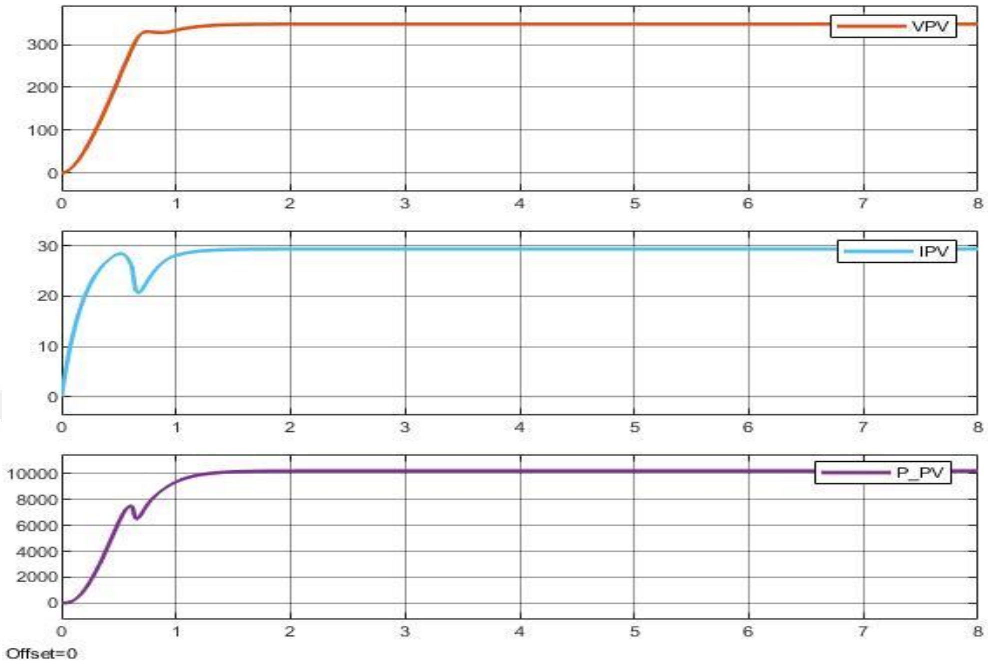

Figure 5.18. Voltage, current and power values of PV panels

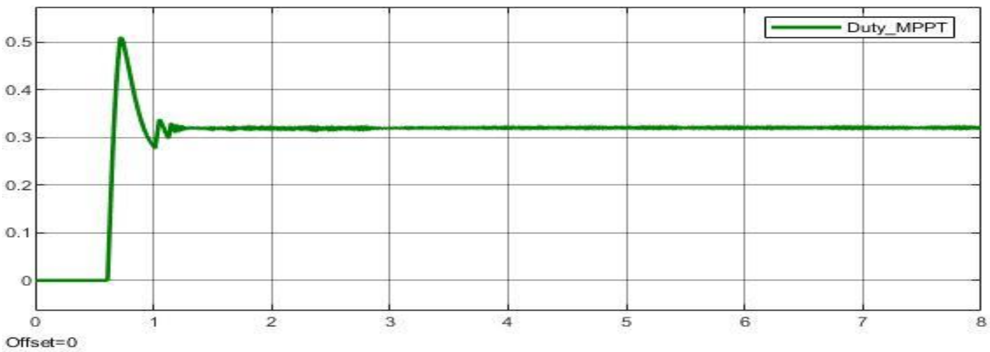

Figure 5.19. MPPT-PI output duty value

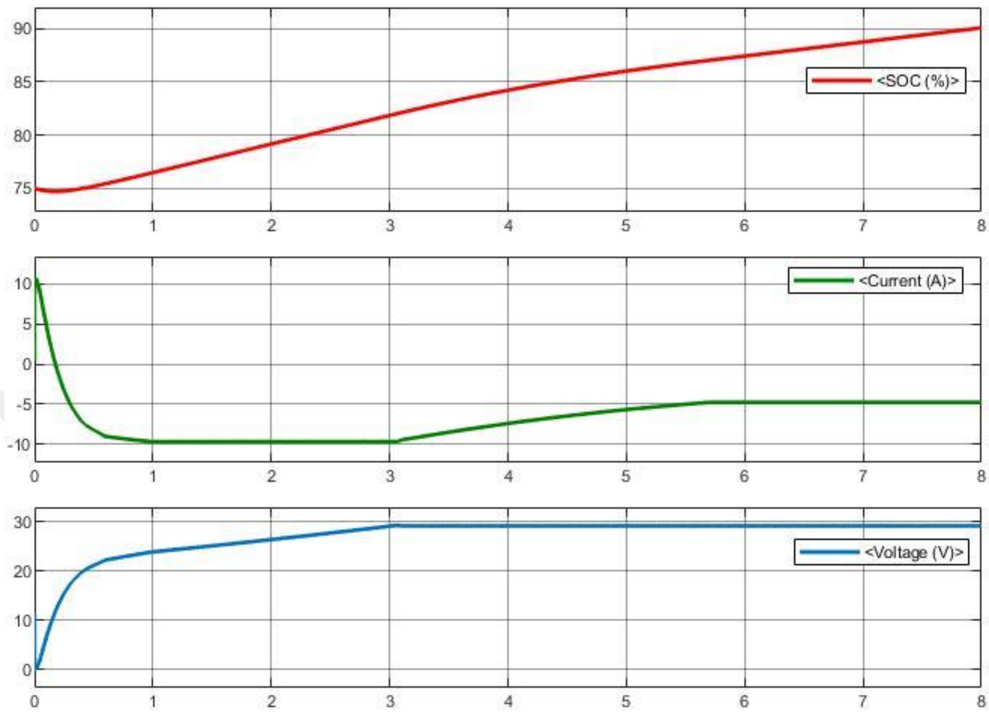

Figure 5.20. SoC, current and voltage values of one battery

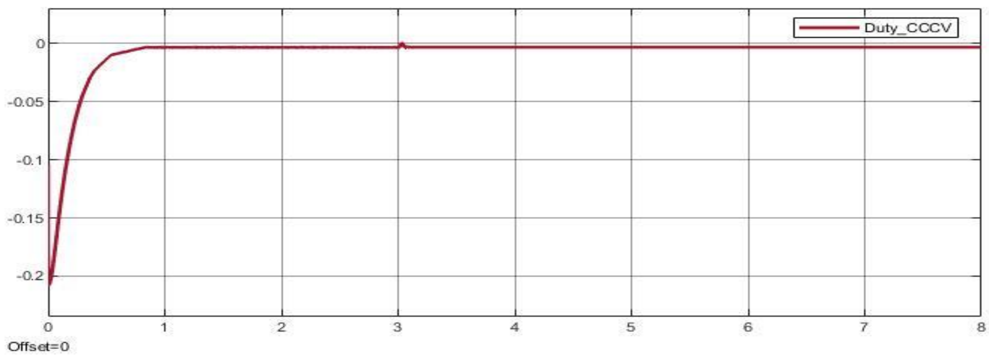

Figure 5.21. CC-CV control PI output duty value

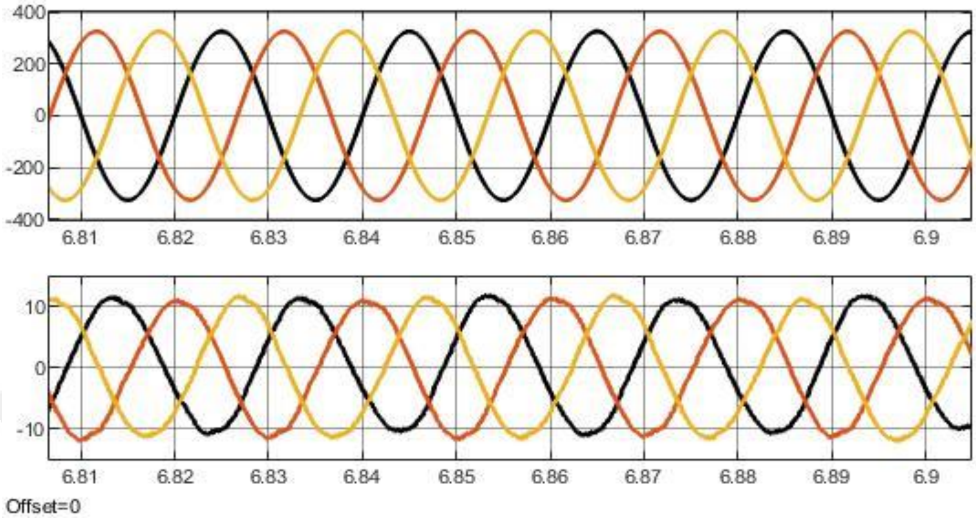

Figure 5.22. Grid voltage and current waveforms

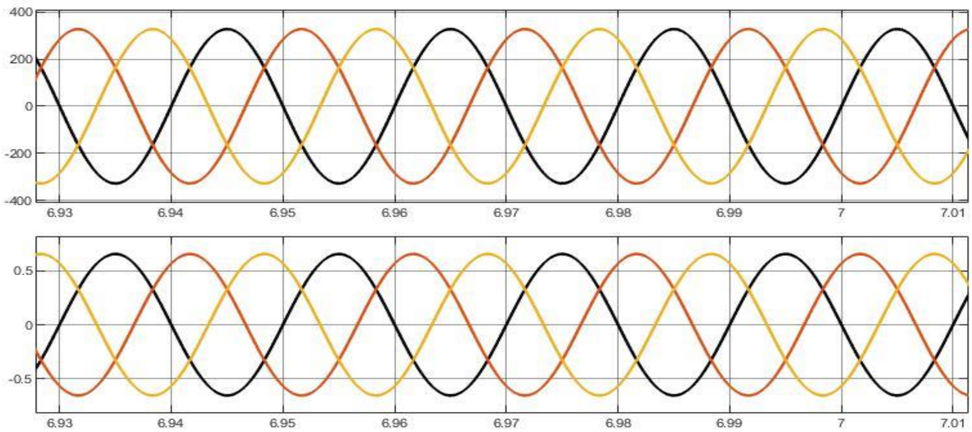

Figure 5.23. AC Load voltage and current waveforms

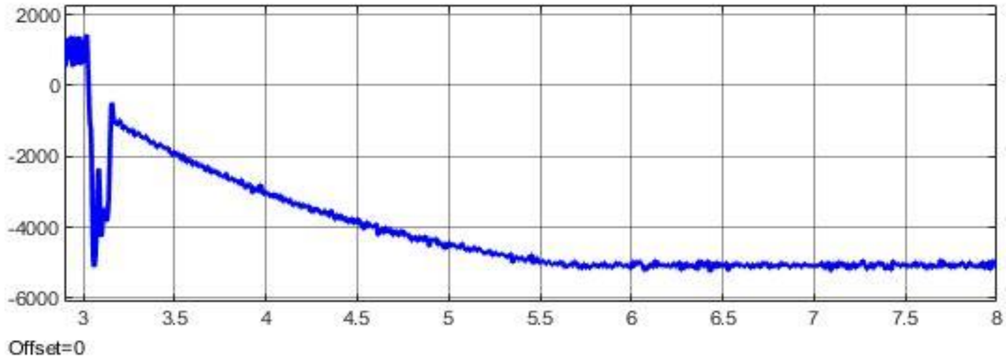

Figure 5.24. Injected Power of Grid

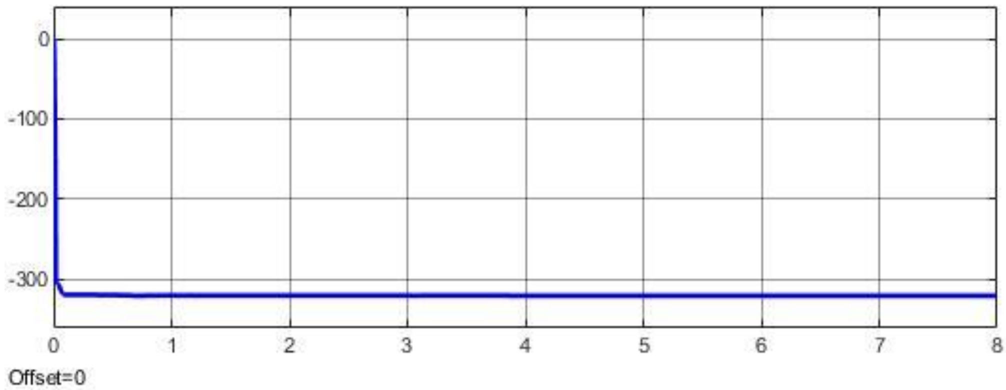

Figure 5.25. Injected AC-Load Power

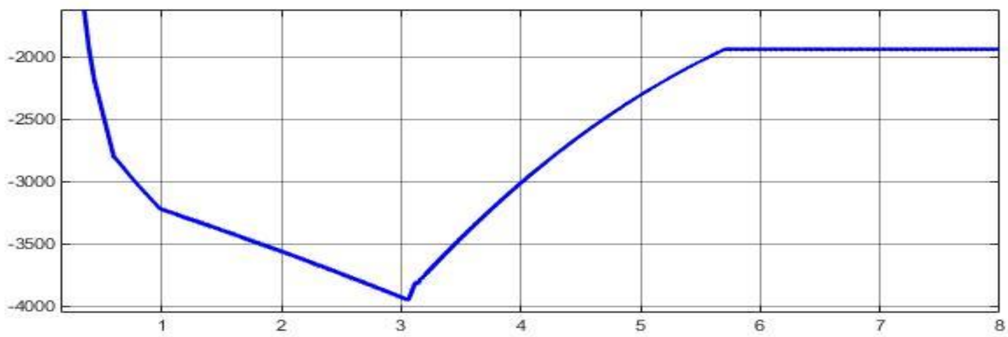

Figure 5.26. Batteries Total Charge Power

Power Balance and System Efficiency Calculations:

Between 6 – 8 seconds;

Input Power (from PV panels) = 10200 W

DC-Load Power = (700 / 350) x 700 = 1400 W

Injected AC-Load Power = 320 W

Batteries Charged Power = 4.8 A x 29.4 V x 14 = 1976 W

Injected Grid Power = 5000 W

Power Loss of the System = 10200 – 1400 – 320 – 1976 – 5000 =1504 W

Efficiency = ((10200 – 1504) / 10200) x 100 = % 85.25

5.4. Results of Double Line Discharge Mode (Scenario-4)

- Grid connected inverter operates with DC-Link voltage control for holding the DC-Link voltage to 700 V.
- Batteries are discharged by 6 A with discharge current control at batteries connected IBDC topology.
- PV panels connected UDC operates with MPPT-P&O algorithm at 1000 W/m^2 irradiance and 25 °C temperature.
- All of the related graphics of power system components are given at next figures with DLD power flow scenario.
- DC Load = 100 Ω and AC Loads = 500 Ω in the simulation. Different load values, different irradiance – temperature levels and discharge current can be adjusted in this scenario.

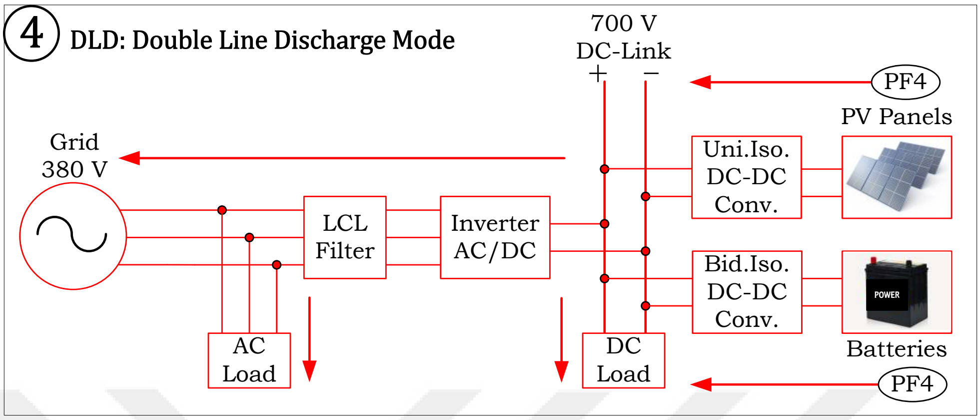

Figure 5.27. Double Line Discharge Mode (Scenario-4)

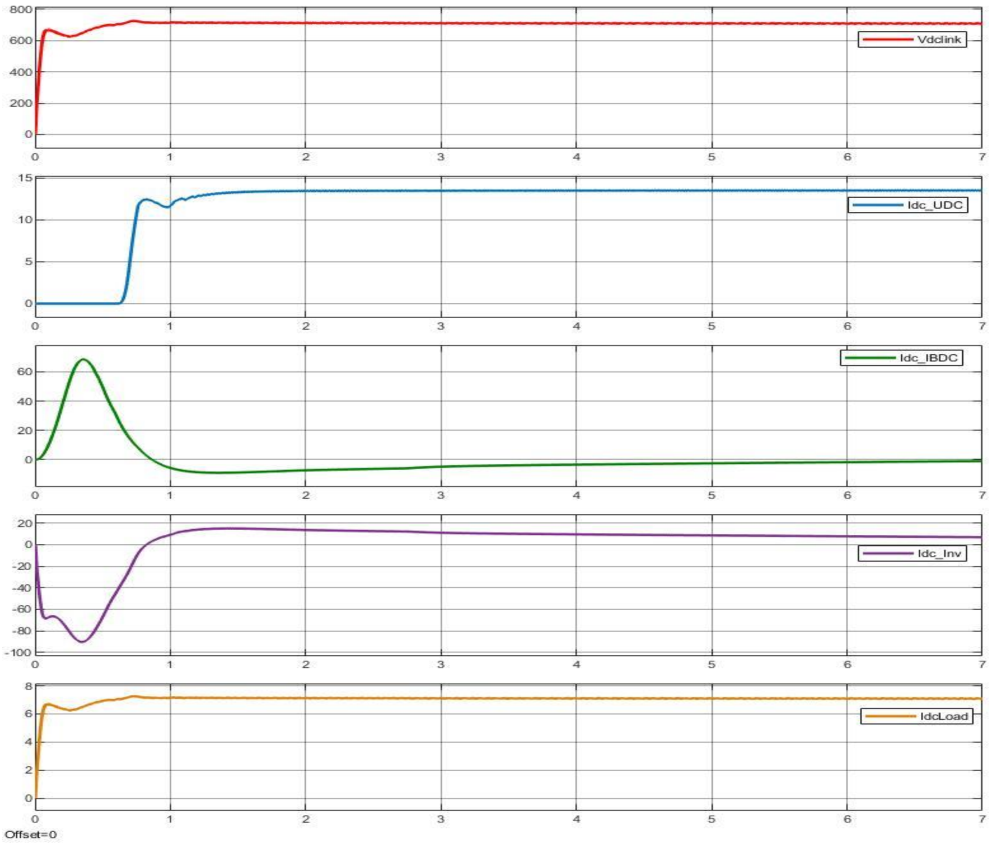

Figure 5.28. DC-Link voltage, UDC output current, IBDC output current, Inverter input current and DC-Load current

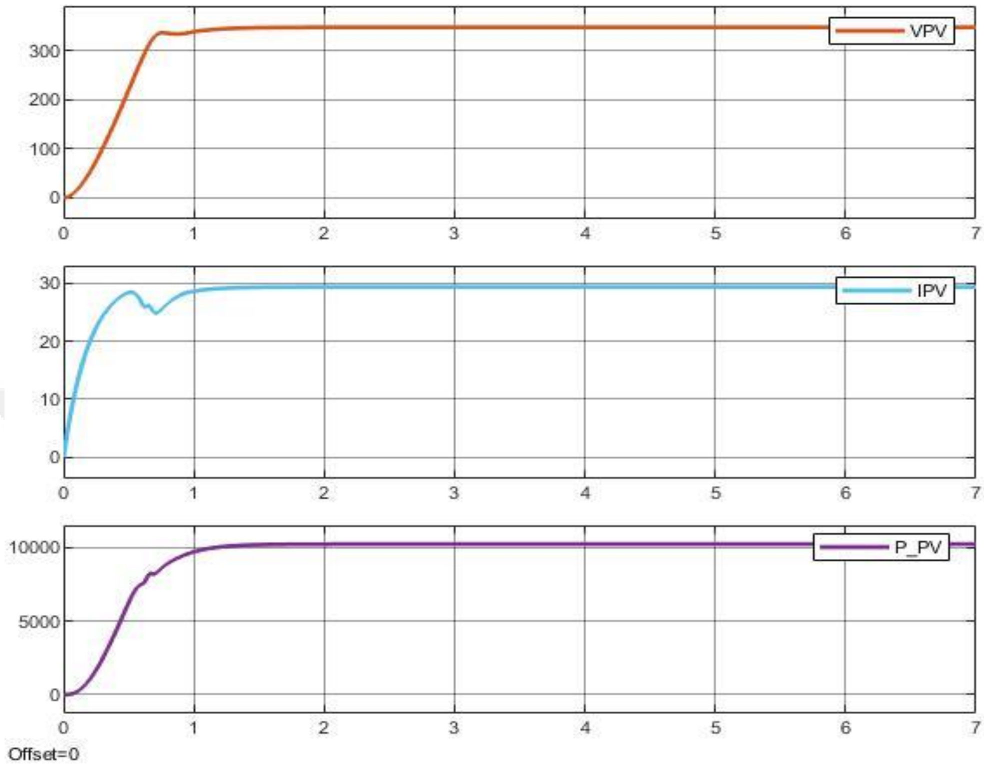

Figure 5.29. Voltage, current and power of PV panels

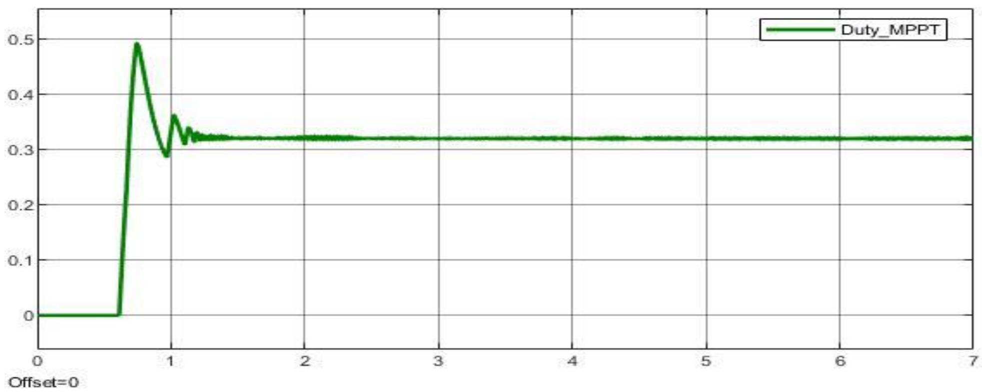

Figure 5.30. MPPT-PI output duty value

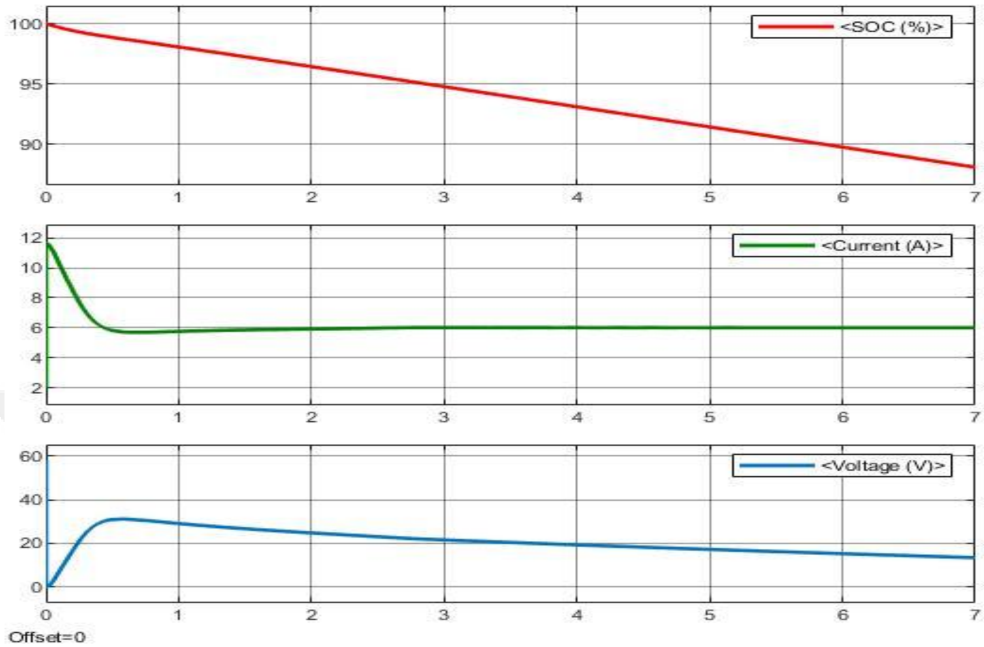

Figure 5.31. SoC, current and voltage values of one battery

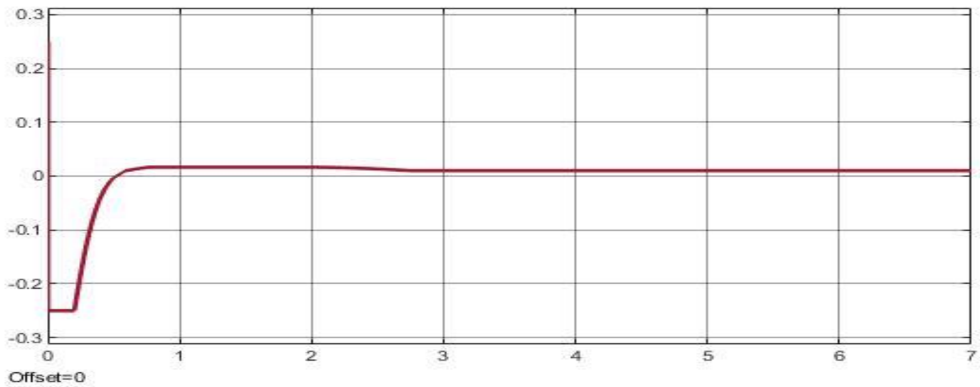

Figure 5.32. Discharge current control PI output duty value

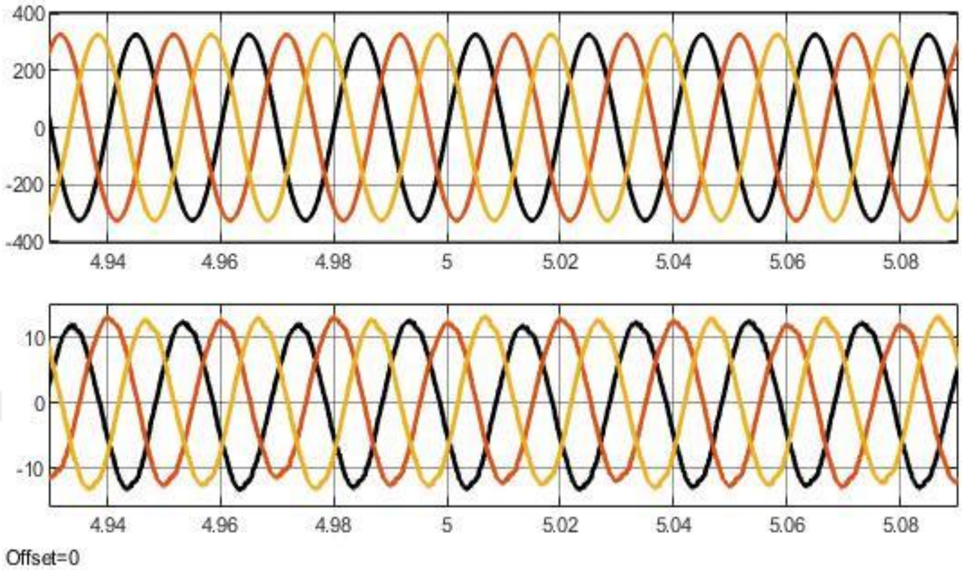

Figure 5.33. Grid voltage and current waveforms

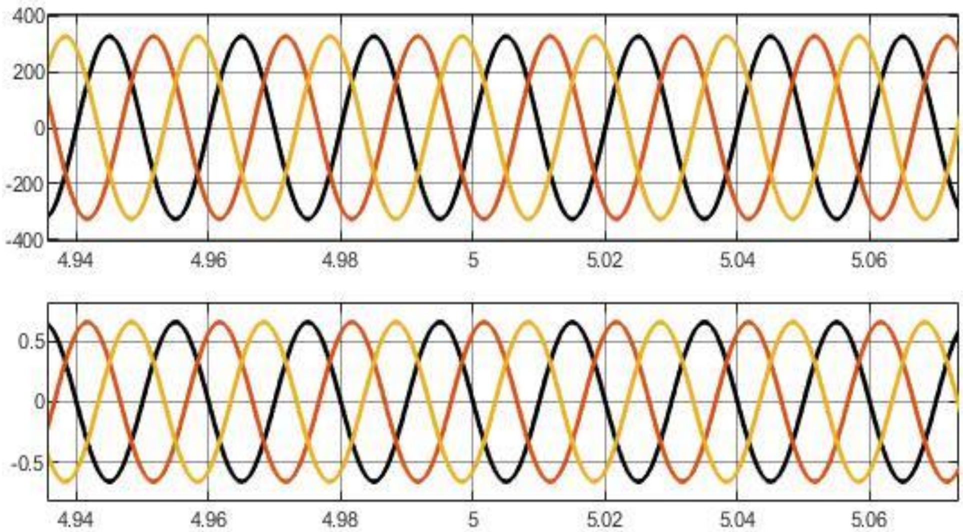

Figure 5.34. AC-Load voltage and current waveforms

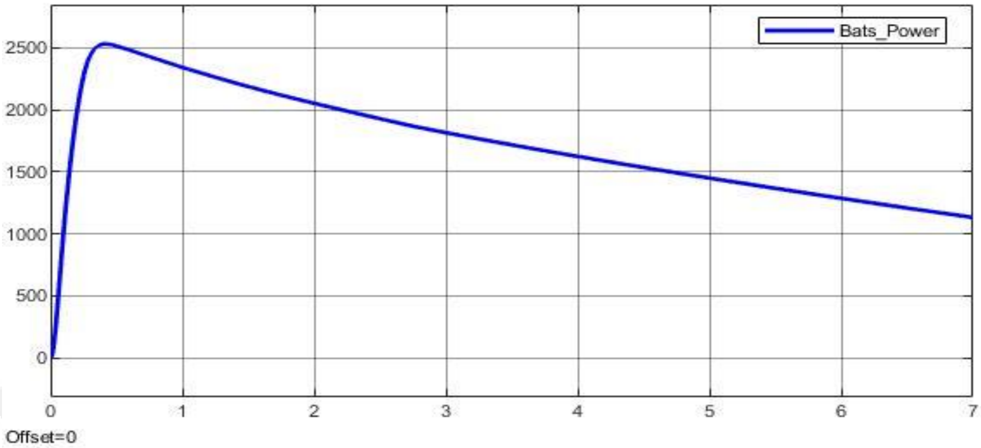

Figure 5.35. Batteries Total Discharge Power

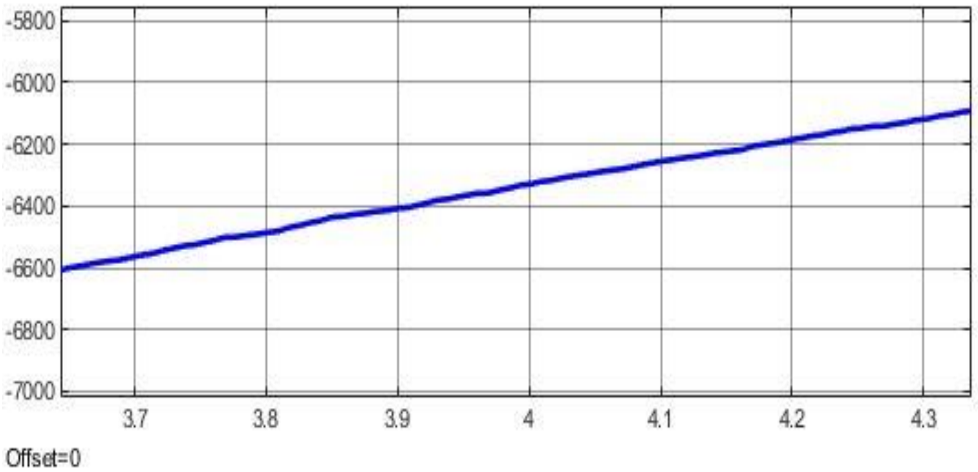

Figure 5.36. Injected Grid Power

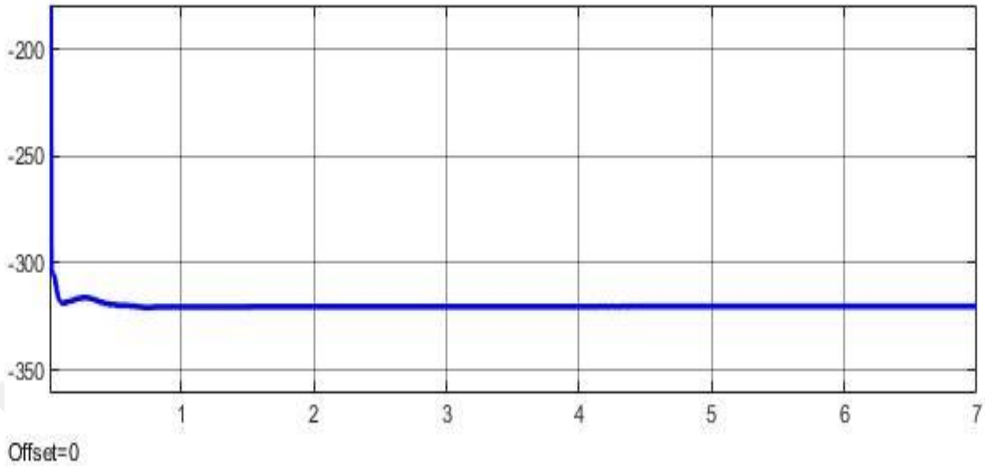

Figure 5.37. Injected AC-Load Power

Power Balance and System Efficiency Calculations:

For average value at 4th second;

Input power (from batteries discharge power and PV panels) = 1625 W + 10200 W = 11825 W

Injected Grid Power = 6325 W

DC Load Power = 700 x 7 = 4900 W

AC Load Power = 320 W

Power Loss of the System = 11825 – (6325 + 4900 + 320) = 280 W

Efficiency = ((11825 – 280) / 11825) x 100 = % 97.63

5.5. Results of OFF-Batteries Mode (Scenario-5)

- All of the components are combined in the proposed HRPS.
- Grid connected inverter operates with DC-Link voltage control for holding the DC-Link voltage to 700 V.
- PV panels connected UDC operates with MPPT-P&O algorithm at 1000 *W/*m^2 irradiance and 25 *°C* temperature.
- All of the related graphics of power system components are given at next figures with OB power flow scenario.
- DC Load = 350 Ω and AC Loads = 500 Ω in the simulation.

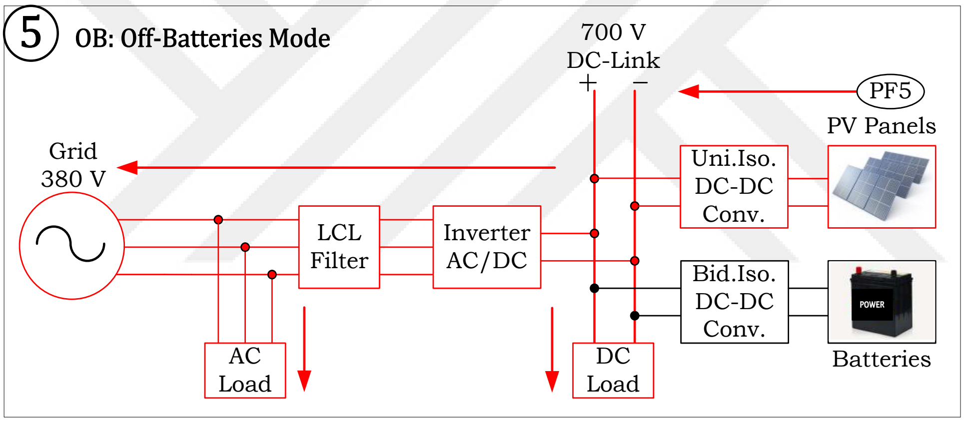

Figure 5.38. OFF-Batteries Mode (Scenario-5)

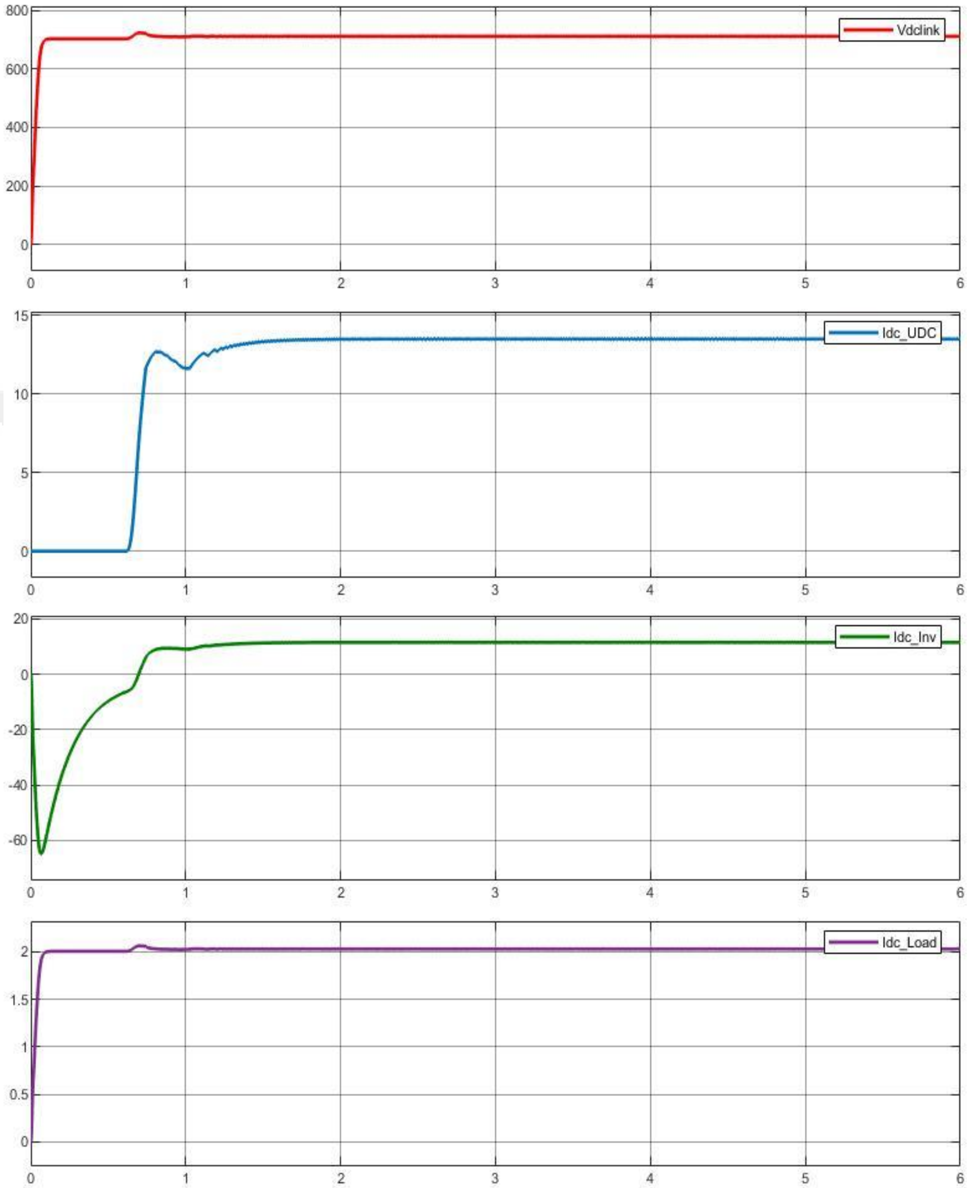

Figure 5.39. DC-Link voltage, UDC output current, Inverter input current and DC-Load current

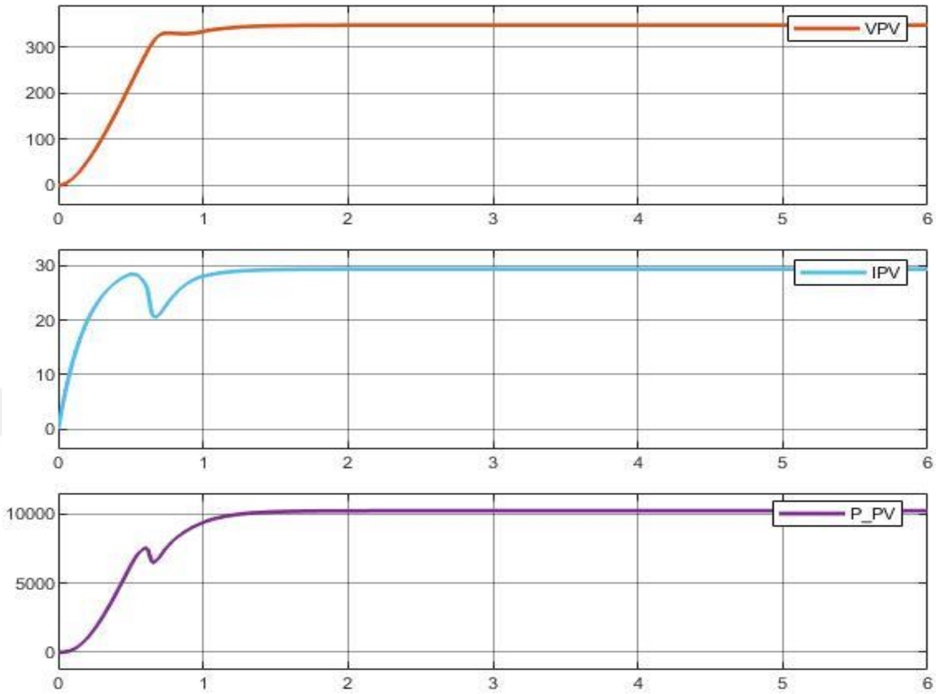

Figure 5.40. Voltage, current and power of PV panels

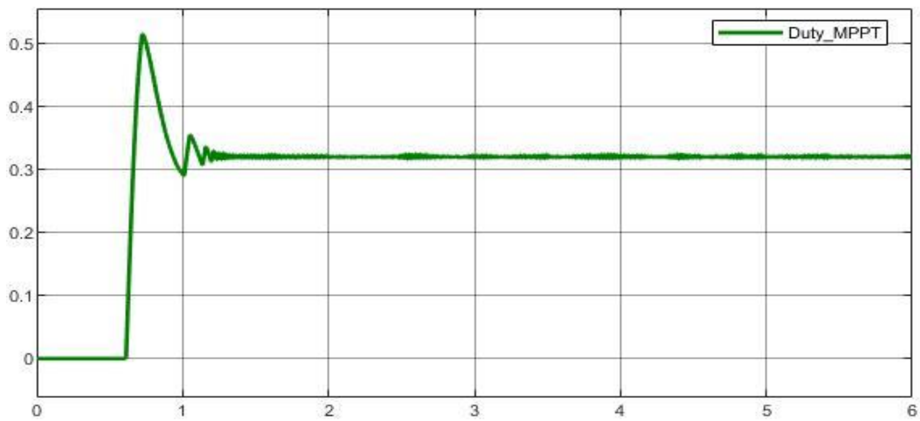

Figure 5.41. MPPT-PI output duty value

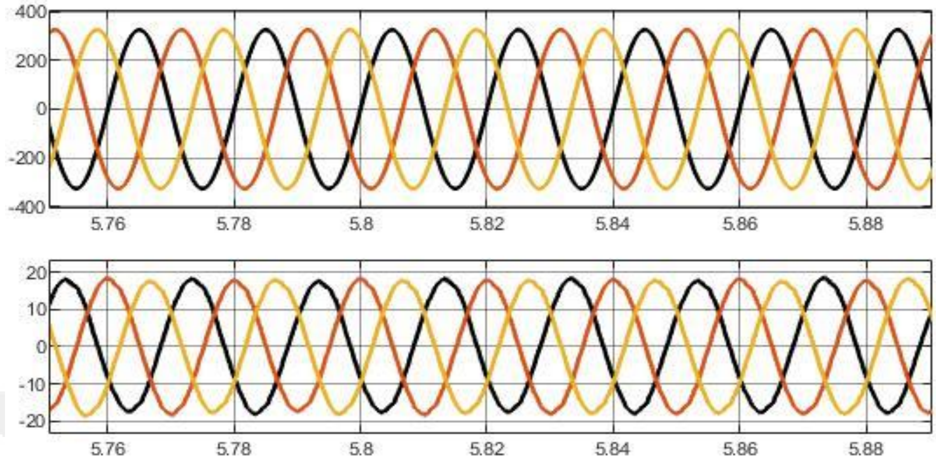

Figure 5.42. Grid voltage and current waveforms

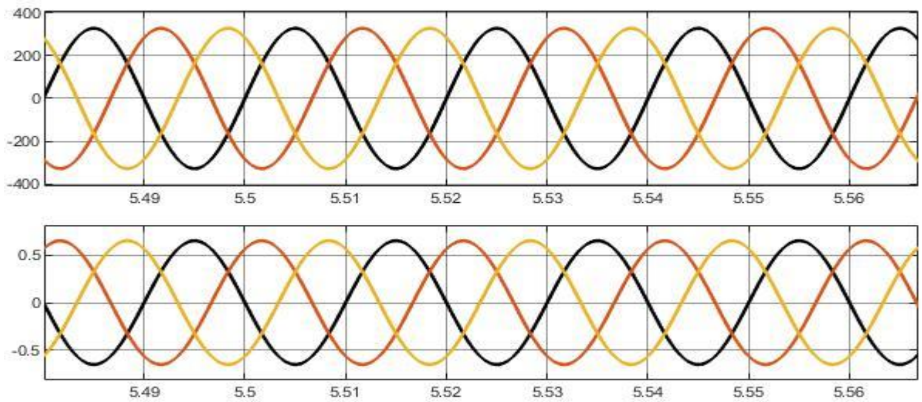

Figure 5.43. AC-Load voltage and current waveforms

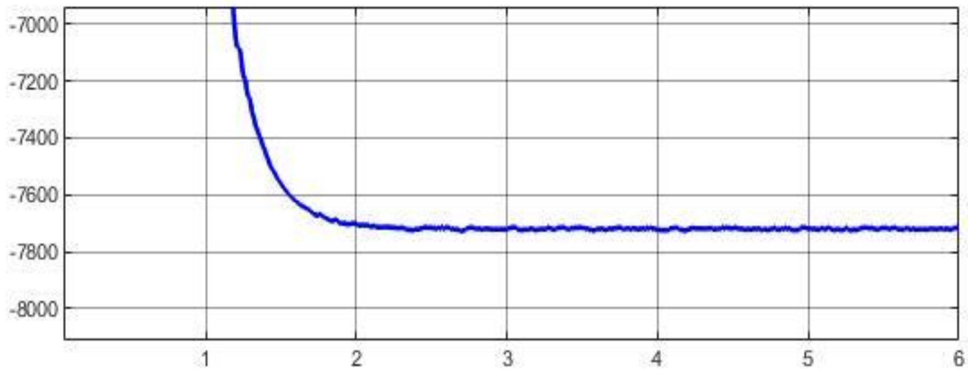

Figure 5.44. Injected Grid Power

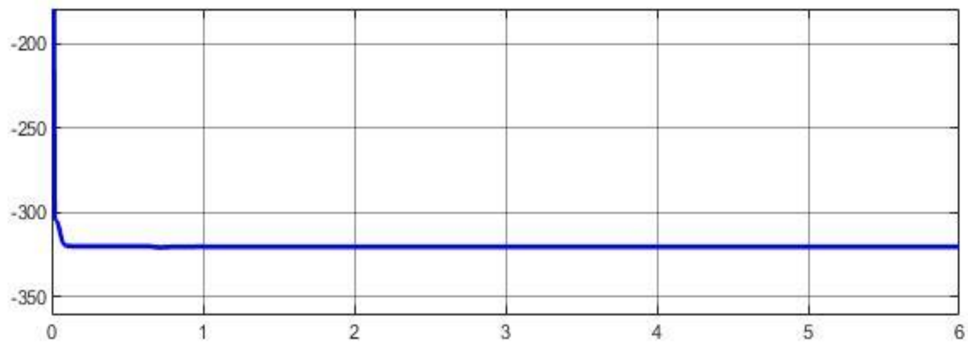

Figure 5.45. Injected AC-Load Power

Power Balance and System Efficiency Calculations:

Input power (from PV panels) = 10200 W

Injected Grid Power = 7725 W

DC Load Power = 700 x 2 = 1400 W

AC Load Power = 320 W

Power Loss of the System = 10200 – (7725 + 1400 + 320) = 755 W

Efficiency = ((10200 – 755) / 10200) x 100 = % 92.60

5.6. Results of Bypass Mode or Fault Mode (Scenario-6)

- All of the components are combined in the proposed HRPS.
- Grid connected inverter operates with DC-Link voltage control for holding the DC-Link voltage to 700 V.
- Batteries and Photovoltaic power systems do not operate in this power flow scenario.
- All of the related graphics of power system components are given at next figures with BY power flow scenario.
- DC Load = 100 Ω and AC Loads = 500 Ω in the simulation.

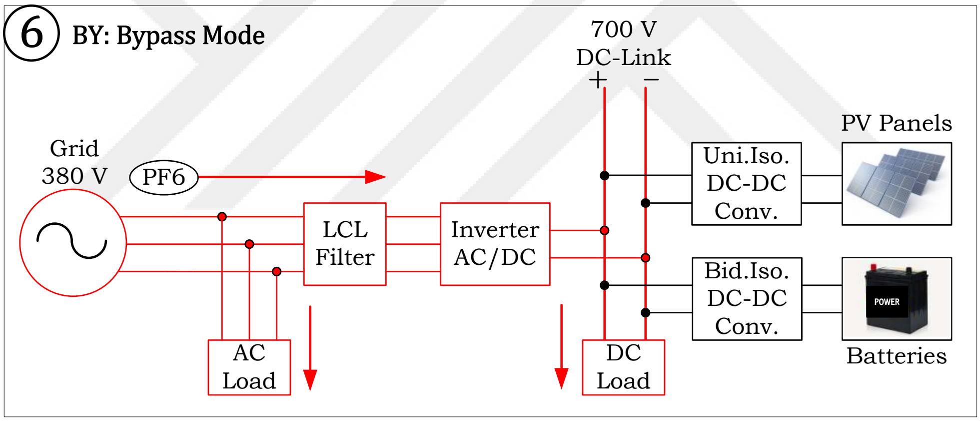

Figure 5.46. Bypass Mode (Scenario-6)

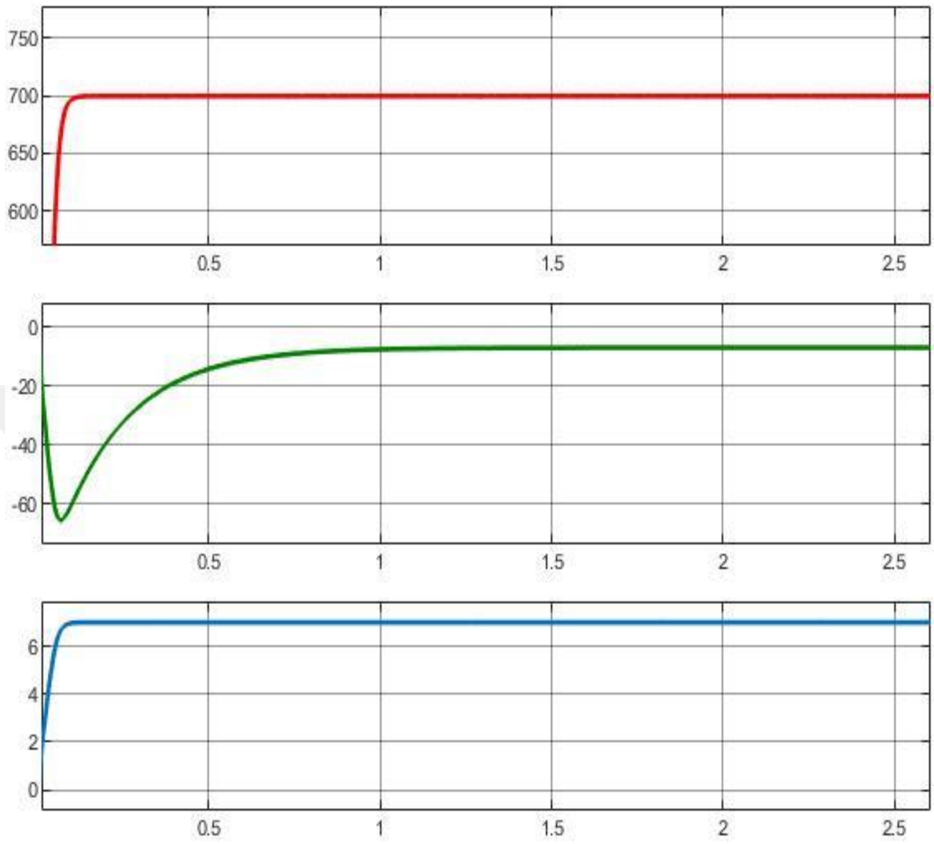

Figure 5.47. DC-Link Voltage, Inverter output current and DC-Load current

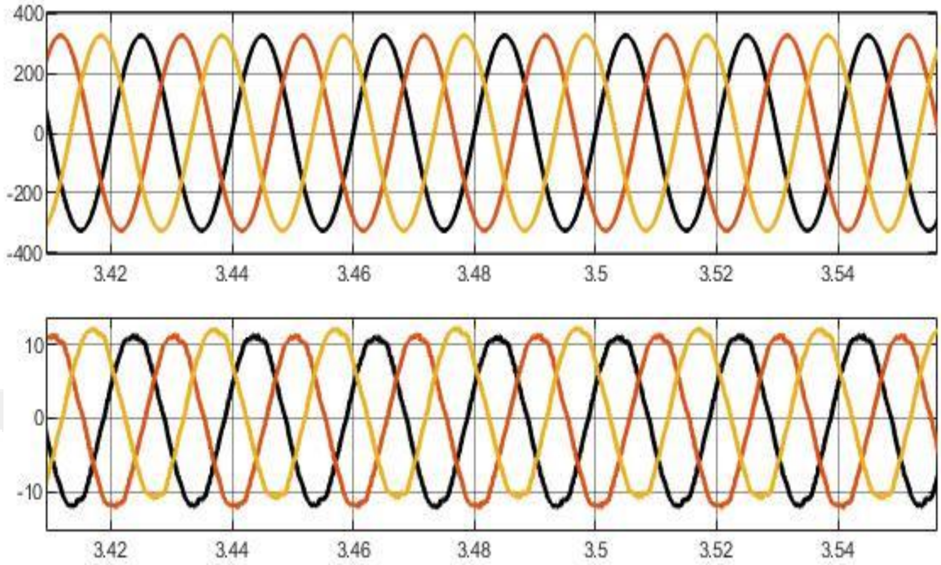

Figure 5.48. Grid voltage and current waveforms

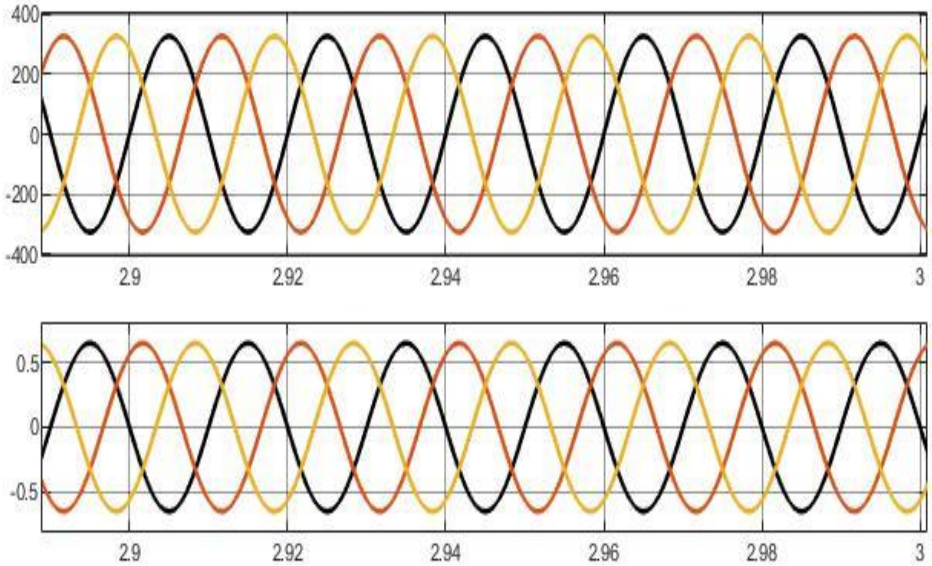

Figure 5.49. AC-Load voltage and current waveforms

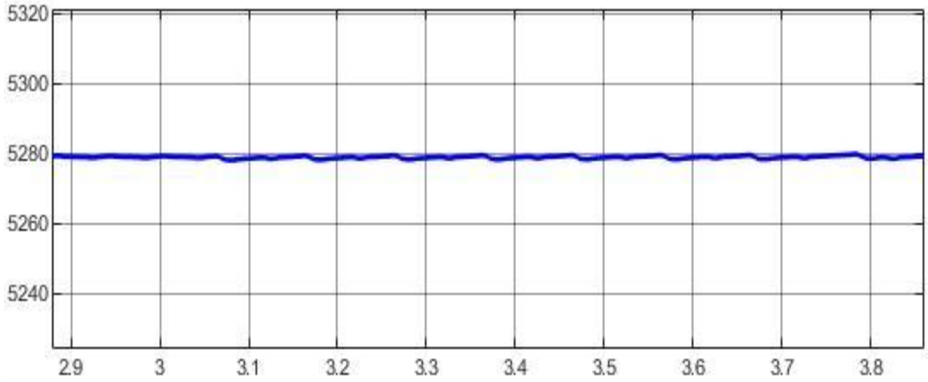

Figure 5.50. Grid Power

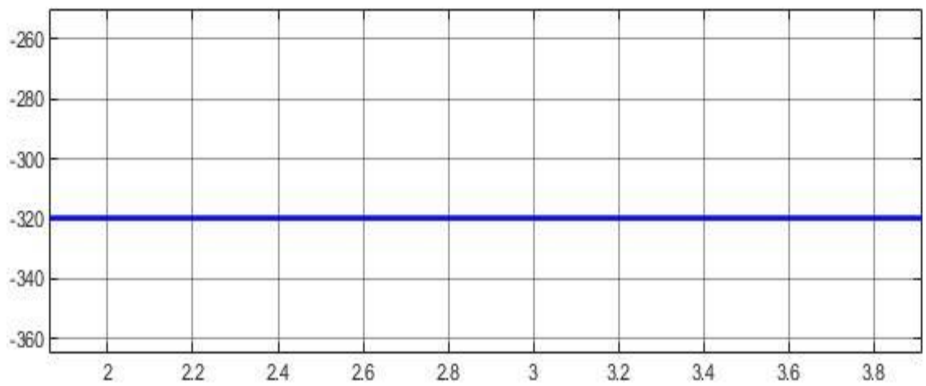

Figure 5.51. AC-Load Power

Power Balance and System Efficiency Calculations:

Between 0.5-4 seconds;

Input power (from Grid) = 5280 W

AC Load Power = 320 W

DC Load Power = 700 x 7 = 4900 W

Power Loss of the System = 5280 – (320 + 4900) = 60 W

Efficiency = ((5280 – 60) / 5280) x 100 = % 98.86

5.7. Results of OFF-Grid Mode or Island Mode (Scenario-7)

- All of the components are combined in the proposed HRPS.
- Grid connected inverter does not operate in this scenario. Thus, DC-Link voltage control of the inverter does not execute for holding the DC-Link voltage to 700 V.
- Batteries are discharged by 6 A with discharge current control at batteries connected IBDC topology.
- PV panels connected UDC operates with MPPT-P&O algorithm at 500 W/m^2 irradiance and 25 $°C$ temperature.
- All of the related graphics of power system components are given at next figures with OG power flow scenario.
- DC Load = 100 Ω and AC Loads are not fed in the simulation.

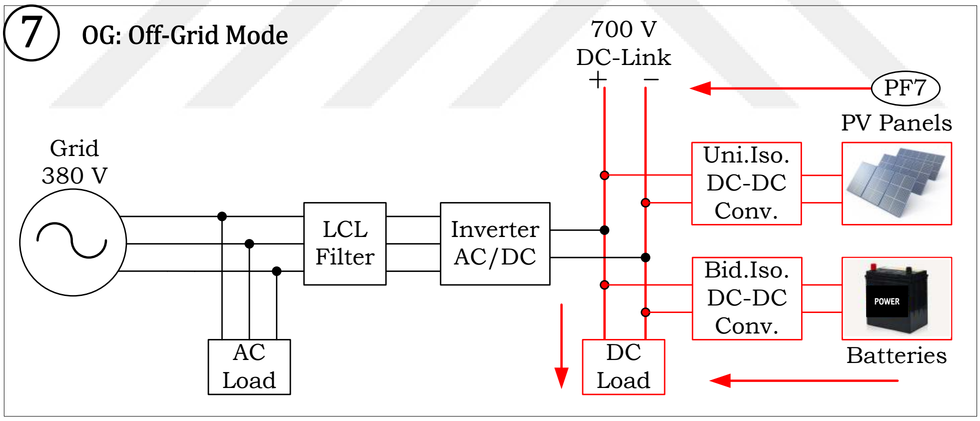

Figure 5.52. OFF-Grid Mode (Scenario-7)

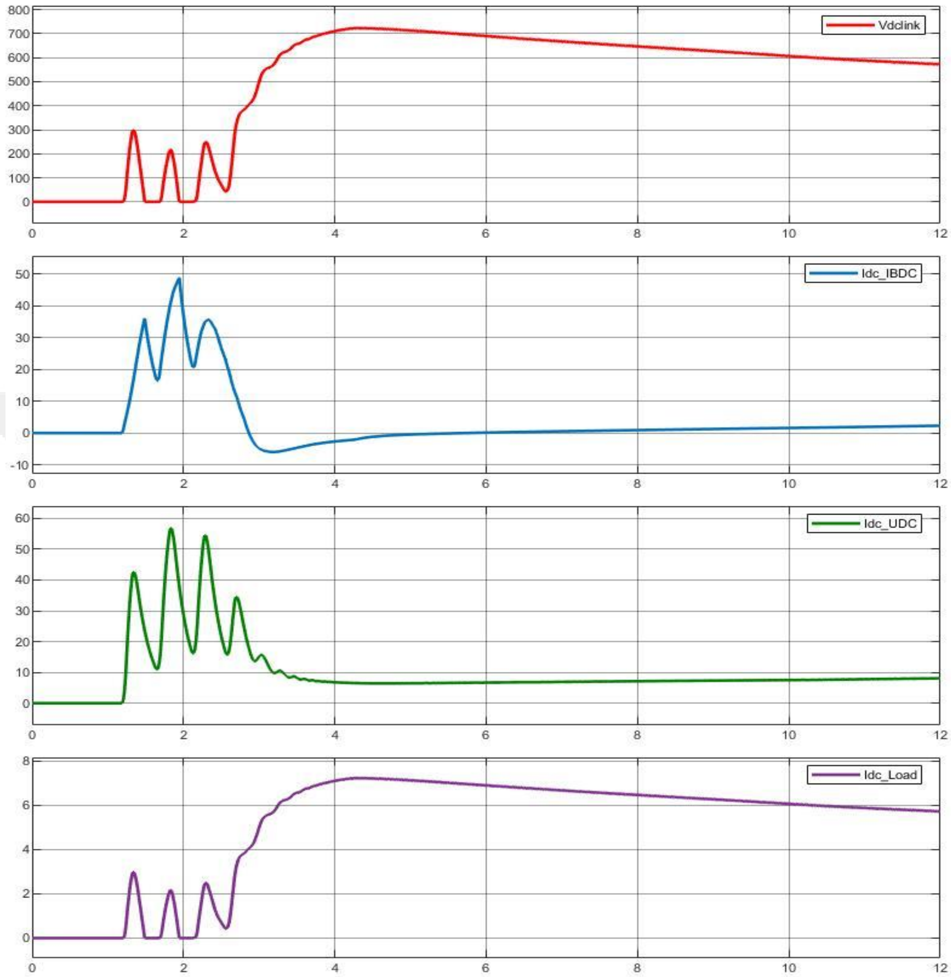

Figure 5.53. DC-Link voltage, IBDC output current, IUDC output current and DC-Load current

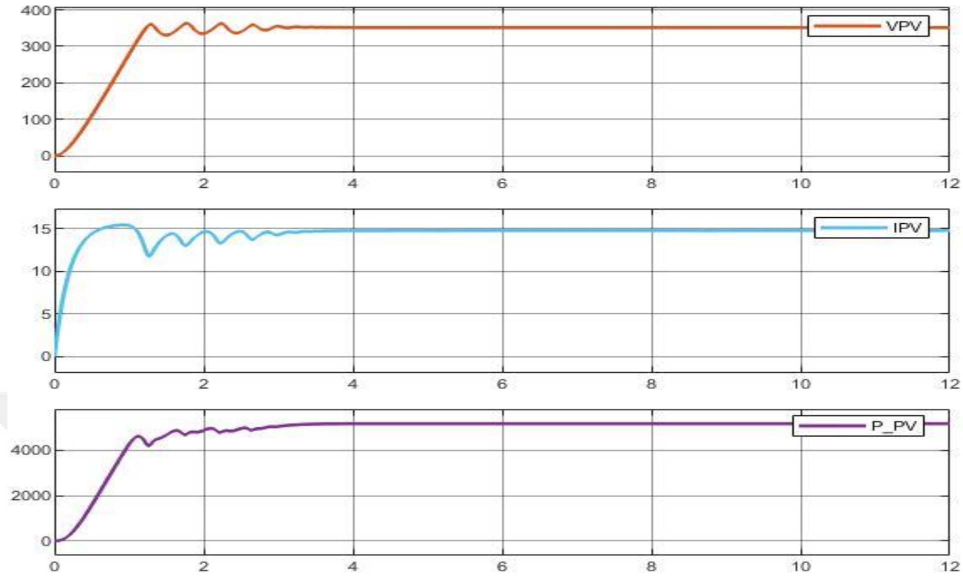

Figure 5.54. Voltage, current and power of PV panels

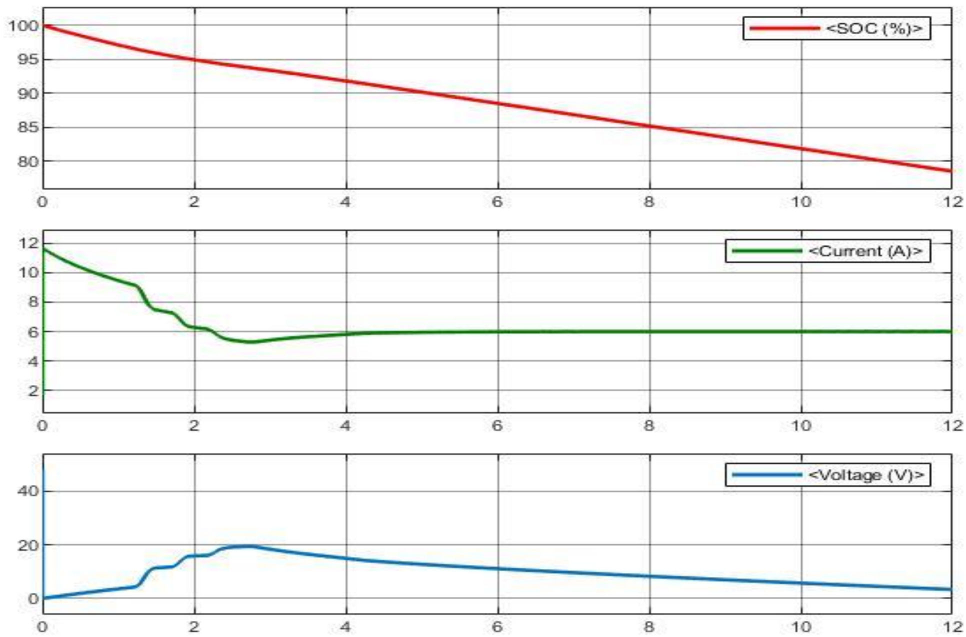

Figure 5.55. SoC, current and voltage of one battery

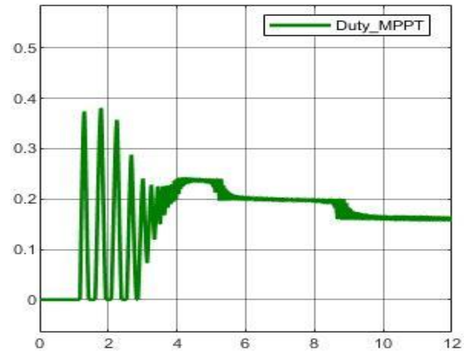

Figure 5.56. MPPT-PI output duty value

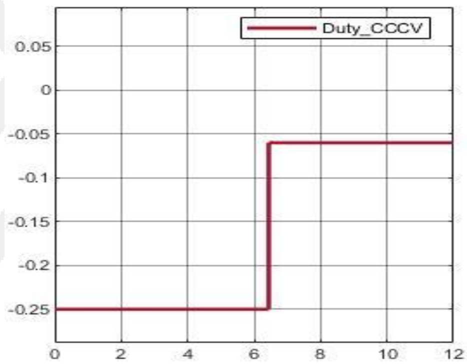

Figure 5.57. Discharge current control duty ratio

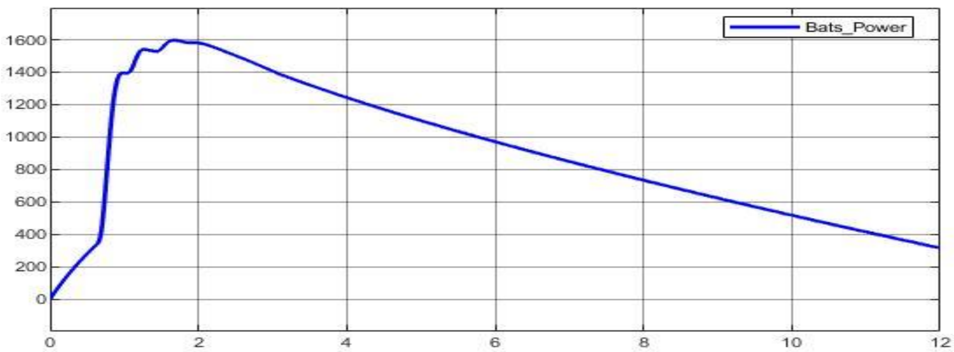

Figure 5.58. Batteries total discharge power

Power Balance and System Efficiency Calculations:

At 6th second;

Input power (from PV Panels) = 5180 W

Input power (from Batteries) = 920 W

AC Load Power = 0 W

DC Load Power = 700 x 7 = 4900 W

Power Loss of the System = (5180 + 920) – 4900 = 1200 W

Efficiency = (4900 / (5180 + 920)) x 100 = % 80.32

5.8. Results of HRPS with The Proposed EMS

In this section, HRPS is automatically operated depends on the proposed rule-based EMS and its results are given. The power flow scenario numbers are changeable according to the simulation seconds of the HRPS operated with the EMS are shown in Figure 5.62. first graphic below. The working order and duration of the scenarios may vary according to the conditions in the loads, power balances of equipments, SoC of batteries and weather conditions. The working principle of the EMS algorithm is described in chapter 4.2.6 which is completely based on the explained example and its results are obtained in the simulation here.

The simulation results in this section are taken by considering the following situations. Proposed EMS decides which power flow scenario will work according to the above mentioned conditions. After the selection of power flow scenario type by the EMS, switch states and controller of converters are chosen by the switch controller that is demonstrated at Figure 4.12.. In this way, all power flow scenarios are running according to Table-4.2 switch states. Irradiance and temperature spectrums are shown at Figure 4.8 and 4.9 respectively. These spectrums are very important for MPPT of PV panels and simulation is operated according to these spectrums. Lastly, simulation is operated with variable load conditions and these load conditions are given at Figure 4.6. and 4.7.

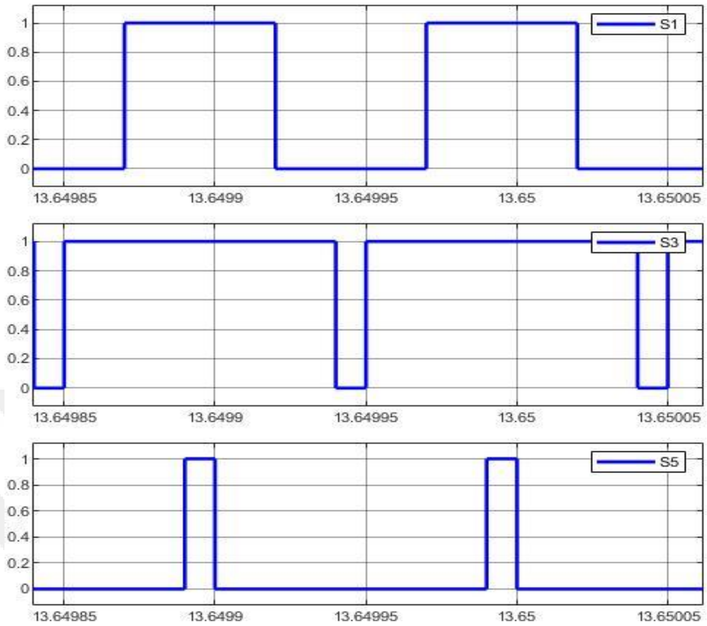

Figure 5.59. S1, S3, S5 inverter switching signals (S4, S6, S2 are opposite)

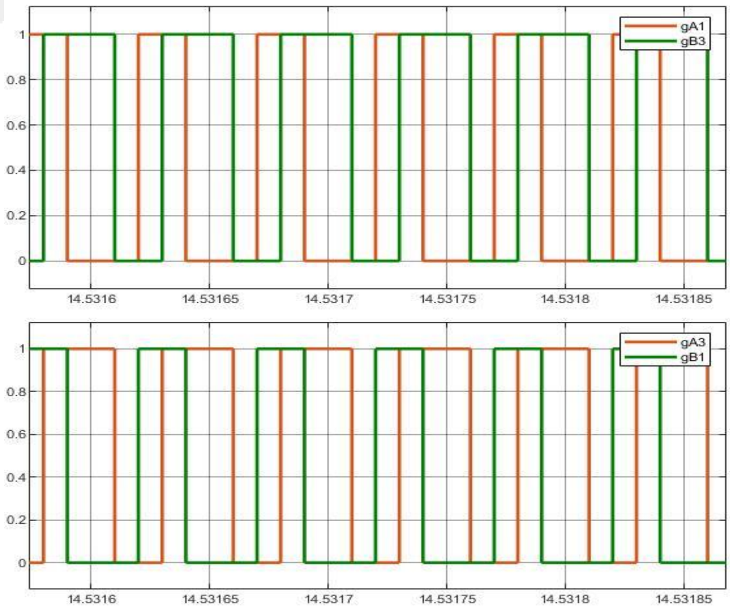

Figure 5.60. DPS condition of gA1-gB3 and gA3-gB1 switches at IBDC

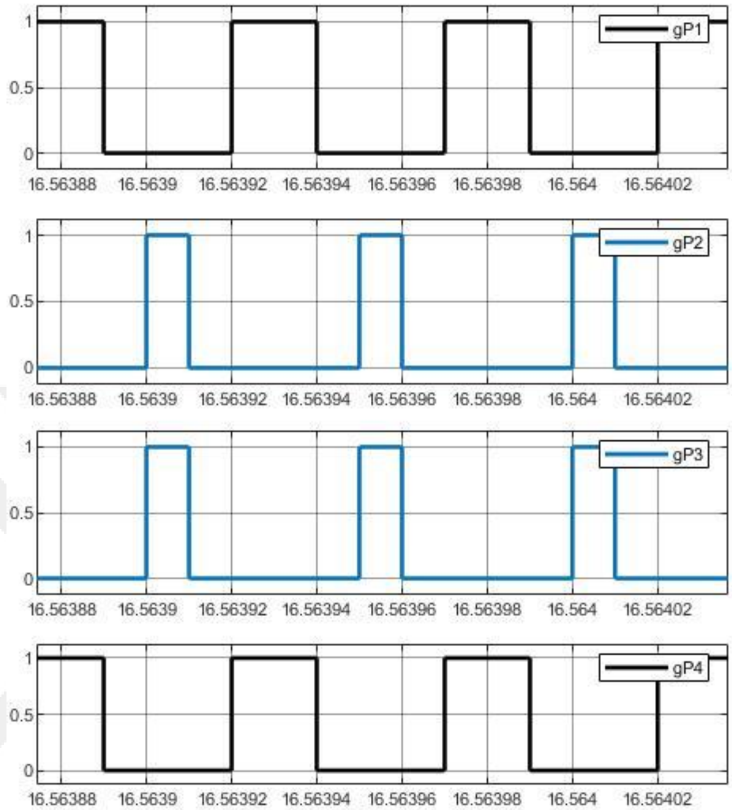

Figure 5.61. Switching signals of IUDC, gP1=gP4 (black) and gP2=gP3 (blue)

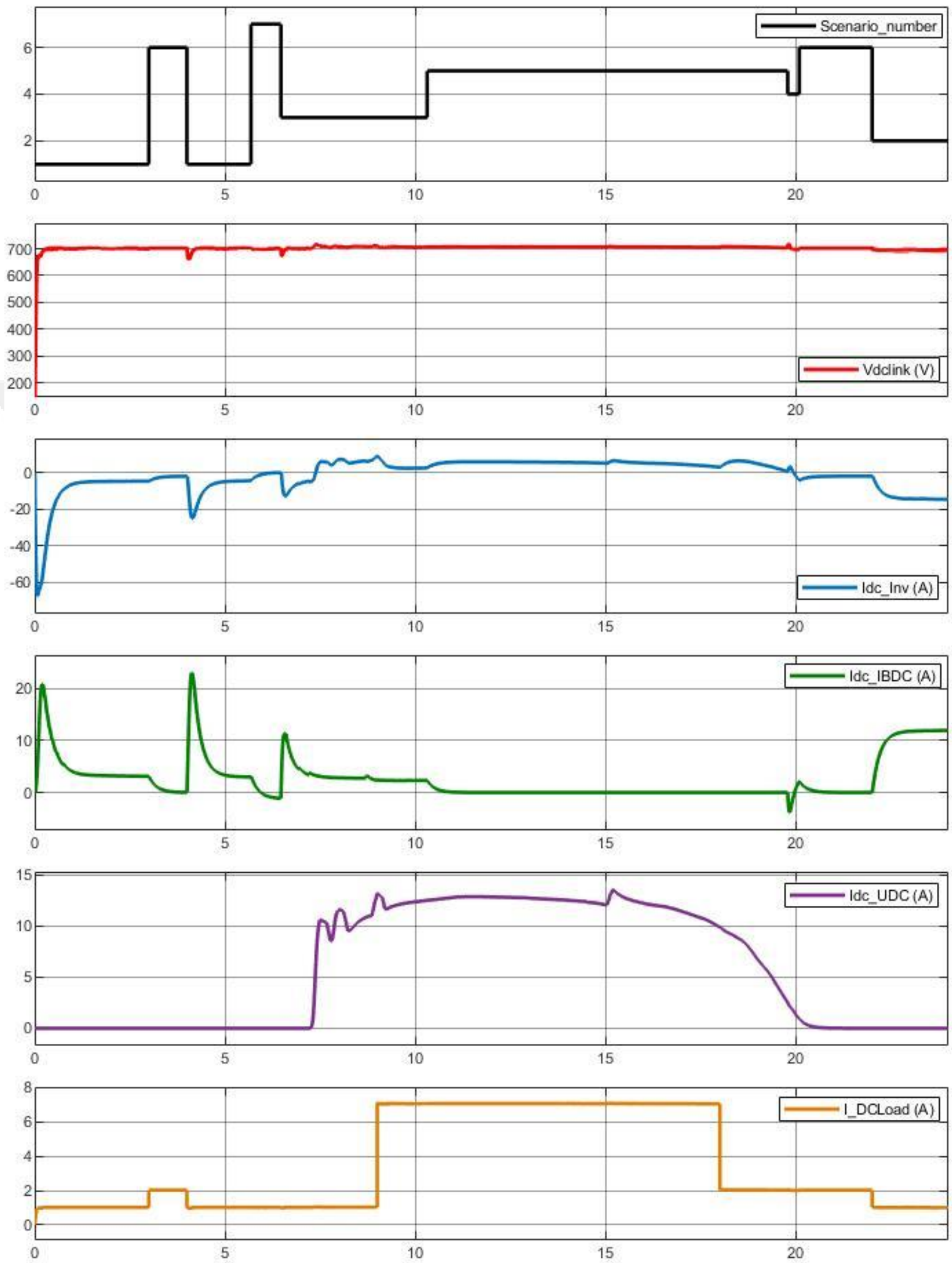

Figure 5.62. DC Link Voltage and currents of components with power flow scenarios

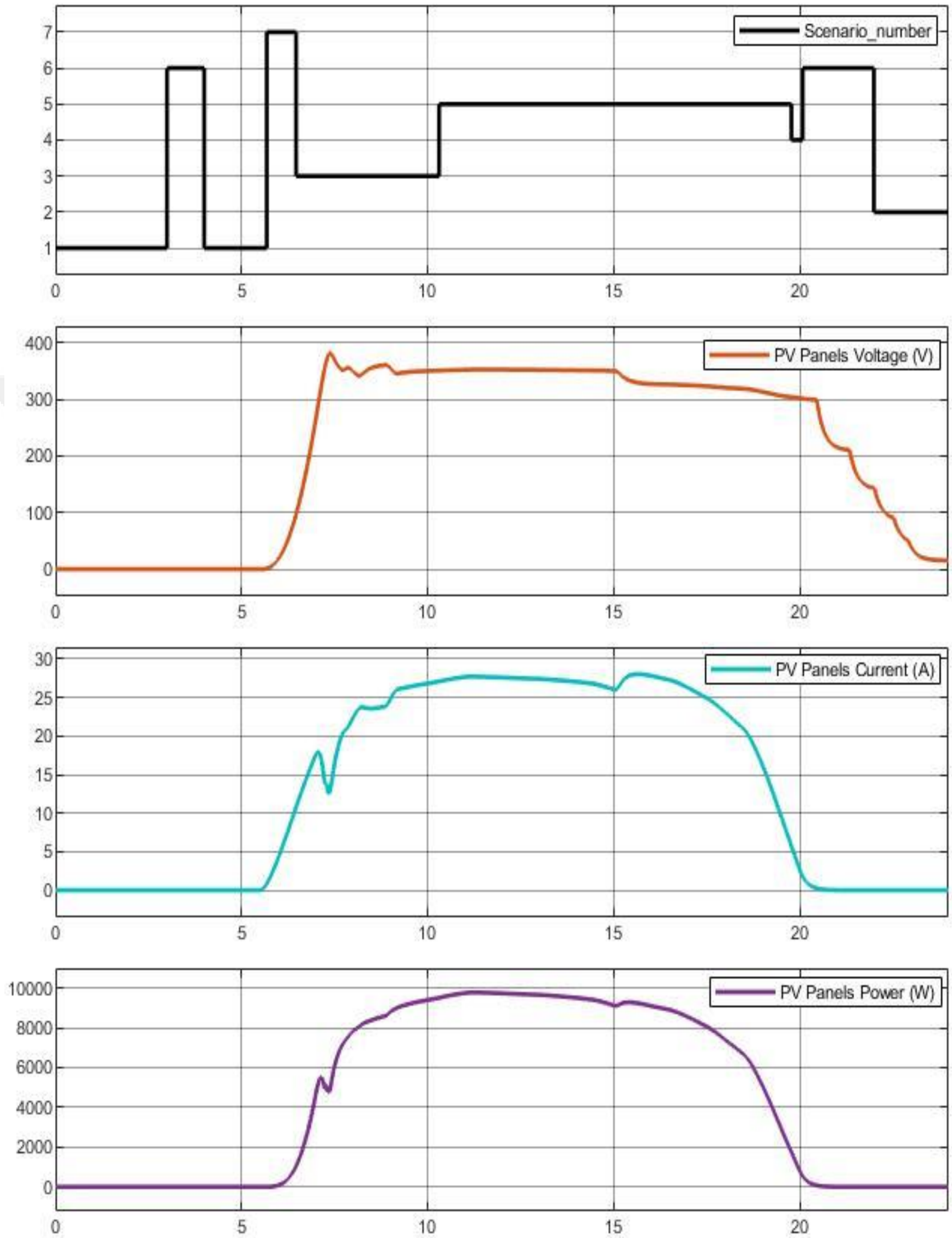

Figure 5.63. Voltage, current and power of PV panels with power flow scenarios

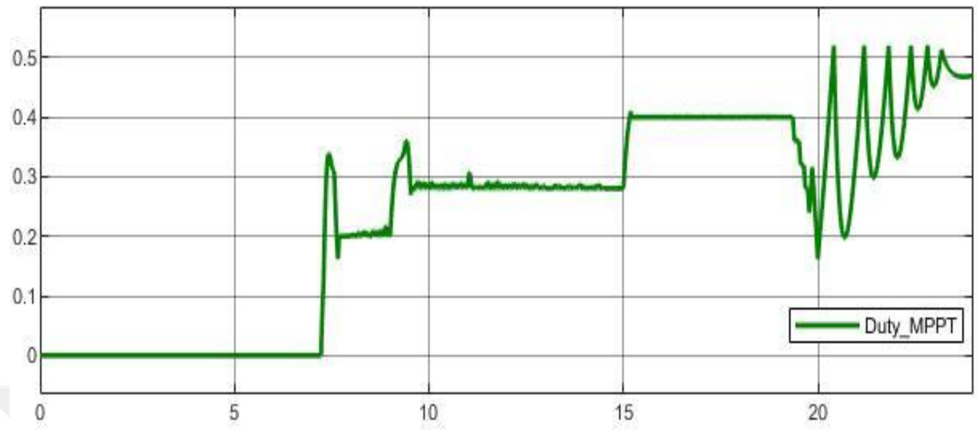

Figure 5.64. MPPT-P&O algorithm PI output waveform

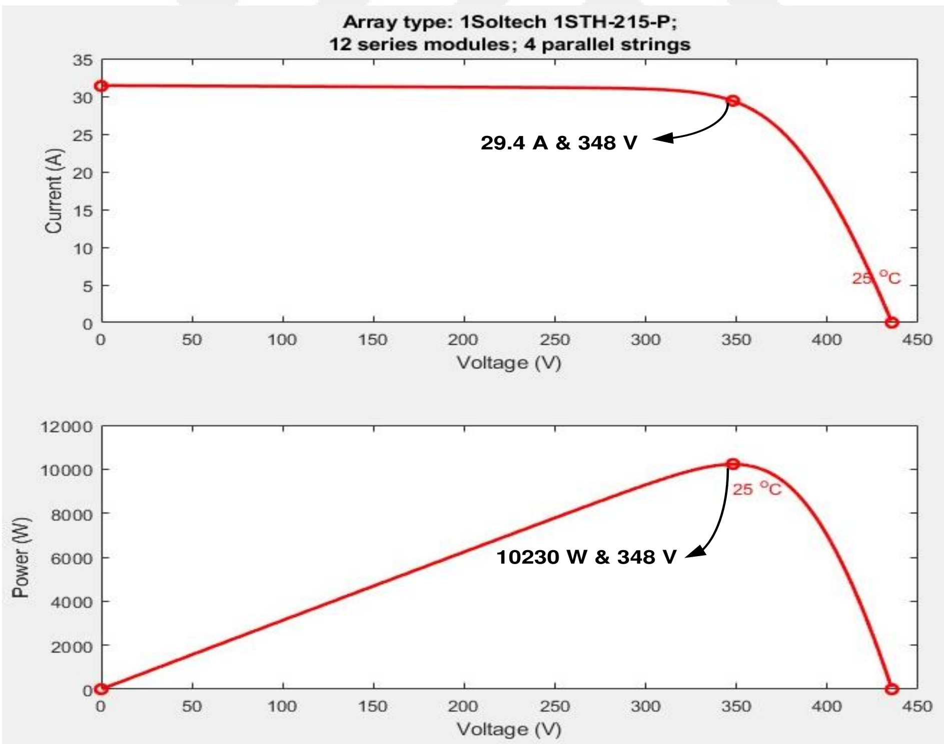

Figure 5.65. PV panels array MPP parameters at 1000 W/m^2 and 25°C

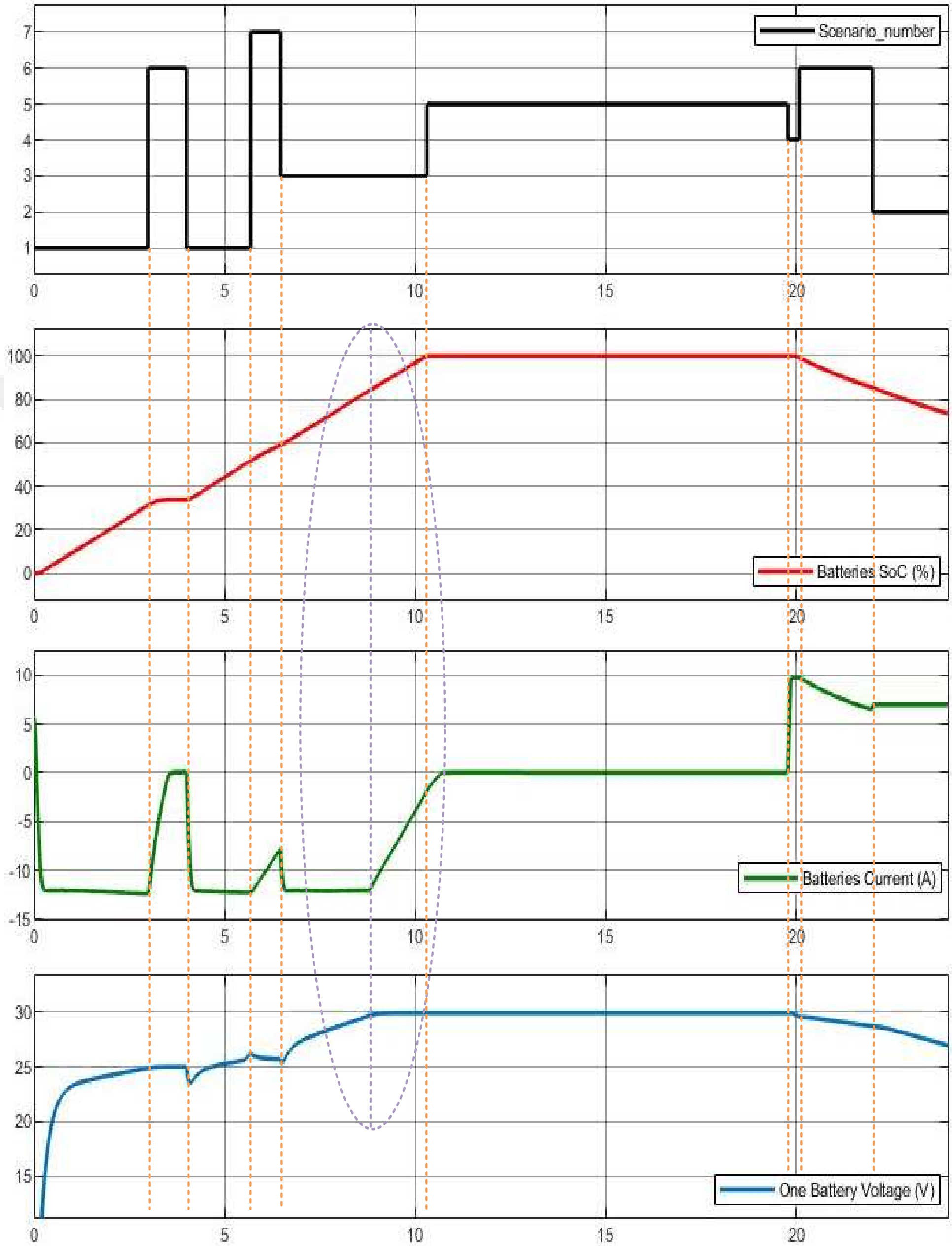

Figure 5.66. Batteries SoC, current and one battery voltage with power flow scenarios

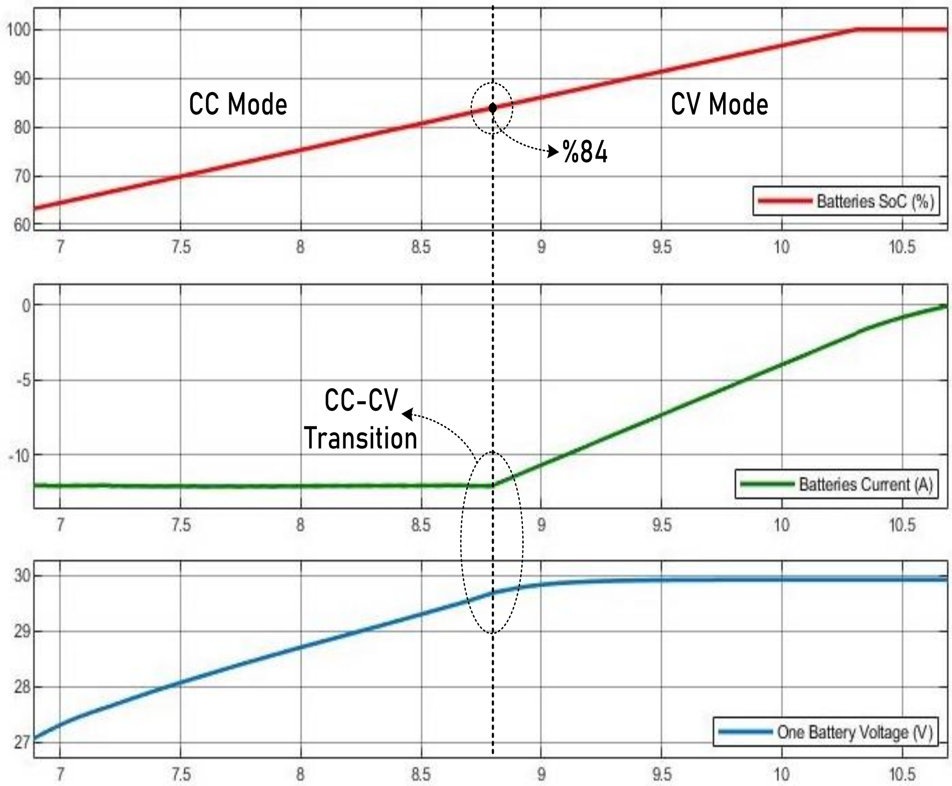

Figure 5.67. CC mode, CC-CV transition and CV mode

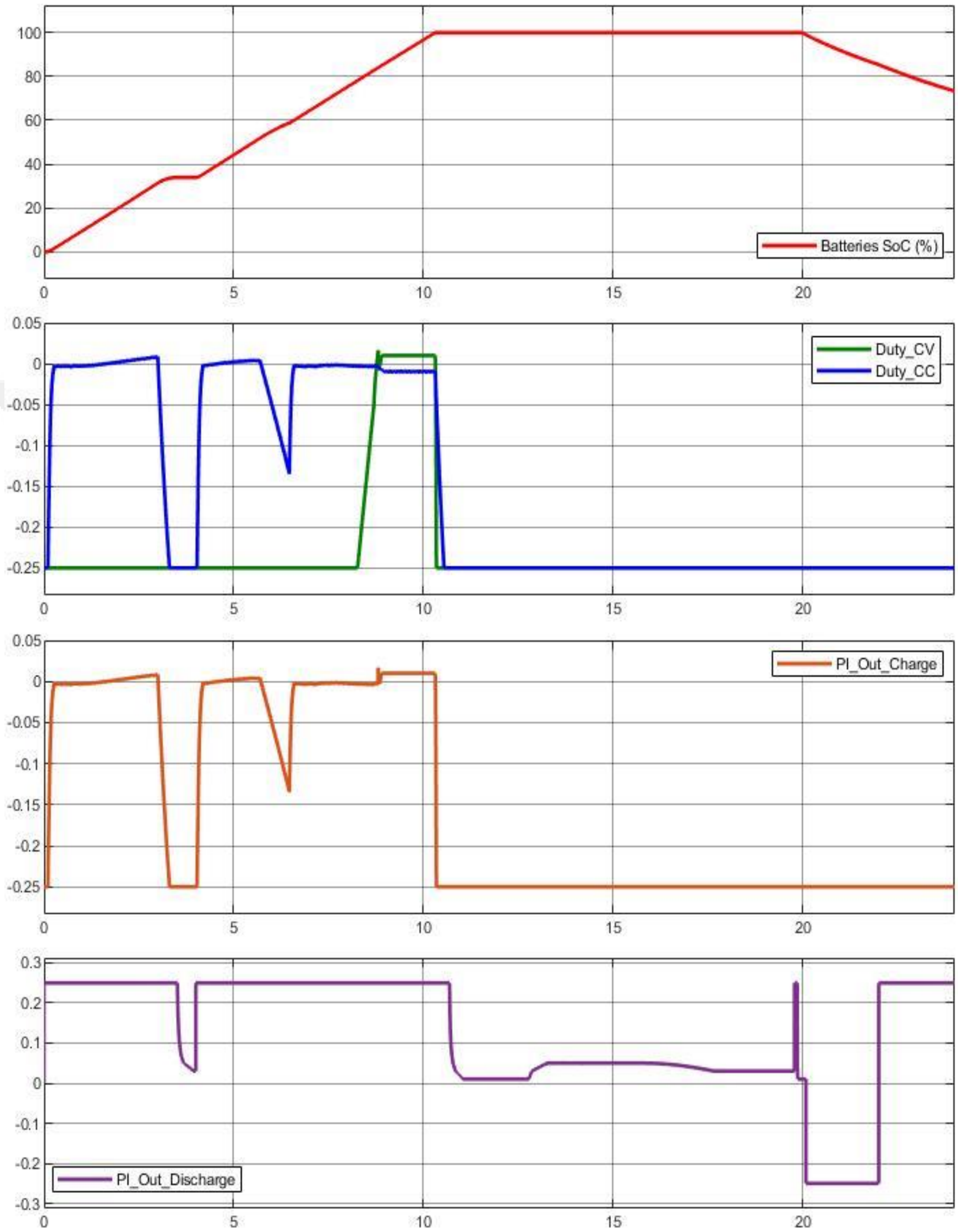

Figure 5.68. Duty_CV, Duty_CC, PI_Out_Charge, PI_Out_Discharge with SoC graphics

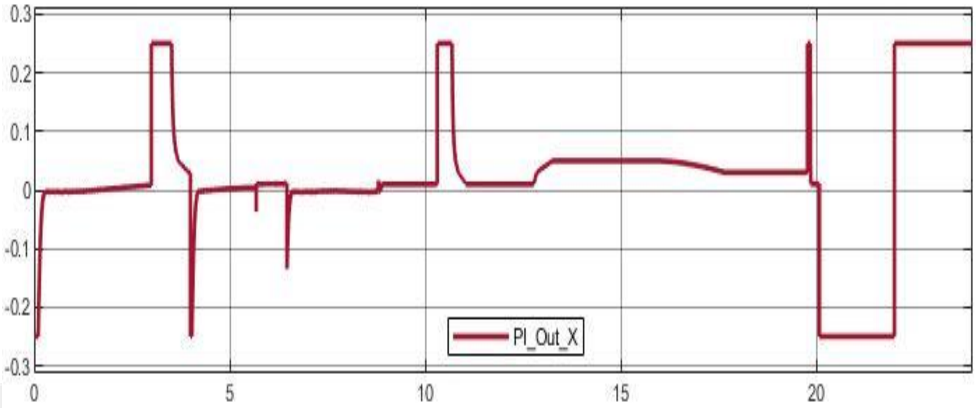

Figure 5.69. PI_Out_X Graphic (combined with PI_Out_Charge and PI_Out_Discharge)

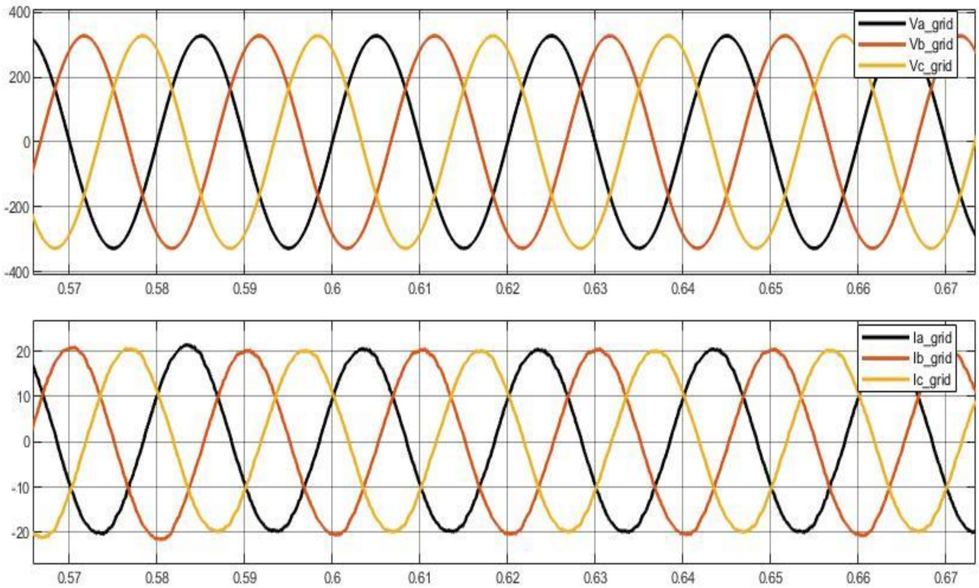

Figure 5.70. Scenario-1 (OPC) Grid Voltage and Current waveforms

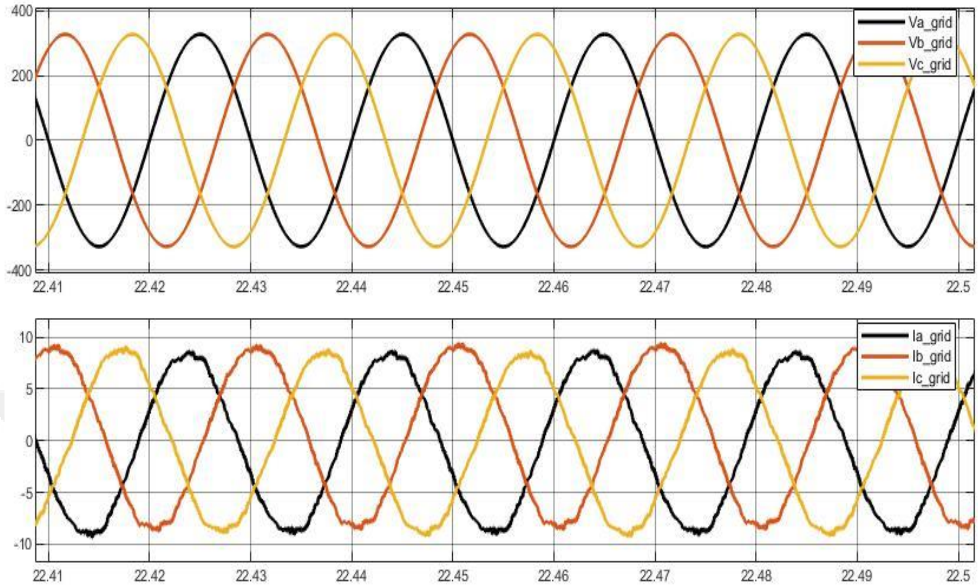

Figure 5.71. Scenario-2 (OPD) Grid Voltage and Current waveforms

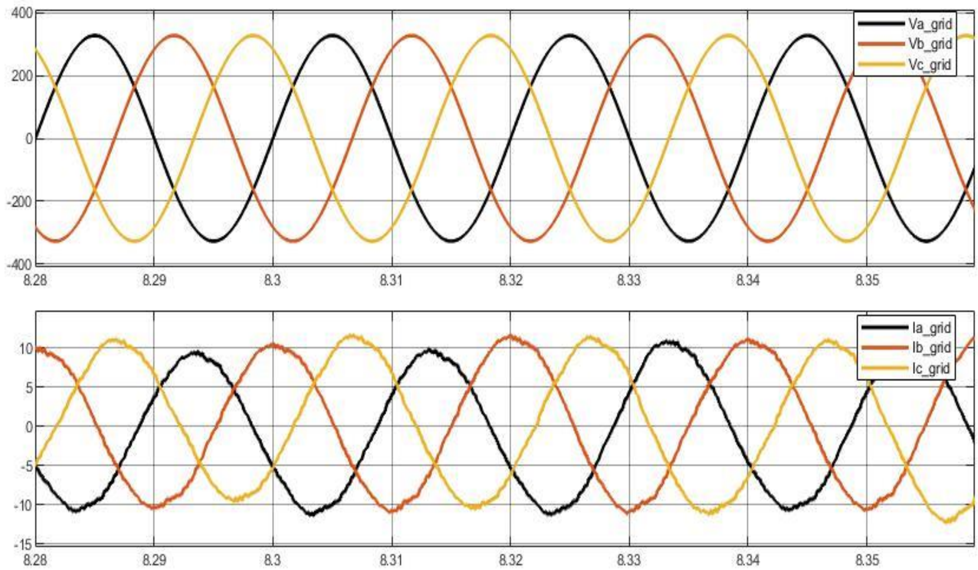

Figure 5.72. Scenario-3 (LC) Grid Voltage and Current waveforms

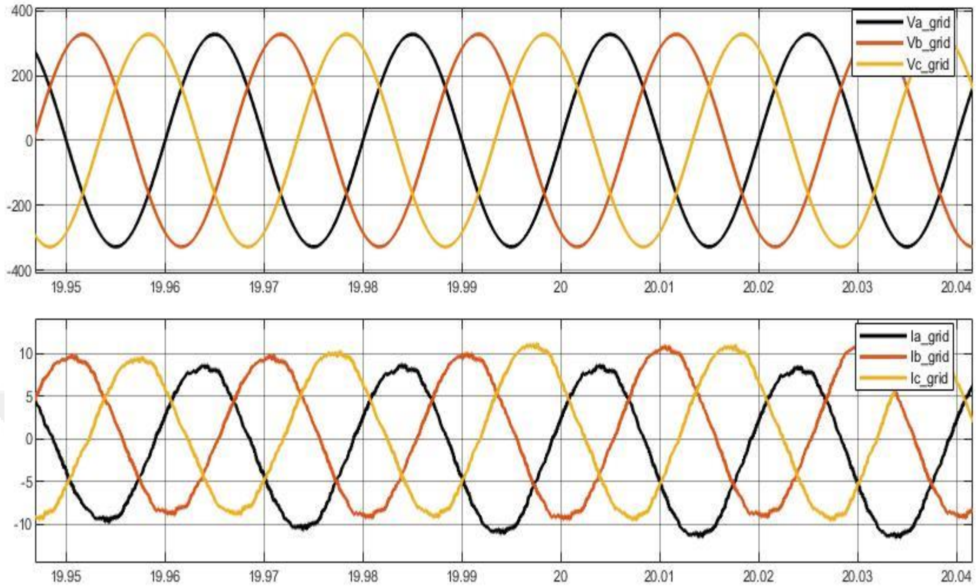

Figure 5.73. Scenario-4 (DLD) Grid Voltage and Current waveforms

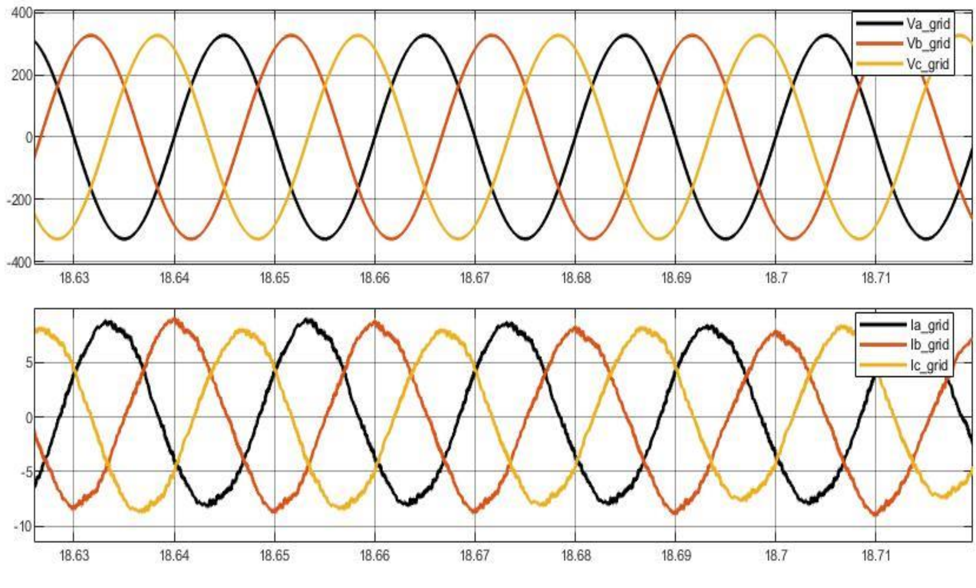

Figure 5.74. Scenario-5 (OB) Grid Voltage and Current waveforms

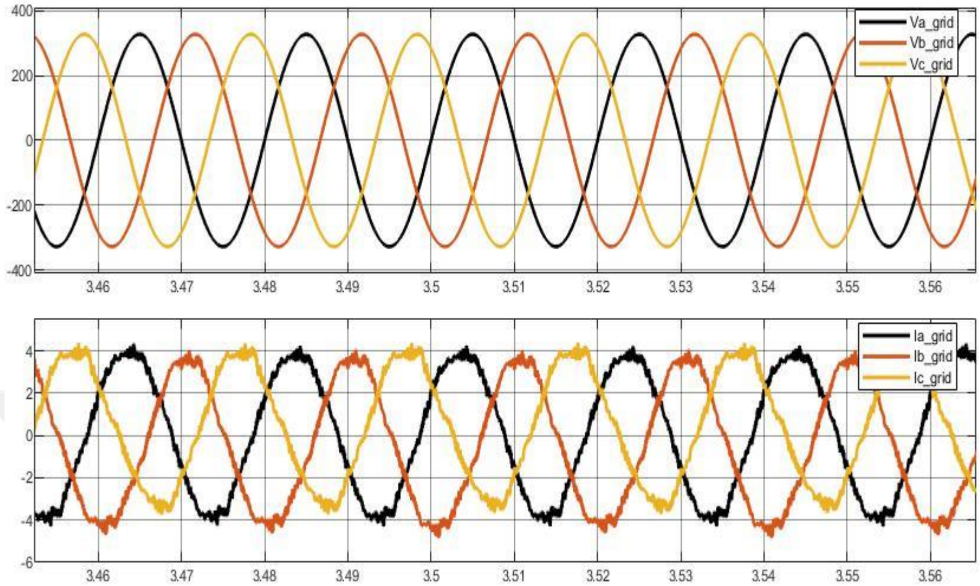

Figure 5.75. Scenario-6 (BY) Grid Voltage and Current waveforms

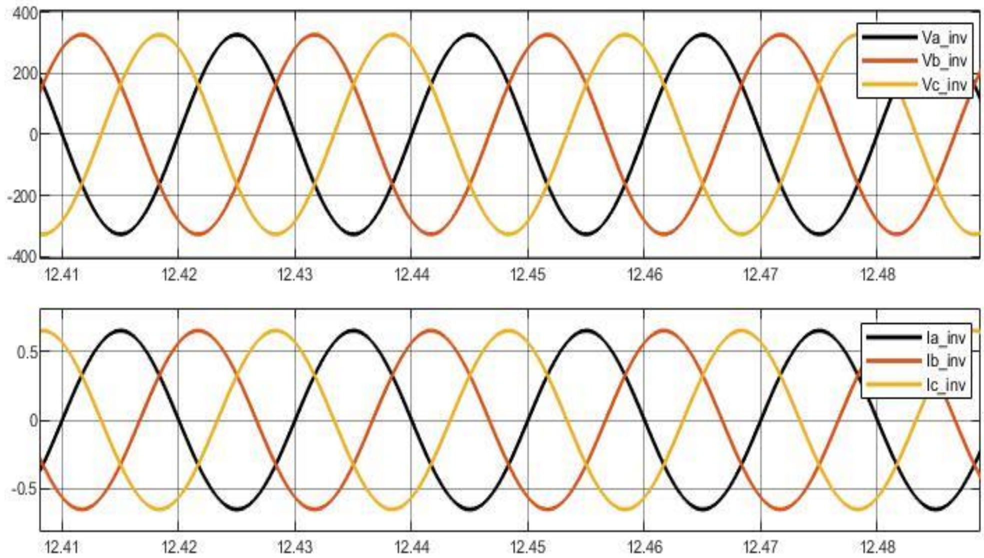

Figure 5.76. AC Load Voltage and Current waveforms

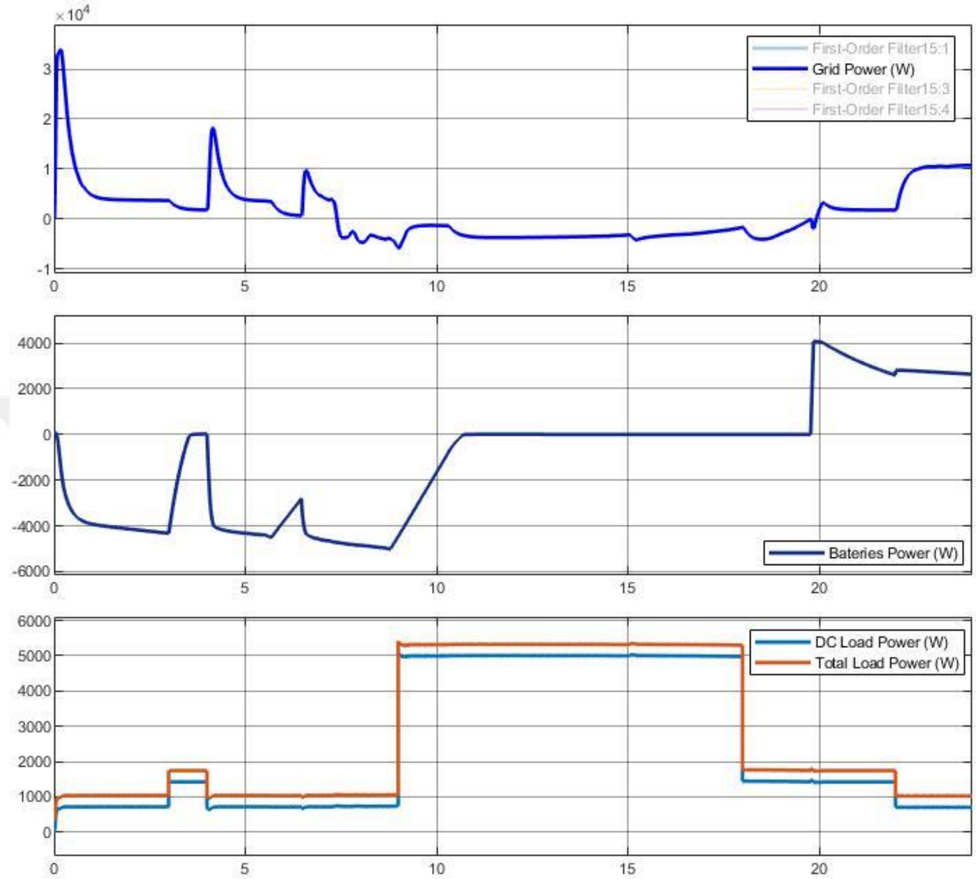

Figure 5.77. Grid Power, Batteries Power, DC Load and Total Load Power

5.9. Cost Analysis and Efficiency Calculations for HRPS with EMS Operation

The power values drawn from the grid appear as positive, while the power values transferred to the grid appear in the negative direction according to Figure 5.78. The amount paid can be found by multiplying the total power consumed over time and the kWh fee. While the pricing tariff is 0.7063 TL/kWh for workplaces in our country, it is 0.4743 TL/kWh for residential areas. According to this;

Since every 1 second is taken as 1 hour on the simulation, the average of the consumed and produced power values in 1 second is taken and added according to 24 hours by multiplying with the hourly tariff rate.

Table-5.1. Average hourly consumed or produced powers and hourly wages

Hours	Ave. Hourly Consumed or Produced Powers	Hourly Wage for Businesses	Hourly Wage for Residences
00:00 – 01:00	13754 W	9.71 TL	6.52 TL
01:00 – 02:00	4737 W	3.35 TL	2.25 TL
02:00 – 03:00	4655 W	3.29 TL	2.21 TL
03:00 – 04:00	2342 W	1.65 TL	1.11 TL
04:00 – 05:00	7768 W	5.49 TL	3.68 TL
05:00 – 06:00	3764 W	2.66 TL	1.79 TL
06:00 – 07:00	3718 W	2.63 TL	1.76 TL
07:00 – 08:00	491 W	0.35 TL	0.23 TL
08:00 – 09:00	-4552 W	-3.22 TL	-2.16 TL
09:00 – 10:00	-2234 W	-1.58 TL	-1.06 TL
10:00 – 11:00	-2345 W	-1.66 TL	-1.11 TL
11:00 – 12:00	-3784 W	-2.67 TL	-1.79 TL
12:00 – 13:00	-3558 W	-2.51 TL	-1.69 TL
13:00 – 14:00	-3532 W	-2.49 TL	-1.68 TL
14:00 – 15:00	-3456 W	-2.44 TL	-1.64 TL
15:00 – 16:00	-3685 W	-2.60 TL	-1.75 TL
16:00 – 17:00	-3176 W	-2.24 TL	-1.51 TL
17:00 – 18:00	-2427 W	-1.72 TL	-1.15 TL
18:00 – 19:00	-3482 W	-2.46 TL	-1.65 TL
19:00 – 20:00	-1112 W	-0.79 TL	-0.53 TL
20:00 – 21:00	1980 W	1.40 TL	0.94 TL

21:00 – 22:00	1642 W	1.16 TL	0.78 TL
22:00 – 23:00	8208 W	5.80 TL	3.89 TL
23:00 – 24:00	10573 W	7.47 TL	5.01 TL

The wages in the 3rd and 4th columns of Table-13 are collected separetly as positive and negative.

Total spent power charge = Sum of positive charges

Total recovered power charge = Sum of negative charges

When calculated with workplaces;

Percent recovery by regenerative effect = (total recovered power charge / total power spent charge) X 100

(26.38 TL / 44.96 TL) X 100 = 58.67 % profit.

Charge payable per day = Total consumed power charge – Total recovered power charge

44.96 – 26.38 = 18.58 TL

When calculated for residences;

(17.72 TL / 30.17 TL) X 100 = 58.73 % profit.

The daily fee;

30.17 – 17.72 = 12.45 TL

6. CONCLUSION AND FUTURE WORK

6.1. Conclusion and Comments of Results

- In HRPS operated with EMS, the power flow scenario number 1 (OFF-PV Charge Mode) works at first. In this scenario, while the batteries are charged in CC mode with a current of 12 A with the power drawn from the grid, the inverter working with the DC-Link voltage controller keep the DC-Link voltage of 700 V. Since this scenario takes place at night, the power produced from the PV panels is still very low and the switches of the IUDC connected to the PV panels are not included in the system because they are in the 0 state. Therefore, the Idc_UDC current is also seen as 0 A. At the beginning of the operation, there is a power demand of 700 W at the DC load. Together with AC loads, this demand total is 1020 W and the current in DC load is seen as 1 A.
- Total load demand increased from 1020 W to 1720 W at 3rd second (03:00). In this case, the charging of the batteries is stopped (Idc_IBDC=0 A) and the scenario number 6 (Bypass Mode or Fault Mode) is passed, and the loads are only fed from the grid. Then, since the total demand power in the reloads is 1020 W, scenario 1 is returned. While scenario 6 is running, since the DC load is 350 ohms, the current in the DC load is seen as 2 A.
- In scenario 7 (OFF-Grid Mode or Island Mode), DC-Link voltage controller is not used at the inverter because grid connected inverter is not used in this scenario. DC-Link voltage is kept by batteries connected IBDC which operates DC-link voltage controller at the results of HRPS with EMS (last case). Discharge current controller is operated while obtaining the results of scenario 7 without EMS. Grid voltage and current waveforms are not shown at last case because of grid and inverter are not used in this scenario.
- DC-Link voltage is stable at 700 V while operating HRPS with EMS. It is seen that only 3 times distortion of the voltage waveform. The biggest

voltage distortion is seen at transition from scenario 6 to scenario 2. It is 25 V falling but DC-Link voltage is set to 700 V again rapidly by using the DC-Link voltage controller. Thus, it is not harmful for converters of HRPS because of it is 3.28% percentage of 700 V.

- In scenario 3 (Line Charge Mode), power is transferred by the PV panels to the grid, to the loads and to charge the batteries. In this case, the total demand power at the loads is defined as 5220 W and the DC load is 100 ohms. For this reason, it is seen as IdcLoad=7 A. The CC-CV transition that occurs during the charging of the batteries is also shown in Figure 5.67. CC-CV transition is occurred at 84% SoC. This percentage is a little bit low. But if the transition is occurred at high percentages, it will causes batteries have more heat or exploding effect. Thus, transition from CC to CV can be lower SoC values. This case can made defining a little bit value than maximum total batteries voltage when designing CC-CV controller. In this way, this defined voltage value is complementary with lower SoC values.
- In scenario 5 (OFF-Batteries Mode), the total load demand power is 5220 W and power is transferred to the grid during scenarios 3 and 5. Therefore, the Idc_Inv current is seen as positive. While power is being transferred from the network to the system, negative current values are seen in other scenarios. The only difference between scenario 5 and 3 is that the batteries are not charged. Therefore, the Idc_IBDC current is seen as 0 A.
- In scenario number 4 (Double Line Discharge Mode), the batteries are discharged with 7 A. Power of loads is supplied by the grid and PV panels. When the scenario 4 is operated, demand load power is 1720 W and solar power is very low. Grid gets involve in the system by providing extra power for feeding loads because of total power of batteries is not sufficient for loads. Thus, it can be seen that for scenario 4, power is transferred from the grid to the system in Figure 5.73. It has been seen that batteries and solar power can be injected to grid when solar power is high enough for demand

power of loads in Figure 5.33. However, this situation is not shown in this latest simulation study.

- The same situation is happened for scenario number 2 (OFF-PV Discharge Mode). Although the demand power in the loads drops to 1020 W, the total power of the batteries is not enough to meet the demand here and grid supplies extra power to the loads. Load demand power should be very low or system should be operated at no-dc-load condition for injecting power to grid. When this scenario is operated without EMS, injection power to grid can be seen in Figure 5.13. Higher power batteries can be used to avoid this situation. But it should be noted that it will be more costly.
- Finally, it is seen that designed LCL filter is operated properly at obtained results. All of THD values are less than 3% at grid side current when injecting power to grid scenarios.
- Consequently, HRPS is operated with proposed rule-based EMS accurately.

6.2. Future Work

In future studies can be about … according to the obtained results in this thesis;

- EMS can be applied at higher powers by adding wind turbines to the hybrid regenerative power system topology.
- If low power operation is continued, the factors affecting system efficiency can be examined in detail and controller-based solutions can be produced to increase efficiency.
- A similar EMS structure can be used for EVs in combination with PV panels.
- In addition to one day in summer, the operating performance of the system can be analyzed by choosing a day from winter months, since the radiation time is less.
- By making a low power experimental prototype; theoretical, simulation and experimental results can be compared.

REFERENCES

Abdi H., Mohammadi-Ivatloo B., Javadi S., Khodaei A. R., and Dehnavi E., 2017. "Distributed Generation Systems" book, chapter 7, "Energy Storage Systems".

Agamy M. S., Chi S., Elasser A., Harfman-Todorovic M., Jiang Y., Mueller F. and Tao F., 2013. "A High-Power-Density DC-DC Converter for Distributed PV Architectures", IEEE Journal of Photovoltaics, 3 (2): 791-798.

Agamy M. S., Chi S., Elasser A., Todorovic M. H., Jiang Y., Mueller F. and Tao F., 2012. "A High-Power-Density DC-DC Converter for Distributed PV Architectures", 2012 IEEE 38th Photovoltaic Specialist Conference (PVSC / Part 2): 1-8.

Ahmed M. E.-S., Orabi M., and AbdelRahim O. M., 2013. "Two-stage micro-grid inverter with high-voltage gain for photovoltaic applications", IET Power Electronics, 6 (9): 1812-1821.

Ahmed O. A. and Bleijs J. A. M., 2015. "An overview of DC-DC converter topologies for fuel cell-ultracapacitor hybrid distribution system", Renewable and Sustainable Energy Reviews, 42: 609-626.

Akagi H. and Kitada R., 2011. "Control and Design of a Modular Multilevel Cascade BTB System Using Bidirectional Isolated DC/DC Converters", IEEE Transactions on Power Electronics, 26 (9): 2457-2464.

Alam M. S., and Arefifar S. A., 2019. "Energy Management in Power Distribution Systems: Review, Classification, Limitations and Challenges", IEEE Access, 7: 92979-93001.

Alonso O., Sanchis P., Gubia E., and Marroyo L., 2003. "Cascaded Hbridge multilevel converter for grid connected photovoltaic generators with independent maximum power point tracking of each solar array," IEEE Power Electronics Specialists Conference, PESC2003.

Anglani N., Oriti G., and Colombini M., 2017. ``Optimized energy management system to reduce fuel consumption in remote military microgrids,"IEEE Trans. Ind. Appl., 53 (6): 5777-5785.

Armstrong S., Glavin M. E., and Hurley W. G., 2008. "Comparison of Battery Charging Algorithms for Stand Alone Photovoltaic Systems", IEEE Power Electronics Specialists Conference: 1469-1475.

Ban M., Shahidehpour M., Yu J., and Li Z., 2019. ``A cyber-physical energy management system for optimal sizing and operation of networked nanogrids with battery swapping stations,"IEEE Trans. Sustain. Energy, 10 (1): 491-502.

Barrios M. A., Cardenas V., Sandoval J. M., Gonzalez M. and Miranda H., 2018. "DC-AC-AC Converter for PV Plant in Medium Voltage Grid-Connected Systems", IEEE CIEP Conference: 146-154.

Bhattacharjee A., 2012. "Design and Comparative Study of Three Photovoltaic Battery Charge Control Algorithms in MATLAB/SIMULINK Environment", International Journal of Advanced Computer Research, 2 (3): 129-135.

Borrega M., Marroyo L., Gonzalez R., Balda J. and Agorreta J. L., 2013. "Modeling and Control of a Master-Slave PV Inverter With N-Paralleled Inverters and Three-Phase Three-Limb Inductors", IEEE Trans. On Power Electronics, 28 (6): 2842-2855.

Bouharchouche A., Berkouk E. M., Ghennam T., 2013. "Control and Energy Management of a Grid Connected Hybrid Energy System PV-Wind with Battery Energy Storage for Residential Applications", IEEE Eighth International Conference and Exhibition on Ecological Vehicles and Renewable Energies".

Boynueğri A. R., Yağcıtekin B., Baysal M., Karakaş A., and Uzunoğlu M. 2013. “Energy Management Algorithm for Smart Home with Renewable Energy Sources”, 4th International IEEE Conference on Power Engineering, Energy and Electrical Drives 1753-1758.

Bragard M., Soltau N., Thomas S. and De Doncker R. W., 2010. “The Balance of Renewable Sources and User Demands in Grids: Power Electronics for Modular Battery Energy Storage Systems”, IEEE Trans. On Power Electronics, 25 (12): 3049-3056.

Bukar A. L., Tan C. W., Yiew L. K., Ayop R., and Tan W.-S., 2020. “A rule-based energy management scheme for long-term optimal capacity planning of grid- independent microgrid optimized by multi-objective grasshopper optimization algorithm”, Energy Conversion and Management, Elsevier: 1-22.

Byrne R. H., Nguyen T. A., Copp D. A., Chalamala B. R., and Gyuk I., 2018. “Energy Management and Optimization Methods for Grid Energy Storage Systems”, Special Section on Battery Energy Storage and Management Systems, IEEE Access, 6: 13231-13260.

Calais M., Agelidis V. G., and Meinhardt M., 1999. "Multilevel converters for single-phase grid connected photovoltaic systems: an overview," Solar Energy, 66: 325-335.

Cao J. and Emadi A., 2012. “A new battery/ultracapacitor hybrid energy storage system for electric, hybrid, and plug-in hybrid electric vehicles,” Power Electron. IEEE Trans. On, 27 (1): 122–132.

Chakir A., Tabaa M., Moutaouakkil F., Medromi H., Julien-Salame M., Dandache A., and K. Alami, 2019. ”Optimal energy management for a grid connected PV-battery system”, EURACA Conf. And Energy Reports, Elsevier: 218-231.

Chandini G. S., Shiny G., and Baiju M. R., 2016. "Common-Mode Voltage Eliminated 2-Level PWM Inverter Based on a Cascaded 3-level Inverter", IEEE ICEEOT Conference: 561-566.

Chen M., Rincon-Mora G. A., 2006. "Accurate, Compact, and Power-Efficient Li-ion Battery Charger Circuit", IEEE Transactions on Circuits and Systems, 53 (11): 1180-1184.

Cheng T., Lu D. D.-C. and Qin L., 2017. "Non-isolated Single Inductor DC/DC Converter with Fully Reconfigurable Structure for Renewable Energy Applications", IEEE Transactions on Circuits and Systems II: Express Briefs: 1-5.

Chiang H. C., Ma T. T., Cheng Y. H., Chang J. M., Chang W. N., 2010. "Design and implementation of a hybrid regenerative power system combining grid–tie and uninterruptible power supply functions", IET Renewable Power Generation, 4 (1): 85-99.

Choi H., Ciobotaru M. and Agelidis V. G., 2012a. "High Gain DC/DC Converter for the Grid Integration of Large Scale PV Systems", 2012. IEEE International Symposium on Industrial Electronics: 1011-1016.

Choi H., Ciobotaru M., and Agelidis V. G., 2014. "Cascaded H-bridge Converter with Multiphase Isolated DC/DC Converter for Large-Scale PV System", IEEE International Conference on Industrial Technology (ICIT): 455-461.

Choi H., Ciobotaru M., Jang M. and Agelidis V. G., 2015. "Performance of Medium-Voltage DC-Bus PV System Architecture Utilizing High-Gain DC-DC Converter", IEEE Trans. On Sustainable Energy: 6 (2): 464-473.

Choi H., Zhao W., Ciobotaru M. and Agelidis V. G., 2012b. "Large Scale PV System based on the Multiphase Isolated DC/DC Converter", 2012 3rd IEEE International Symposium on Power Electronics for Distributed Generation Systems (PEDG): 801-807.

Costa L. F., Mussa S. A., Barbi I., 2013. “Steady-State Analysis of a 5-Level Bidirectional Buck+Boost DC-DC Converter,” IEEE IECON 2013, Vienna: 1290-1295.

Çolak İ., and Tuncay N., 2008. “High Current, Low Voltage Modular Power Converter for Lead Acid Battery Charging”, IEEE ICSET Conference: 1042-1046.

Daher S., Schmid J., and Antunes F. L. M., 2008. "Multilevel Inverter Topologies for Stand-Alone PV Systems," IEEE Trans. on Industrial Electronics, 55: 2703-2712.

Dash V., and Bajpai P., 2015. “Power management control strategy for a stand-alone solar photovoltaic-fuel cell-battery hybrid system”, Sustainable Energy Technologies and Assesments: 68-80.

Del Moral D. L., Barrado A., Sanz M., Zumel P., Raga C., Lazaro A. and Miniguano H., 2015. “Improvement of the Synchronous Buck Converter Dynamic Performance Applied to Hybrid Electric Vehicle Regenerative Power Systems”, 9th International Conference on Compatibility and Power Electronics (CPE): 437-442.

Dou C. X. and Liu B., 2013. ``Multi-agent based hierarchical hybrid control for smart microgrid,"IEEE Trans. Smart Grid, 4 (2): 771-778.

Dung L.-R., Chen C.-E., and Yuan H.-F., 2016. “A Robust, Intelligent CC-CV Fast Charger for Aging Lithium Batteries”, IEEE 25th ISIE Conference: 268-273.

Duryea S., Islam S., and Lawrance W., 2001. “A Battery Management System for Stand-Alone Photovoltaic Energy Systems”, IEEE Industry Applications Magazine, 7 (3): 67-72.

Elgammal A. and El-Naggar M., 2018. “Energy management in smart grids for the integration of hybrid wind-PV-FC-battery renewable energy resources using multi-objective particle swarm optimisation (MOPSO),"J. Eng., 2018 (11): 1806-1816.

Elsayad N. and Mohammed O. A., 2017. “A Cascaded High Frequency AC Link System with Reduced Switch Count and Low-Voltage Ride-Through Capability for Large-Scale PV Systems”, IEEE Power & Energy Society General Meeting.

Esram T. and Chapman P. L., 2007. "Comparison of photovoltaic array maximum power point tracking techniques," in IEEE Trans. on Energy Conversion, 22: 439-449.

Essakiappan S., Krishnamoorthy H. S., Enjeti P., Balog R. S. and Ahmed S., 2012. “Independent Control of Series Connected Utility Scale Multilevel Photovoltaic Inverters”, IEEE ECCE Conference: 1760-1766.

Essakiappan S., Manjrekar M., Enslin J., Ramoz-Ruiz J., Enjeti P. and Garg P., 2015. “A utility scale battery energy storage system for intermittency mitigation in multilevel medium voltage photovoltaic system”, IEEE ECCE Conf.: 54-61.

Falahi M., Lotfifard S., Ehsani M., and Butler-Purry K., 2013. “Dynamic Model Predictive-Based Energy Management of DG Integrated Distribution Systems”, IEEE Transactions on Power Delivery, 28 (4): 2217-2227.

Farivar G., Hredzak B., and Agelidis V. G., 2016. “A DC-Side Sensorless Cascaded H-Bridge Multilevel Converter-Based Photovoltaic System”, IEEE Transactions on Industrial Electronics, 63 (7): 4233-4241.

Fei X., Feng Z., PuQi N. and Xuhui W., 2018. “Analyzing ZVS Soft Switching using Single Phase Shift Control Strategy of Dual Active Bridge Isolated DC-DC Converters”, ICEMS 2018: 2378-2381.

Femia N., Petrone G., Spagnuolo G. and Vitelli M., 2009. “A Technique for Improving P&O MPPT Performances of Double-Stage Grid-Connected Photovoltaic Systems”, IEEE Transactions on Industrial Electronics, 56 (11): 4473-4482.

Feng B., Wang Y. and Man J., 2014. “A Novel Dual Phase Shift Control Strategy for Dual Active Bridge DC-DC Converter,” IECON 2014: 4140-4145.

Filsoof K., Lehn P. W., 2013. “Design and Control of Bidirectional Triangular Modular Multilevel DC-DC Converter,” IEEE COMPEL 2013, Salt Lake City: 1-7.

Gangatharan S., Rengasamy M., Elavarasan R. M., Das N., Hossain E., and Sundaram V. M., 2020. “A Novel Battery Supported Energy Management System fort he Effective Handling of Feeble Power in Hybrid Microgrid Environment”, IEEE Open Access Journal, 8: 217391-217415.

Giacomini J. C., Michels L., Pinheiro H., and Rech C., 2017. “Design Methodology of a Passive Damped Modified LCL Filter for Leakage Current Reduction in Grid-connected Transformerless Three-Phase PV Inverters” IET Renewable Power Generation”, 11 (14): 1769-1777.

Gupta B. K., Gedam A. I. and Sekhar K. R., 2019. “A Dual Inverter Based Grid Connected Solar Power Conditioning System With Coordinated Closed Loop Control”, IEEE PES Innovative Smart Grid Technologies: 2178-2183.

Han L., Morstyn T., and McCulloch M., 2019. ``Incentivizing prosumer coali-tions with energy management using cooperative game theory," IEEE Trans. Power Syst., 34 (1): 303-313.

Haneda R. and Akagi H., 2020. “Design and Performance of the 850-V 100-Kw 16-kHz Bidirectional Isolated DC-DC Converter Using SiC-MOSFET/SBD H-Bridge Modules”, IEEE Transactions on Power Electronics, Early Access Article.

Hang W., Xiang-jun Z., Mei-mei Z., Ying-ying H., Xiao Z., and Xu Y., 2017. “5L full-scale converter with a dc-link flying-capacitor auxiliary bridge leg for large direct-drive wind turbines”, IET Electric Power Applications, 11 (6): 1001-1012.

Hassan S. Z., Li H., Kamal T., Mumtaz S., Khan L., and Ullah I., 2016. “Control and Energy Management Scheme for a PV/SC/BATTERY Hybrid Renewable Power System”, Sci. Int. (Lahore), 28 (2): 955-964.

Hong J., Yin J., Liu Y., Peng J., and Jiang H., 2019. “Energy Management and Control Strategy of Photovoltaic/Battery Hybrid Distributed Power Generation Systems With an Integrated Three-Port Power Converter”, IEEE Access, 7: 82838-82847.

Hu J., Joebges P., Pasupuleti G. C., Averous N. R. and De Doncker R. W., 2019. “A Maximum-Output-Power-Point-Tracking Controlled Dual-Active Bridge Converter for Photovoltaic Energy Integration Into MVDC Grids”, IEEE Transactions on Energy Conversion, 34 (1): 170-180.

Humayun M., Huawei J., and Hassan M. U., 2017a. “Cascaded Symmetric Flying Capacitor Multilevel Inverter for Statcom Application”, IEEE IECON Conference: 946- 951.

Humayun M., Khan M. M., Weidong Z., Huawei J., and Ullah M., 2017b. “Modelling of Five-Level Symmetric Flying Capacitor Multilevel Inverter for STATCOM Application”, IEEE ICET Conference.

Ionic Batteries Company model: IC-24V10-EP datasheet

Inoue S. and Akagi H., 2007. “A Bidirectional DC-DC Converter for an Energy Storage System With Galvanic Isolation,” IEEE Trans. Power Electron., 22 (6): 2299-2306.

Islam R., Mahfuz-Ur-Rahman A. M., Islam M., Guo Y. G., Zhu J. G., 2017. “Modular Medium-Voltage Grid-Connected Converter with Improved Switching Techniques for Solar Photovoltaic Systems”, IEEE Trans. On Industrial Electronics 64 (11): 8887–8896.

Islam R., Mahfuz-Ur-Rahman A. M., Muttaqi K. M. and Sutanto D., 2019. “State-of-the-Art of the Medium-Voltage Power Converter Technologies for Grid Integration of Solar Photovoltaic Power Plants”, IEEE Trans on Energy Conversion, 34 (1): 372-384.

Itani K., De Bernardinis A., Jammal A. and Oueidat M., 2016. “Control Strategy for Extreme Conditions Regenerative Breaking of a Hybrid Energy Storage System for an Electric Vehicle”, IEEE 14th International Conference on Industrial Informatics (INDIN): 264-269.

Jafari M., Malekjamshidi Z., Lu D. D., and Zhu J., 2019. ``Development of a fuzzy-logic-based energy management system for a multiport multioper-ation mode residential smart microgrid,''IEEE Trans. Power Electron., 34 (4): 3283-3301.

Jalbrzykowski S. and Citko T., 2009. “A bidirectional DC-DC converter for renewable energy systems”, Bulletin of the Polish Academy of Sciences Technical Sciences, 57 (4): 363-368.

Karshenas H. R., and Saghafi H., 2006. “Basic Criteria in Designing LCL Filters for Grid Connected Converters”, IEEE ISIE Conference:1996-2000.

Katerchi M., Belhadj J., and Elleuch M., 2014. “Integration of a Large Scale Photovoltaic System in the Distribution Grid under Partially Shading,” 2014 International Conference on Electrical Sciences and Technologies in Maghreb (CISTEM): 1-5.

Kayaalp R. İ., Demirdelen T., and Tümay M., 2015. “Modelling and Analysis of Bidirectional DC-DC Converter”, International Journal for Innovation Education and Research, IJIER, 3 (11): 16-30.

Kazmierkowski M., Krishnan R., and Blaabjerg F., 2002. Control in Power Electronics –Selected Problem: Academic Pres.

Kebede F. S., Olivier J.-C., Bourguet S., and Machmoum M., 2021. “Reliability Evaluation of Renewable Power Systems through Distribution Network Power Outage Modelling”, Energies: 1-26.

Khanam J. and Foo S. Y., 2018. “Modeling of a Photovoltaic Array in Matlab Simulink and Maximum Power Point Tracking Using Neural Network”, Journal of Electrical & Electronic Systems, 7 (3): 1-8.

Kim M., Rosekeit M., Sul S. K., and De Doncker R. W., 2011. “A dual-phase-shift control strategy for dual-active-bridge DC-DC converter in wide voltage range,” in Proc. IEEE ECCE: 364-371.

Kouro S., Asfaw K., Goldman R., Snow R., Wu B. and Rodriguez J., 2010. “NPC Multilevel Multistring Topology for Large Scale Grid Connected Photovoltaic Systems”, IEEE 2nd International Symposium on Power Electronics for Distributed Generation Systems: 400-405.

Krishna K. V., Suryawanshi H. M., Shitole A. B. and Ajmal T., 2015. “Comparison between 2-level and 3-level grid connected inverters implemented using SRF PLL technique”, IEEE ICEPE Conference.

Krismer F., Round S., and Kolar J. W., 2006. “Performance Optimization of a High Current Dual Active Bridge with a Wide Operating Voltage Range”, IEEE 37th Annual Conference on Power Electronics Specialist Conference.

Kumar A., Bhat A. H. and Agarwal P., 2017. “Comparative Analysis of Dual Active Bridge Isolated DC to DC converter with Single Phase Shift and Extended Phase Shift Control Techniques”, CERA 2017: 257-262.

Lashab A., Sera D., Guerrero J. M., Mathe L., and Bouzid A., 2018. “Discrete Model Predictive Control-Based Maximum Power Point Tracking for PV Systems: Overview and Evaluation”, IEEE Transactions on Power Electronics, 33 (8): 1-14.

Li R. and Shi F., 2019. “Control and Optimization of Residential Photovoltaic Power Generation System With High Efficiency Isolated Bidirectional DC-DC Converter”, IEEE Access, 7: 116107-116122.

Lin C.-H., Hsieh C.-Y., and Chen K.-H., 2010. “A Li-Ion Battery Charger With Smooth Control Circuit and Built-In Resistance Compensator for Achieving Stable and Fast Charging”, IEEE Transactions on Circuits and Systems-I: Regular Papers, 57 (2): 506-517.

Liserre M., Blaabjerg F., and Hansen S., 2005. "Design and Control of an LCL-Filter-Based Three-Phase Active Rectifier", IEEE Transactions on Industry Applciations, 41 (5): 1281-1291.

Lu S., Li Y., and Xia H., 2018. ``Study on the conguration and operation optimization of CCHP coupling multiple energy system,"Energy Convers. Manage.,177: 773-791.

Lu S., Sun K., Shi H., Jiang S. and Li Y. W., 2018. "Comparison of High Power DC-DC Converters for Photovoltaic Generation Integrated into Medium Voltage DC Grids", IEEE PEAC Conf.: 978-984.

Madaci B., Chenni R., Kurt E., and Hemsas K. E., 2016. "Design and control of a stand-alone hybrid power system", International Journal of Hydrogen Energy, 1-12.

Marzband M., Sumper A., Dominguez-Garcia J. L., and Gumara-Ferret R., 2013. ``Experimental validation of a real time energy management system for microgrids in islanded mode using a local day-ahead electricity market and MINLP," Energy Convers. Manage, 76: 314-322.

Marzband M., Yousefnejad E., and Sumper A., 2016. ``Real time experimental implementation of optimum energy management system in standalone microgrid by using multi-layer ant colony optimization,"Int. J. Elect. Power Energy Syst., 75: 265-274.

McCann A. J., Zhang L. and Mueller F., 2012. "A High Efficiency DC-DC Converter Topology Suitable for Distributed Large Commercial and Utility Scale PV Systems", 2012 15th International Power Electronics and Motion Control Conference (EPE/PEMC): 1-6.

Merabet A., Khandker T.A., Hussein I., and Beguenane R. 2016. "Energy Management and Control System for Laboratory Scale Microgrid based Wind-PV-Battery", IEEE Trans. On Sustainable Energy, 8 (1): 145-154

Mi C., Bai H., Wang C., and Gargies S., 2008. "Operation, design and control of dual H-Bridge-based isolated bidirectional DC-DC converter", IET Power Electronics, 1 (4): 507-517.

Mnati M. J., Abed J. K., Bozalakov D. V., and Van den Bossche A., 2018. "Analytical and Calculation DC-Link Capacitor of a Three-Phase Grid-Tied Photovoltaic Inverter", IEEE CPE-POWERENG Conference.

Moghaddam S. H. A., Ayatollahi A., and Rahmati A., 2012. "Modelling and Current Programmed Control of a Bidirectional Full-Bridge DC-DC Converter", Energy and Power Engineering (EPE), 4: 107-116.

Morstyn T., Savkin A. V., Hredzak B., and Tuan H. D., 2018. ``Scalable energy management for low voltage microgrids using multi-agent storage system aggregation,"IEEE Trans. Power Syst., 33 (2): 1614-1623.

Mukundan C. M. N., and Jayaprakash P., 2017. "Isolated SEPIC Converter fed Trinary Hybrid Cascaded H-bridge Multilevel Inverter for Solar PV System", IEEE Region 10 Symposium (TENSYMP).

Nair U. R, and Costa-Castello R., 2020. "A Model Predictive Control-Based Energy Management Scheme for Hybrid Storage System in Islanded Microgrids", IEEE Access, 8: 97809-97822.

Nasr M., Nasr-Azadani E., Rabiee A., and Hosseinian S. H., 2019. ``Risk-averse energy management system for isolated microgrids considering generation and demand uncertainties based on information gap deci-sion theory," IET Renew. Power Gener., 13 (6): 940-951.

Okyere H. K., Nouri H., and Miedzinski B., 2006. "Bus Voltage Control Through 5 and 11 Level Voltage-Sourced Inverter STATCOM", IEEE Proceedings of the 41th International Universities Power Engineering Conference, 2: 795-799.

Peng J., He H. and Xiong R., 2017. "Rule based energy management strategy for a series- parallel plug-in hybrid electric bus optimized by dynamic programming", Applied Energy, 185: 1633-1643.

Pereira P., De Paula H., Filho B. J. C., Brito J. A. S., Rocha A. V., 2014. “Analysis of High Frequency Phenomena in Medium-Power Photovoltaic Systems”, IEEE Industry Application Society Annual Meeting: 1-8.

Phanikumar C. and Agarwal V., 2013. “Single Phase 9 Level Grid Connected Inverter for Photovoltaic Applications”, 4th IEEE International Symposium on Power Electronics for Distributed Generation Systems (PEDG).

Pippia T., Sijs J., De Schutter and B., 2020. “A Single-Level Rule-Based Model Predictive Control Approach for Energy Management of Grid-Connected Microgrids”, IEEE Trans. On Control Systems Technology, 28 (6): 2364-2376.

Rana M. J., and Abido M. A., 2017. “Energy management in DC microgrid with energy storage and model predictive controlled AC-DC converter”, IET Gener., Transmiss. Distrib., 11 (15): 3694-3702.

Rangel C. A. S., Canha L., Sperandio M., and Severiano R., 2018. “Method-ology for ESS-type selection and optimal energy management in dis-tribution system with DG considering reverse ow limitations and cost penalties,"IET Gener., Transmiss. Distrib., 12 (5): 1164-1170.

Rani B. I., Ilango G. S., and Nagamani C., 2013. “Control Strategy for Power Flow Management in a PV System Supplying DC Loads”, IEEE Trans. On Industrial Electronics, 60 (8): 3185-3194.

Reznik A., Simoes M. G., Al-Durra A., and Muyeen S. M., 2014. “LCL Filter and Performance Analysis for Grid Interconnected Systems”, IEEE Transactions on Industry Applications, 50 (2): 1-7.

Riffonneau Y., Bacha S., Barruel F., and Ploix S., 2011. “Optimal Power Flow Management for Grid Connected PV Systems with Batteries”, IEEE Trans. On Sustainable Energy, 2 (3): 309-320.

Rivera S., Kouro S., Wu B., Leon J. I., Rodriguez J. and Franquelo L.G., 2011. “Cascaded H-Bridge Multilevel Converter Multistring Topology for Large Scale Photovoltaic Systems”, IEEE International Symposium on Industrial Electronics: 1837-1844.

Rivera S., Kouro S., Wu B., Leon J. I., Rodriguez J., and Franquelo L. G., 2011. "Cascaded H-bridge multilevel converter multistring topology for large scale photovoltaic systems," IEEE International Symposium on Industrial Electronics, ISIE2011.

Rivera S., Wu B., Kouro S., Wang H. and Zhang D., 2012. “Cascaded H-Bridge Multilevel Converter Topology and Three-phase Balance Control for Large Scale Photovoltaic Systems”, IEEE PEDG Conf.: 690-697.

Sahoo A. K., Shahani A., Basu K., and Mohan N., 2014. “LCL Filter Design for Grid-Connected Inverters by Analytical Estimation of PWM Ripple Voltage”, IEEE APEC Conference: 1281-1286.

Saiju R., Kroggel A. and Wiese N., 2019. “Photovoltaic model based on data sheet values using Matlab simulation tool”, 1st Global Power, Energy and Communication Conference (IEEE GPECOM): 259-264.

Sangsun K. and Enjeti P. N., 2002. "A parallel-connected single phase power factor correction approach with improved efficiency," in IEEE Applied Power Electronics Conference and Exposition, APEC 2002, 1: 263-269.

Sassi A., Zaidi N., Nasri O., and Slama J. B. H., 2017. “Energy Management of PV/Wind/Battery Hybrid Energy System Based on Batteries Utilization Optimization”, IEEE International Conference on Green Energy Conversion Systems (GECS), Hammamet, Tunisia.

Sayed S., Elmenshawy Mena, Elmenshawy Mariam, Ben-Brahim L., Massoud A., 2018. “Design and Analysis of High-Gain Medium-Voltage DC-DC Converters for High-Power PV Applications”, IEEE CPE-POWERENG Conference.

Segaran D., Holmes D. G., and McGrath B. P., 2008. “Comparative Analysis of Single and Three-phase Dual Active Bridge Bidirectional DC-DC Converters”, Australasian Universities Power Engineering Conference.

Sochor P., Tan N. M. L. and Akagi H., 2018. “Low-Voltage-Ride-Through Control of a Modular Multilevel Single-Delta Bridge-Cell (SDBC) Inverter for Utility-Scale Photovoltaic Systems”, IEEE Trans. On Industry Applications, 54 (5): 4739-475.

Song C., Chen A., Chen J., Du C. and Zhang C., 2017. “Current stressed optimized strategy of dual active bridge DC-DC converter with dead-time effect in single phase shift control”, IECON 2017: 1013-1018.

Sorour A., Fazeli M., Monfared M., Fahmy A. A., Searle J. R., and Lewis R. P., 2021. “Forecast-Based Energy Management for Domestic PV-Battery Systems: A U.K. Case Study”, IEEE Open Access Journal, 9: 58953-58965.

Tabari M., and Yazdani A., 2016. “An Energy Management Strategy for a DC Distribution System for Power System Integration of Plug-In Electric Vehicles”, IEEE Transactions on Smart Grid, 7 (2): 659-668.

Tafti H. D., Maswood A. I., Konstantinou G., Pou J. and Townsend C. D., 2016. “Low-Voltage Ride-Through Capability of Full-Row Connected Cascaded H-Bridge Converters”, IEEE Region 10 Conference (TENCON): 984-987.

Tehrani M. M., and Dahmardeh M., 2018. “A Novel Power Distribution System Employing State of Available Power Estimation for a Hybrid Energy Storage System”, IEEE Transactions on Industrial Electronics, 65 (8): 6676-6685.

Teodorescu R., Blaabjerg F., Liserre M. and Dell’Aquila A., 2003. “A stable three-phase LCL-filter based active rectifier without damping”, IEEE 38th IAS Annual Meeting on Conference Record of the Industry Applications Conference: 1552-1557.

Thomson S. J., Thomas P., Anjali R., and Rajan E., 2018. "Design and Prototype Modelling of a CC/CV Electric Vehicle Battery Charging Circuit", IEEE International Conference on Circuits and Systems in Digital Enterprise Technology (ICCSDET).

Todorčević T., Bauer P., and Ferreira J. A., 2013b. "Comparison of bidirectional medium- voltage dc-dc converters for energy harvesting using dielectric elastomers," PCIM Europe 2013b, Germany: 673-680.

Todorčević T., Bauer P., Ferreira J. A., van Kessel R., 2013a. "Bidirectional Modular Multilevel DC-DC Converter Control and Efficiency Improvements through Separate Module Control Method," IEEE ECCE 2013, Denver: 2038-2043.

Twining E., and Holmes D. G., 2003. "Grid Current Regulation of a Three-Phase Voltage Source Inverter With an LCL Input Filter", IEEE Transactions on Power Electronics, 18 (3): 888-895.

Valencia F., Collado J., Saez D., and Marin L. G., 2016. "Robust Energy Management System for a Microgrid Based on a Fuzzy Prediction Interval Model", IEEE Transactions on Smart Grid, 7 (3): 1486-1494.

Veerappan Dr. N., Rattan kumar V. and Archana V., 2014. "Smart Self Regenerative Illumination-Solar Energy Based Hybrid Power Generation System", IEEE National Conference on Emerging Trends In New & Renewable Energy Sources And Energy Management (NCET NRES EM): 181-185.

Venayagamoorthy G. K., Sharma R. K., Gautam P. K., and Ahmadi A., 2016. "Dynamic Energy Management System for a Smart Microgrid", IEEE Transactions on Neural Networks and Learning Systems, 27 (8): 1643-1656.

Villanueva E., Correa P., Rodriguez J., and Pacas M., 2009. "Control of a Single-Phase Cascaded H-Bridge Multilevel Inverter for Grid-Connected Photovoltaic Systems," IEEE Trans. on Industrial Electronics, 56: 4399-4406.

Vinod B. R., and Baiju M. R., 2016. "Space Vector based DTC Scheme for a 3-Level Inverter Realized by Cascading Two 2-Level Inverters", IEEE ICPEICES Conference: 1-6.

Walter J., De Doncker R. W., 2003. "High Power Galvanically Isolated DC/DC Converter Topology for Future Automobiles", IEEE 34th Annual Conference on Power Electronics Specialists Conference, 1: 27-32.

Wang B., Zhang X., Song C., and Cao R., 2019. "A New Arrangement of LCL Filter for Dual-Inverter Fed Open-End Winding Transformer Topology in PV Applications", IEEE ECCE-Asia Conference: 2442-2447.

Wang P., Liu F., Zha X., Zhu F., Gong J. and Feng K., 2017. "A Segmented Power Distribution Control System Based on Hybrid Regenerative Cascaded Multilevel Converter", IEEE Applied Power Electronics Conference and Exposition (APEC): 724-728.

Wang Z. and Li H., 2012. "A Soft Switching Three-phase Current-fed Bidirectional DC-DC Converter with High Efficiency Over a Wide Input Voltage Range", IEEE Transactions on Power Electronics, 27 (2): 669-684.

Windarko N. A., Qudsi O. A., Tjahjono A., Okky A. D., and Purnomo M. H., 2014. "Optimized PI Constant for Current Controller of Grid Connected Inverter with LCL Filter Using Genetic Algorithm", IEEE MICEEI Conference: 9-13, 2014.

Wu X., Hu X., Yin X., and Moura S. J., 2018. "Stochastic Optimal Energy Management of Smart Home With PEV Energy Storage", IEEE Transactions on Smart Grid, 9 (3): 2065-2075.

Wu Z., Zhang X.-P., Brandt J., Zhou S.-Y., and Li J.-N., 2015. "Three Control Approaches for Optimized Energy Flow With Home Energy Management System", IEEE Power and Energy Technologies Journal, 2 (1): 21-31.

Yazdani F., Haghbin S., Zolghadri M., and Thiringer T., 2017. "Accurate Analysis of a Single-Phase Dual Active Bridge Converter for ZVS and Deadband Conditions", IEEE International Conference on Environment and Electrical Engineering.

Yoon C., Kim J., and Choi S., 2011. "Multiphase DC-DC Converters Using a Boost-Half- Bridge Cell for High-Voltage and High-Power Applications," IEEE Trans. on Power Electronics, 26: 381-388.

Zhang Z., Cai Y.-Y., Zhang Y., Gu D.-J., and Liu Y.-F., 2016 "A Distributed Architecture Based on Microbank Modules With Self-Reconfiguration Control to Improve the Energy Efficiency in the Battery Energy Storage System", IEEE Transactions on Power Electronics 31 (1): 304-317.

Zhang L., Zhang Z., Qin J., Shi D. and Wang Z., 2018. "Design and Performance Evaluation Evaluation of the Modular Multilevel Converter (MMC)-based Grid-tied PV-Battery Conversion System", IEEE ECCE Conf: 2649-2654.

Zhao B., Yu Q., and Sun W., 2012. "Extended-Phase-Shift Control of Isolated Bidirectional DC-DC Converter for Power Distribution in Microgrid," IEEE Trans. Power Electron., 27 (11): 4667-4680.

Zhao W., Choi H., Konstantinou G., Ciobotaru M. and Agelidis V. G., 2012. "Cascaded H-bridge Multilevel Converter for Large-scale PV Grid-Integration with Isolated DC-DC Stage", IEEE PEDG Conf.: 849-856.

Zhou Y., Huang Z., Liao H., Li H., Jiao Y., and Peng J., 2019. "A Predictive Set-Point Modulation Energy Management Strategy for Hybrid Energy Storage Systems", IEEE Transactions on Industry Applications, 25 (6): 6266-6277.

Zulauf G., Treichler W. and Castelaz J., 2015. "System, method, and results for the regenerative burn-in testing of high-power DC-DC converter", IEEE Transportation Electrification Conference and Expo (ITEC): 1-6.

CURRICULUM VITAE

Rahmi İlker KAYAALP, He graduated from Seyhan ÇEAŞ Anatolian High School in Adana in 2007. He received his BSc degree from Electrical and Electronics Engineering department of Çukurova University in 2013. Then, he started MSc education and passed the academic exam to be research assistant at Kırşehir Ahi Evran University in the same year. In 2015, he received his MSc degree from Electrical and Electronics Engineering department of Çukurova University. Then, he started PhD education at the same department. He has been working as a research assistant in the Electrical and Electronics Engineering department of the Çukurova University since 2013.

His research interests are renewable energy systems, power electronic converters, electrical machines, smart grid, energy management system applications and energy efficiency studies.